Pacific Northwest
NATIONAL LABORATORY

PNNL-32826, Rev. 0
EWG-RPT-039, Rev. 0

Hanford Low-Activity Waste Glass Minor Component Concentration Boundary Expansion

November 2022

RL Russell
JD Vienna
S Baird
D Cutforth

U.S. DEPARTMENT OF ENERGY

Prepared for the U.S. Department of Energy
under Contract DE-AC05-76RL01830

DISCLAIMER

PACIFIC NORTHWEST NATIONAL LABORATORY
operated by
BATTELLE
for the
UNITED STATES DEPARTMENT OF ENERGY
under Contract DE-AC05-76RL01830

Printed in the United States of America

Available to DOE and DOE contractors from the
Office of Scientific and Technical Information,
P.O. Box 62, Oak Ridge, TN 37831-0062;
ph: (865) 576-8401
fax: (865) 576-5728
email: reports@adonis.osti.gov

Available to the public from the National Technical Information Service
5301 Shawnee Rd., Alexandria, VA 22312
ph: (800) 553-NTIS (6847)
email: orders@ntis.gov <https://www.ntis.gov/about>
Online ordering: http://www.ntis.gov

PNNL-32826, Rev. 0
EWG-RPT-039, Rev. 0

Hanford Low-Activity Waste Glass Minor Component Concentration Boundary Expansion

November 2022

RL Russell
JD Vienna
S Baird
D Cutforth

Prepared for
the U.S. Department of Energy
under Contract DE-AC05-76RL01830

Pacific Northwest National Laboratory
Richland, Washington 99354

Executive Summary

This study investigated the effects of increasing concentrations of minor components on simulated Hanford low-activity waste (LAW) glass properties to allow for LAW glass composition envelope expansion. A test matrix of ten glasses was generated by spiking three previously studied simulated Hanford LAW glass compositions with increasing concentrations of minor component mixes up to a total concentration of 2 wt%. In this study, the ten glasses were fabricated, and key properties were measured including crystal formation after canister centerline cooling (CCC), crystallinity as a function of temperature, density, viscosity, electrical conductivity, glass durability using the Vapor Hydration Test (VHT), product consistency using the Product Consistency Test (PCT), and sulfur solubility.

The measured viscosity and electrical conductivity at 1150 °C, PCT, and VHT responses of the spiked glasses were all found to be within experimental uncertainty of the associated unspiked baseline glasses. All of the differences in property responses were found to be within the 90% prediction intervals, suggesting the models accurately predict the effect of spiking on all modelled properties. These results strongly suggest that an expansion of sum-of-minors (SOM) component concentration range to 2 wt% is justified.

Based on these results, we recommend increasing the validity range of SOM from 0.33 wt% to 2 wt% for the Vienna et al. (2022) LAW glass property models.

Acknowledgments

The authors gratefully acknowledge the financial support provided by the U.S. Department of Energy Office of Environmental Management, with technical oversight by Dr. Nicholas Machara. Product consistency test and glass composition analyses were performed under the Waste Treatment and Immobilization Plant project under the supervision of Albert Kruger.

The authors thank Madison Hsieh of Savannah River National Laboratory for her help in the analysis and testing of the glasses. We also thank Tongan Jin (PNNL) for his technical review, Matt Wilburn (PNNL) for his editorial review, and David MacPherson and Chrissy Charron (PNNL) for programmatic support during the conduct of this work.

Acronyms and Abbreviations

ARG-1	Analytical Reference Glass-1
CCC	container centerline cooling (heat treatment)
CF	crystal fraction
CI	confidence interval
DIW	deionized water
DWPF	Defense Waste Processing Facility
DOE	Department of Energy
EC	electrical conductivity
EM	DOE Office of Environmental Management
IC	ion chromatography
ICP-OES	inductively coupled plasma – optical emissions spectroscopy
KH	potassium hydroxide digestion
LAW	low-activity waste
LM	lithium metaborate/tetraborate fusion
LRM	low-activity waste reference material
MV	model validity
NIST	National Institute of Standards and Technology
NQAP	Nuclear Quality Assurance Program
ORP	Office of River Protection
PCT	Product Consistency Test
PF	sodium peroxide fusion
PI	prediction interval
PNNL	Pacific Northwest National Laboratory
QA	quality assurance
SOM	sum-of-minors
SRNL	Savannah River National Laboratory
SSM	sulfur saturated melt
S/V	glass surface area-to-solution volume ratio
TM	melting temperature
TRL	technology readiness level
VHT	Vapor Hydration Test
WTP	Waste Treatment and Immobilization Plant
XRD	X-ray diffraction

Contents

Figures

Tables

1.0 Introduction

This task, *Low-Activity Waste (LAW) Composition Boundary Expansion*, supports the Department of Energy (DOE) Office of Environmental Management (EM) mission by expanding the range of LAW glass compositions that can be processed in the Hanford's Waste Treatment and Immobilization Plant (WTP). The long-term objective of this work is to expand the Hanford Site waste glass database and property-composition models to add flexibility to operate the LAW facility with a broader range of waste compositions and site flowsheet options.

1.1 Background

In 2020, Pacific Northwest National Laboratory (PNNL) issued the *Glass Property-Composition Models for Support of Hanford WTP LAW Facility Operation* (recently revised version Vienna et al. 2022) along with the glass optimization approach (Lu et al. 2021), which expanded the composition region of processable LAW by roughly 50% compared to the current WTP baseline (Kim and Vienna 2012). However, some constraints are still relatively tight. Options for Hanford near-tank processing also broaden the potential operational space, depending on the presence or absence of washing, leaching, and other pretreatment strategies and incidental blending as retrieval strategies are evaluated. Expanding compositional boundaries is intended to create a maximum flexibility in processing options. Analyses have shown that the current projected composition envelope is limited by the:

- concentrations of salt components (e.g., SO_3, Cl, Cr_2O_3, P_2O_5, F), which are constrained by salt accumulation;
- concentrations of waste alkali (e.g., Na and K), which are constrained by durability and melter corrosion; and
- concentrations of minor components (everything besides the 19 major components modeled in Vienna et al. (2022), e.g., NiO, PbO, BaO, La_2O_3, Nd_2O_3, CdO), which are constrained by data availability.

To broaden the composition region of glass in the WTP LAW Facility, additional data and model development and/or validation are needed. Each of these areas will be investigated separately due to the differences in constraining factors. Expansion of the processing composition region will enable both (1) higher waste loading, translating to higher plant throughput; and (2) higher process flexibility, translating to fewer process upsets and the ability to manage unplanned composition variations.

The current WTP baseline glass formulation boundaries are limited to processing glasses with the sum-of-minors (SOM) concentration no larger than 0.28 wt% (Kim and Vienna 2012). In this context, SOM is comprised of all chemical components other than the 17 major components: Al_2O_3, B_2O_3, CaO, Cl, Cr_2O_3, F, Fe_2O_3, K_2O, Li_2O, MgO, Na_2O, P_2O_5, SiO_2, SO_3, TiO_2, ZnO, and ZrO_2. The enhanced waste glass models (Vienna et al. 2022) include two additional major components: SnO_2 and V_2O_5 and limit the SOM to less than 0.33 wt%. The Hanford tanks contain nearly the full periodic table of elements and many of the minor components (e.g., Ni, Pb, Ba, La, Nd, Cd, etc.) are not well characterized and their partitioning during various process steps are not fully understood. This leads to a relatively high risk that the SOM may exceed the limiting concentration of 0.33 wt% by a far margin.

This report presents the glass compositions and glass property data of the expanded minor component concentrations. Section 1.2 documents the quality assurance (QA) program used in performing the work discussed in this report.

1.2 Quality Assurance

This work was performed in accordance with the PNNL Nuclear Quality Assurance Program (NQAP). The NQAP complies with DOE Order 414.1D, *Quality Assurance*, and 10 CFR 830 Subpart A, *Quality Assurance Requirements*. The NQAP uses NQA-1-2012, *Quality Assurance Requirements for Nuclear Facility Application*, as its consensus standard and NQA-1-2012, Subpart 4.2.1, as the basis for its graded approach to quality.

The NQAP works in conjunction with PNNL's laboratory-level Quality Management Program, which is based on the requirements as defined in DOE Order 414.1D, *Quality Assurance*, and 10 CFR 830, Nuclear Safety Management, Subpart A, *Quality Assurance Requirements*.

The work of this report was performed to the QA technology readiness level (TRL) 6. This work was performed to support technology development. Data obtained may be used to support design input. Work and deliverables will comply with the PNNL NQAP QA Program for this grading level and any additional controls.

2.0 Test Methods

This section describes how the 10 LAW boundary expansion glasses were designed and data obtained. The descriptions include the methods for (1) glass matrix design, (2) glass fabrication, (3) chemical composition analysis, (4) density determination, (5) secondary phase identification from container centerline cooling (CCC), (6) viscosity measurement, (7) electrical conductivity (EC) measurement, (8) crystal fraction (CF) determination, (9) Product Consistency Test (PCT) response, (10) Vapor Hydration Test (VHT) measurement, and (11) sulfur solubility measurement for these glasses.

2.1 Waste Glass Composition Region and Test Matrix

The three baseline glass compositions (Gervasio et al. 2022) were determined by calculating the predicted properties using the 2020 models (Vienna et al. 2022). For this matrix, the minor oxides were divided into 17 groups based on like chemistry on equimolar basis (e.g., alkali, alkaline earth, lanthanide, and many groups for transition metals using their charge state and cation field strength) (Table 2.1). The minor components in each group were separated into two spikes with a different oxide in each spike representing the maximum concentrations for each group, where the difference of the weighted summation of the cation field strength between the two spikes was minimized. The 10 glasses were then formulated based on three compositions of the baseline test matrix (LAWALG-02, LAWALG-08, and LAWALG-10) using the two minor component spikes with different spike levels up to a maximum of 2 wt%. This maximum spike level was determined arbitrarily to expand the composition range of the total minor component range of the total minor components by about six times.

Table 2.1. Grouping of minor components*

Ele	Z	r	CFS	IP	Period	Grp	Oxide	S1	S2
Cs	1	1.67	0.110	0.331	1	1	Cs_2O	1.48%	0.00%
Rb	1	1.61	0.114	0.338	1	1	Rb_2O	0.00%	1.00%
Tl	1	1.5	0.123	0.351	M-NM	1	Tl_2O	0.00%	0.00%
Ba	2	1.35	0.274	0.741	2	2	BaO	2.85%	0.00%
Sr	2	1.18	0.312	0.791	2	2	SrO	0.00%	1.96%
Be	2	0.27	0.762	1.235	2	3	BeO	0.00%	0.00%
Se	4	0.5	1.169	2.162	C	4	SeO_2	0.00%	1.15%
Te	4	0.66	0.990	1.990	C	4	TeO_2	1.63%	0.00%
Ge	4	0.39	1.321	2.299	M-NM	6	GeO_2	0.00%	0.00%
As	5	0.335	1.761	2.967	M-NM	7	As_2O_5	0.00%	0.00%
Sb	5	0.6	1.315	2.564	M-NM	7	Sb_2O_5	0.46%	0.47%
Am	3	1.09	0.504	1.230	R	8	Am_2O_3	0.00%	0.00%
Ce	3	1.143	0.483	1.203	R	8	Ce_2O_3	0.00%	0.00%
Cm	3	0.97	0.557	1.293	R	8	Cm_2O_3	0.00%	0.00%
Eu	3	1.066	0.514	1.242	R	8	Eu_2O_3	12.14%	0.00%
La	3	1.16	0.476	1.195	R	8	La_2O_3	0.00%	11.45%
Nd	3	1.109	0.496	1.220	R	8	Nd_2O_3	0.00%	11.82%
Pr	3	1.126	0.489	1.212	R	8	Pr_2O_3	11.38%	0.00%
Sm	3	1.079	0.508	1.235	R	8	Sm_2O_3	0.00%	0.00%
Y	3	0.9	0.593	1.333	R	8	Y_2O_3	0.20%	0.20%
Np	4	0.87	0.812	1.802	R	9	NpO_2	0.00%	0.00%
Pu	4	0.86	0.819	1.810	R	9	PuO_2	0.00%	0.00%
Th	4	1.05	0.694	1.667	R	9	ThO_2	0.00%	0.00%
U	6	0.81	1.286	2.778	R	9	UO_3	0.00%	0.00%

Ele	Z	r	CFS	IP	Period	Grp	Oxide	S1	S2
Ag	1	0.67	0.245	0.495	T	10	Ag_2O	0.92%	0.00%
Cd	2	0.95	0.378	0.870	T	10	CdO	0.00%	1.51%
Co	2	0.58	0.537	1.036	T	10	CoO	0.87%	0.00%
Cu	2	0.6	0.263	0.513	T	10	CuO	0.00%	0.64%
Mn	2	0.66	0.495	0.995	T	10	MnO	54.50%	0.00%
Ni	2	0.55	0.554	1.053	T	10	NiO	0.00%	58.45%
Pb	2	1.19	0.310	0.787	T	10	PbO	7.70%	0.00%
Pd	2	0.64	0.505	1.005	T	10	PdO	0.00%	0.00%
Bi	3	1.03	0.530	1.261	T	11	Bi_2O_3	7.89%	0.00%
Hf	4	0.71	0.943	1.942	T	12	HfO_2	0.00%	0.00%
Re	4	0.63	1.020	2.020	T	13	ReO_2	1.80%	0.00%
Ru	4	0.62	1.031	2.030	T	13	RuO_2	0.00%	1.12%
Nb	5	0.64	1.263	2.513	T	15	Nb_2O_5	0.07%	0.00%
Ta	5	0.64	1.263	2.513	T	15	Ta_2O_5	0.00%	0.11%
Mo	6	0.41	1.937	3.409	T	16	MoO_3	2.42%	0.00%
Tc	7	0.37	2.366	4.070	T	16	Tc_2O_7	0.00%	0.00%
W	6	0.6	1.578	3.077	T	16	WO_3	3.83%	0.00%
Rh	3	0.665	0.739	1.489	T	17	Rh_2O_3	0.00%	0.00%

* Ele = element, Z = formal valance, r = ionic radius in A (from Shannon 1976), CFS = crystal field strength (= $Z/[r_{ele}+r_O]^2$), IP = ion potential (=$Z/[r_{ele}+r_O]$), Grp = group defined for this effort, S1 = concentration in first spike group in wt%, S2 = concentration in second spike group in wt%.

The baseline glass compositions are shown in Table 2.2. For each baseline glass, each spike composition was added at 1 wt% individually and combined to generate nine test matrix glasses. A tenth test matrix glass was developed by adding each spike composition at 0.5 wt% to base LAWALG-10 glass. Table 2.2 shows the normalized values of the glass compositions used in this testing with the minor component spikes added to them.

Table 2.2. Baseline Glass Compositions Used for EMHQ LAW Boundary Expansion Glass Matrix (Gervasio et al. 2022)

Compound	LAWALG-02 (wt%)	LAWALG-08 (wt%)*	EMHQ-LBE-04B (wt%)*	LAWALG-10 (wt%)
Al_2O_3	5.405	3.574	3.525	8.780
B_2O_3	13.006	13.677	13.448	8.724
CaO	9.751	12.363	12.193	7.710
Cl	0.119	0.076	0.078	0.078
Cr_2O_3	0.055	0.025	0.025	0.169
F	0.115	0.096	0.095	0.068
Fe_2O_3	0.133	0.132	0.130	0.125
K_2O	0.128	0.088	0.088	0.072
Li_2O	0.000	1.671	1.648	0.000
MgO	0.145	0.182	0.180	0.116
MnO	0.010	0.013		0.008
Na_2O	19.601	9.905	11.145	23.479
P_2O_5	0.308	0.160	0.158	0.314
SO_3	1.556	1.702	1.680	0.192
SiO_2	41.709	50.150	49.456	39.761
SnO_2	0.000	0.000	0.000	4.381
TiO_2	0.128	0.092	0.090	0.141
UO_3	0.003	0.001	0.001	0.004
V_2O_5	4.047	4.072	4.016	0.000
ZrO_2	3.783	2.019	1.990	5.878
SUM	100.00	100.00	100.00	100.00

* LAWALG-08 was nominally selected for spiking. However, after spiked glasses were fabricated, they were high in Na_2O due to a source chemical challenge. A new glass with the composition very close to LAWALG-08 with Na_2O content matching the spiked glasses – EMHQ-LBE-04B was fabricated and tested for comparison with the high SO_3 spiked glasses.

Table 2.3. Target EMHQ LAW Boundary Expansion Glass Composition Matrix (mass fraction)

	Glass ID									
Component	EMHQ-LBE-01	EMHQ-LBE-02	EMHQ-LBE-03	EMHQ-LBE-04	EMHQ-LBE-05	EMHQ-LBE-06	EMHQ-LBE-07	EMHQ-LBE-08	EMHQ-LBE-09	EMHQ-LBE-10
Al_2O_3	0.05351	0.05351	0.05297	0.03538	0.03538	0.03503	0.08693	0.08693	0.08605	0.08693
B_2O_3	0.12876	0.12876	0.12745	0.13540	0.13540	0.13403	0.08637	0.08637	0.08550	0.08637
CaO	0.09753	0.09753	0.09556	0.12240	0.12240	0.12116	0.07632	0.07632	0.07555	0.07632
Cl	0.00118	0.00118	0.00117	0.00076	0.00076	0.00075	0.00077	0.00077	0.00076	0.00077
Cr_2O_3	0.00054	0.00054	0.00054	0.00025	0.00025	0.00025	0.00167	0.00167	0.00165	0.00167
F	0.00114	0.00114	0.00113	0.00095	0.00095	0.00094	0.00067	0.00067	0.00066	0.00067
Fe_2O_3	0.00132	0.00132	0.00131	0.00131	0.00131	0.00129	0.00124	0.00124	0.00123	0.00124
K_2O	0.00126	0.00126	0.00125	0.00087	0.00087	0.00087	0.00071	0.00071	0.00071	0.00071
Li_2O	0.00000	0.00000	0.00000	0.01665	0.01665	0.01638	0.00000	0.00000	0.00000	0.00000
MgO	0.00144	0.00144	0.00142	0.00180	0.00180	0.00179	0.00115	0.00115	0.00114	0.00115
MnO	0.00010	0.00010	0.00010	0.00013	0.00013	0.00013	0.00008	0.00008	0.00008	0.00008
Na_2O	0.19405	0.19405	0.19209	0.09806	0.09806	0.09707	0.23244	0.23244	0.23010	0.23244
P_2O_5	0.00305	0.00305	0.00301	0.00158	0.00158	0.00157	0.00310	0.00310	0.00307	0.00310
SiO_2	0.41292	0.41292	0.40874	0.49649	0.49649	0.49147	0.39363	0.39363	0.38965	0.39363
SO_3	0.01540	0.01540	0.01525	0.01685	0.01685	0.01668	0.00190	0.00190	0.00188	0.00190
SnO_2	0.00000	0.00000	0.00000	0.00000	0.00000	0.00000	0.04337	0.04337	0.04294	0.04337
TiO_2	0.00126	0.00126	0.00125	0.00091	0.00091	0.00090	0.00139	0.00139	0.00138	0.00139
UO_3	0.00002	0.00002	0.00002	0.00001	0.00001	0.00001	0.00004	0.00004	0.00004	0.00004
V_2O5	0.04007	0.04007	0.03966	0.04031	0.04031	0.03990	0.00000	0.00000	0.00000	0.00000
ZrO_2	0.03745	0.03745	0.03707	0.01998	0.01998	0.01978	0.05820	0.05820	0.05761	0.05820
Spike 1 (S1)	0.00000	0.01000	0.01000	0.00000	0.01000	0.01000	0.00000	0.01000	0.01000	0.00500
Spike 2 (S2)	0.01000	0.00000	0.01000	0.01000	0.00000	0.01000	0.01000	0.00000	0.01000	0.00500
Total	1.00000	1.00000	1.00000	1.00000	1.00000	1.00000	1.00000	1.00000	1.00000	1.00000

2.2 Glass Fabrication

The spikes were prepared by weighing out the appropriate chemical oxides in the target masses to form 50 g of the target spike composition for each spike and then placed in a plastic bag. After thoroughly mixing in the plastic bag for at least 30 s until uniform color developed, the powders were transferred into an agate milling chamber and milled for 2 min in the Angstrom vibratory mill. The mixed spike powders were then placed in a labeled plastic bottle.

Glass fabrication was performed according to the PNNL *Glass Batching and Melting* procedure.[1] Single metal oxides, single metal carbonates, boric acid, sodium salts, spike mixture, and glass forming chemical minerals were weighed out in the appropriate masses to form the target glass composition for each glass and then placed in a plastic bag. After thoroughly mixing in the plastic bag for at least 30 s until uniform color developed, the powders were transferred into an agate milling chamber and milled for 2 min in the Angstrom vibratory mill. The powders were then transferred to a clean Pt-10%Rh (hereafter referred to as Pt-alloy) crucible for melting using a two-step melt process. The first melt was of the raw materials after mechanically mixing in an agate milling chamber. Initial melting was performed at a temperature of 1150 °C for 1 h for the compositions to melt and form glasses. A second melt of the glass at 1150 °C for 1 h was accomplished after the first melt was quenched and the glass was ground to a fine powder in a tungsten carbide milling chamber in the Angstrom vibratory mill.

The morphology and color of each quenched glass are shown in Appendix A.

2.3 Chemical Analysis of Glass Composition

To confirm that the "as-fabricated" glasses corresponded to the specified target compositions, a representative sample of each glass was chemically analyzed at Savannah River National Laboratory (SRNL). Three preparation techniques – sodium peroxide fusion (PF), lithium metaborate/tetraborate fusion (LM), and potassium hydroxide digestion (KH) – were used to prepare the glass samples, in duplicate, for analysis. Descriptions of the dissolution processes can be found in Hsieh (2022a).

Each of the duplicate samples (two each for the preparation techniques) was analyzed twice for each element of interest by inductively coupled plasma – optical emission spectroscopy (ICP-OES) and ion chromatography (IC). Glass composition standards were also intermittently prepared and analyzed to assess the performance of the ICP-OES and IC instruments over the course of these analyses. Specifically, several samples of the low-activity reference material (LRM, Ebert and Wolfe 1999) were included as part of the SRNL Process Science Analytical Laboratory analytical plan. The preparation and measurement methods used for each of the reported glass analytes are listed in Table 2.4.

A detailed analysis of the chemical composition measurements is published elsewhere (Hsieh 2022a). A short summary of these analyses is included in Section 3.1.

[1] Russell RL. 2016. *Glass Batching and Melting.* WFDL-GBM-1, Rev. 2.

Table 2.4. Preparation and Measurement Methods Used in Measuring Concentrations of the Analytes in the LAW Boundary Expansion Waste Glasses

Analyte	Preparation Method	Measurement Method
Al	LM	ICP-OES
B	PF	ICP-OES
Ca	LM	ICP-OES
Cr	LM	ICP-OES
F	KH	IC
Fe	LM	ICP-OES
K	LM	ICP-OES
Li	PF	ICP-OES
Mn	LM	ICP-OES
Na	LM	ICP-OES
P	LM	ICP-OES
Si	PF	ICP-OES
S	LM	ICP-OES
Zn	LM	ICP-OES
Zr	PF	ICP-OES

2.4 Glass Density

The room temperature density of each glass was measured according to the PNNL procedure *Density Using a Gas Pycnometer*[2] using a MicroMeritics AccuPyc II 1340 gas pycnometer (MicroMeritics, Norcross, GA) with approximately 1.0 to 1.5 g of glass pieces. The glass was loaded into a vial and placed within the instrument. The instrument then determined the density by the difference in amount of helium gas needed to fill the vial with and without the glass present. After five runs for each glass, the average glass densities were calculated. The pycnometer was calibrated within 6 months of the measurement and checked both before and after measurements for that day using a National Institute of Standards and Technology (NIST)-traceable tungsten carbide sphere standard. These results are discussed in Section 3.2.

[2] Russell RL. 2017. *Density Using a Gas Pycnometer*. EWG-OP-0045.

2.5 Container Centerline Cooling (CCC)

A portion (~5 g) of each test glass was subjected to the simulated CCC temperature profile shown in Table 2.5 and Figure 2.1.

Table 2.5. CCC Heat Treatment Schedule of Hanford LAW Boundary Expansion Glasses

Segment	Time (min)	Start Temp. (°C)	Rate (°C/min)
1	-30	Melt. temp	0
2	0	1114	-7.125
3	0-16	1000	-1.754
4	16-73	900	-0.615
5	73-195	825	-0.312
6	195-355	775	-0.175
7	355-640	725	-0.130
8	640-1600	600	-0.095
9	1600-3710	Room temp.	NA

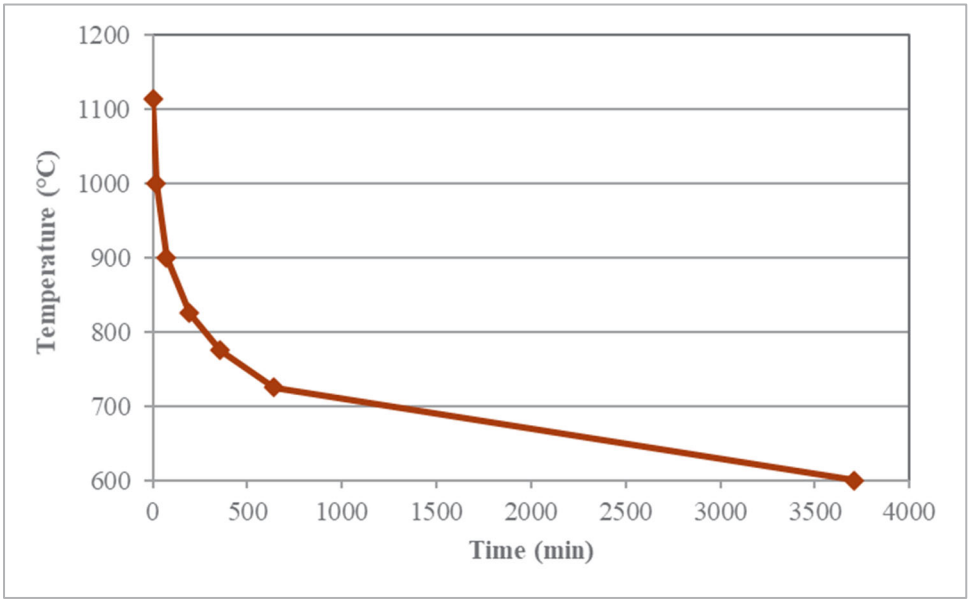

Figure 2.1. Plot of Temperature Schedule during CCC Treatment of Hanford LAW Boundary Expansion Glasses

This profile is the temperature schedule of CCC treatment for Hanford LAW glasses planned for use at the WTP.[3] Pieces of quenched glass, < 3 cm in diameter, were placed in a Pt-alloy crucible and covered with a Pt-alloy lid. The glass samples were placed in a furnace preheated to the glass melting temperature of 1150 °C. After 30 min at the melting temperature, the furnace temperature was quickly dropped to 1114 °C and the cooling profile started. It progressed down to about 400 °C based on six cooling segments shown in Table 2.5. The starting temperatures for the seven segments of cooling were 1000 °C, 900 °C, 825 °C, 775 °C, 725 °C, and 600 °C.

[3] Memorandum, "Low Activity Container Centerline Cooling Data," CCN: 074181, RPP-WTP, October 16, 2003.

The amount and types of crystalline phases that formed during CCC treatment were analyzed by X-ray diffraction (XRD) according to Section 12.4.4 of the standard ASTM International procedure, *Standard Test Method for Determining Liquidus Temperature of Immobilized Waste Glasses and Simulated Waste Glasses* (ASTM C1720). Powdered glass samples were prepared using between 1 and 2 g of glass milled for 1 min in a 10-cm^3 vibratory mill with a tungsten carbide cup and disc. Roughly 5 wt% CeO_2 was added to the powder as an internal standard and milled together with the glass for 30 sec. The powdered glass samples were loaded into XRD sample holders and scanned at a 0.015° 2θ step size, 1.5-s dwell time, from 5° to 75° 2θ scan range. XRD spectra were analyzed with TOPAS® 4.2 Software (Bruker AXS Inc., Madison, Wisconsin) for phase identification and Rietveld refinement to semi-quantify the amounts of crystal phases in samples with crystalline content. These results are discussed in Section 3.5.

2.6 Glass Viscosity

The viscosities of the quenched glasses were measured as a function of temperature using a fully automated Anton Parr FRS 1600 Furnace Rheometer System, according to the PNNL procedure *High-Temperature Viscosity Measurement Using Anton Paar FRS1600*.[4] Approximately 25 to 30 mL, or ~70 g, of glass was placed into a Pt-alloy cylindrical cup. It was then heated to ~1150 °C and maintained at that temperature until thermal equilibrium was reached. A Pt-alloy spindle was then lowered into the cup of molten glass. An initial torque reading at a constant spindle speed was taken at ~1150 °C with subsequent measurements at target temperatures of 1050 °C, 950 °C, 1150 °C, 1250 °C, and then 1150 °C using a hysteresis approach. The hysteresis approach allows for the potential impacts of crystallization (at lower temperatures) to be assessed via reproducibility with duplicate measurements being taken at approximately melting temperature (T_M) and volatilization (at higher temperatures) minimized by measuring viscosity at temperatures above T_M as the final viscosity measurement(s). The soak time was 30 min at each temperature. Prior to quenched glass viscosity measurements, the test instrumentation was calibrated using a standard glass [Defense Waste Processing Facility (DWPF) Startup Frit] as discussed in the literature (Crum et al. 2012). These results are discussed in Section 3.3.

2.7 Electrical Conductivity

The ECs of the quenched glasses were measured with an Anton Parr FRS 1600 Furnace Rheometer System by the high-temperature furnace and a Solartron Analytical 1455 Cell Test System (Solartron Analytical, Oak Ridge, TN) impedance analyzer according to PNNL procedure *High-Temperature Electrical Conductivity Measurement*.[5] Platinum plates (1.3 in. long by 0.28 in. wide) were placed parallel to each other with a separation of 0.367 in. About 30 mL of glass sample was used for EC measurements in a Pt-alloy crucible. Before measuring the ECs of the test matrix glasses, calibration was conducted at room temperature with reference solutions of KCl (0.1 M and 1 M) by measuring the resistance values at three frequencies (1, 10, and 100 kHz). Four readings were taken at each frequency over a period of 2 to 5 min. The calibration was then checked with DWPF standard glass at the higher temperatures (Crum et al. 2012). The averaged values of the four readings were then used to calculate the cell constant.

For glass measurement, the sample was first heated to melting temperature and the probe was slowly lowered into the molten glass to a depth of 12.7 mm. After the temperature was stabilized, a scan from 1 MHz to 0.1 Hz in 3 min was conducted and resistance at 1 kHz was used to calculate the EC. The EC was measured at four different temperatures in a range around the melting temperature of the glass: 1250 °C, 1150 °C, 950 °C, and 1150 °C. Two scans were made for each temperature after the glass was held for 10 min at each temperature before measurement for temperature stabilization. These results are

[4] George JL. 2022. *High-Temperature Viscosity Measurement Using Anton Paar FRS1600*. EWG-OP-0046, Rev. 1.0.
[5] George JL. 2022. *High-Temperature Electrical Conductivity Measurement*. EWG-OP-0047, Rev. 1.0.

discussed in Section 3.4. Selected glass compositions were measured in duplicate due to a change in the measurement configuration midstream of the testing. Both sets of results are reported.

2.8 Crystal Fraction in Isothermal Heat-Treated Glasses

Prior to measuring the CF, the furnace temperature accuracy was verified using Analytical Reference Glass-1 (ARG-1) glass (Smith 1993). Data measured and captured for the standard glass check was stored and maintained with the batch glass data.

The CF as a function of temperature was measured in Pt-alloy boats with tight-fitting lids (to minimize volatility) according to the standard ASTM International procedure *Standard Test Method for Determining Liquidus Temperature of Immobilized Waste Glasses and Simulated Waste Glasses* (ASTM C1720). The heat treatment was performed at 950 °C for 24 h and 850 °C for 48 h.

The amount and type of crystalline phases that formed during the CF treatment were analyzed by XRD according to Section 12.4.4 of the standard ASTM International procedure *Standard Test Method for Determining Liquidus Temperature of Immobilized Waste Glasses and Simulated Waste Glasses* (ASTM C1720). Powdered glass samples were prepared using between 1 g and 2 g of glass milled for 1 min in a 10-cm^3 vibratory mill with a tungsten carbide cup and disc. Roughly 5 wt% CeO_2 was added to the powder as an internal standard and milled together with the glass for 30 sec. The powdered glass samples were loaded into XRD sample holders and scanned at a 0.015° 2θ step size, 1.5-s dwell time, from 5° to 75° 2θ scan range. XRD spectra were analyzed with TOPAS® 4.2 Software (Bruker AXS Inc., Madison, Wisconsin) for phase identification and Rietveld refinement to semi-quantify the amounts of crystal phases in samples with crystalline content. These results are discussed in Section 3.5.

2.9 Product Consistency Test (PCT)

PCT responses were measured in triplicate for quenched samples of each glass using Method A of the standard ASTM International procedure *Standard Test Methods for Determining Chemical Durability of Nuclear, Hazardous, and Mixed Waste Glasses and Multiphase Glass Ceramics: The Product Consistency Test (PCT)* (ASTM C1285). Also included in the PCT experimental test matrix and tested in triplicate were the ARM-1 glass (Mellinger and Daniel 1984) and blanks. Glass samples were ground, sieved to −100 +200 mesh, washed, and prepared according to the standard ASTM C1285 International procedure. The prepared glass was added to water in a 1.5 g to 15 mL ratio, resulting in a glass surface area-to-solution- volume ratio (S/V) of approximately 2000 m^{-1}. The vessels were closed, sealed, and placed into an oven at 90 ± 2 °C for 7 days ± 3 h.

After the 7 days at 90 °C, the vessels were removed from the oven and allowed to cool to room temperature. The final mass of the vessel and the solution pH were recorded on a data sheet. Each test solution was then filtered through a 0.45-µm-size filter and acidified with concentrated, high-purity HNO_3 to 1 vol% to assure that the cations present remained in solution. The resulting solutions were analyzed by ICP-OES at SRNL for Si, Na, B, and Li. Samples of multi-element, standard solutions were also analyzed as a check on the accuracy of the ICP-OES. Normalized releases (g/L) were calculated based on both target and measured glass composition. Results from the PCT work are published elsewhere (Hsieh 2022c), and a short summary of these results is included in Section 3.6.

2.10 Vapor Hydration Test (VHT)

In the VHT, monolithic glass samples were exposed to water vapor at 200 °C in sealed stainless-steel vessels according to the ASTM International standard procedure *Standard Test Method for Measuring Waste Glass or Glass Ceramic Durability by Vapor Hydration Test* (ASTM C1663). Roughly 1.5-mm by

10-mm by 10-mm samples were cut from annealed glass bars using a diamond-impregnated saw. All sides of the cut sample were polished to 600-grit surface finishes with silicon carbide paper.

Polished samples were hung from stainless-steel supports with Pt wire within a stainless-steel container (see Figure 2.2). Deionized water (DIW) was added to the bottom of the vessel so that enough water was present to react with the specimen without enough water to reflux during testing (~0.20 g). The samples were heated and held at 200 °C in a convection oven for 24 days.

After removal from the oven, vessels were weighed and then quenched in cold water. The specimens were removed from the vessels and cross-sectioned with or without epoxy (depending on the stability of each sample) for analysis by optical microscopy-image analysis to determine the amount of glass altered during the test. The solution in the vessel was tested for pH to ensure reflux did not occur.

The remaining glass thickness of the VHT specimen was determined by performing at least 10 measurements distributed (roughly equally) across the crack-free cross section of the sample. Then, the average and standard deviations of the 10 thickness measurements of the remaining glass were calculated. The amount of glass altered per unit surface area of specimen was determined from the average thickness of unaltered glass according to Eq. (2.1):

$$m = \frac{1}{2}\rho(d_i - d_r) \tag{2.1}$$

where d_i, = initial thickness of the specimen (m)
d_r = average thickness of remaining glass layer (m)
m = mass of glass converted to alteration products per unit surface area (g/m^2)
ρ = glass density (g/m^3)

The average rate of corrosion was calculated as $r_a = m/t$, where t is the corrosion time. Vienna et al. (2001) showed that, if the average rate of corrosion at 200 °C is:

$$r_a = m / t < 50\ g/(m^2 \cdot d) \tag{2.2}$$

then the final rate of corrosion, r_a < 50 $g/(m^2 \cdot d)$, meets the current Office of River Protection requirement for LAW glass performance. Although the contract limit for VHT response is stated in rates (50 $g/m^2/d$), the test directly measures alteration depth (D) in µm at different times. In previous studies (Piepel et al. 2007 and Muller et al. 2014), the directly measured parameter of D in µm after 24 days was modeled. This value can be converted to a rate by: D (µm) $*10^{-6}$ (m/µm) *density (g/cm^3) $*10^6$ (cm^3/m^3) /t(d). Assuming a density of 2.65 g/cm^3, the limit of 50 $g/m^2/d$ is equivalent to a D of 453 µm for a 24-day test duration.

These results are discussed in Section 3.7.

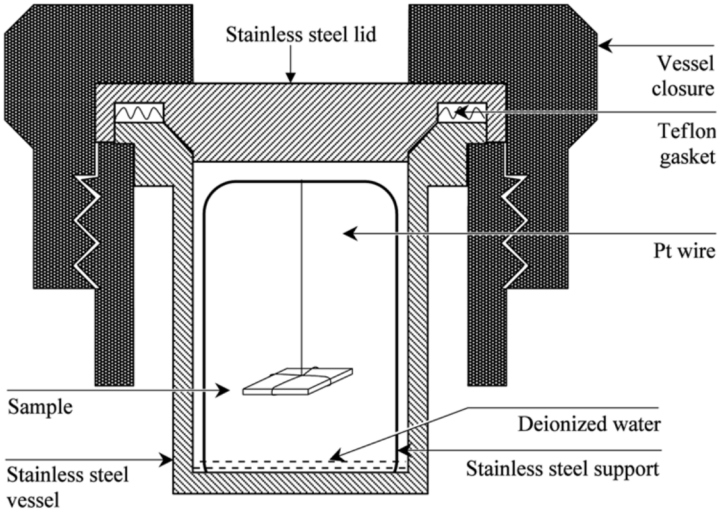

Figure 2.2. Apparatus for Conducting VHTs of Hanford LAW Boundary Expansion Glasses

2.11 Sulfur Solubility

Sulfur solubility was measured on the quenched glass samples. The procedure was developed by PNNL and can be found in Jin et al. (2019). There are three primary phases of testing with each glass: (1) saturation with sodium sulfate, (2) washing with DIW, and (3) analysis.

Saturation of the glass with sodium sulfate was performed by taking 50 g of each glass, grinding it, and then sieving through a #120 sieve (125 µm). Then, 3.82 g of Na_2SO_4 per 50 g of glass was added to the sieved powdered glass to maintain 4 mass% SO_3 added to the glass/salt system, and the combination was mixed for homogeneity. The mixture of baseline glass and Na_2SO_4 was melted at 1150 °C for 1 h in a Pt-alloy crucible with a tight-fitting lid. After melting, the mixture was poured onto a stainless-steel plate and quenched. The mixture was again mixed by crushing and sieving through a #120 sieve (125 µm) and placed back into the Pt-alloy crucible to melt at 1150 °C for 1 h the second time. After the second melting, the mixture was quenched by pouring onto a stainless-steel plate, mixed by crushing and sieving through a #120 sieve (125 µm), and melted under the same conditions for the third time. The glass, after three times re-melting and re-mixing, was crushed and sieved through the #120 sieve (125 µm).

After the third melt, the sieved samples were washed with DIW to remove excess salt prior to further analysis. This was done by adding 2 g of glass/salt mixture to a centrifuge filter in a centrifuge tube and adding 20 g of DIW to the tube. The tube was capped and shaken by hand for 2 min. Samples were then placed in a balanced centrifuge, which was set to 3175 rpm for 5 min. After centrifuging, the solution was decanted into a bottle through a low-density polyethylene filter. The filter was removed, and then was reinserted into the centrifuge tube. A second wash was performed following the same steps and then the glass was weighed and dried at 80 °C overnight. To ensure there was enough sample for analysis, a fresh 2 g of the same glass was obtained, and the procedure described above was repeated with the resulting solutions and washed glass combined.

The washed and filtered glasses were then analyzed by ICP-OES and IC at SRNL and reported by Hsieh (2022b). Also, a representative sample was taken from each of the wash solutions generated from the preparation of the sulfur saturated melt (SSM) samples. The sample was diluted according to expected concentrations of the species of interest in each of the solutions, and each sample was analyzed in triplicate by ICP-OES and IC. Blanks and standards were analyzed intermittently to assess the

performance of each of the instruments and procedures. Methods of measurement are shown in Table 2.6. The results are discussed in Section 3.8.

Table 2.6. Measurement Methods Used in Reporting the Concentrations of Each of the Analytes of the SSM Glasses and Wash Solutions (Hsieh 2022b)

Analyte	Measurement Method
Al	ICP-OES
B	ICP-OES
Ca	ICP-OES
Cr	ICP-OES
F^-	IC
Fe	ICP-OES
K	ICP-OES
Mn	ICP-OES
Na	ICP-OES
P	ICP-OES
PO_4^{3-}	IC
S	ICP-OES
SO_4^{2-}	IC
Si	ICP-OES
Zn	ICP-OES
Zr	ICP-OES

3.0 Results and Discussion

This section describes the results for the chemical composition, density, CCC crystallinity, viscosity, EC, isothermal CF, PCT, VHT, and sulfur solubility for the LAW boundary expansion glasses studied.

3.1 Chemical Analysis of Glass Composition

The targeted and average measured component concentrations (wt%) in the quenched glasses are presented in Appendix B along with the percent differences. The composition analyses of the glass samples were performed as described in Section 2.3.

The results presented in this section are summarized from the report by Hsieh (2022a). The analytical sequences of the measurements were reviewed, the average chemical composition for each glass was determined, and comparisons were made between the measurements and the targeted compositions of the glasses. JMP™ Pro Version 14.3.0 (SAS Institute, Inc.) was used to support these analyses.

Plots of the wt% glass component concentrations measured for each sample by oxide and analytical block were provided in Hsieh (2022a). Plotting the data in this format provides an opportunity to identify gross trends in performance of the analytical instruments within and among calibration blocks. A review of these plots did not identify any gross patterns or trends in the analytical process over the course of these measurements. In all cases, the instrument check standards were within specification. Any minor calibration effects typical of ICP-OES analyses are mitigated by taking the average of the measurements for each analyte.

A comparison of the LRM results to their acceptability limits was performed by SRNL. The results show that all the measurements for the elements present in the LRM standard glass were within the acceptability limits used by SRNL in conducting instrument and procedure assessments during the execution of these analyses.

All the measured sums of oxides for the study glasses fell within the interval of 96.8 to 98.1 wt%, indicating acceptable recovery of the glass components. With all of the spike elements targets added, the sums of the oxides were between 97.3 and 99 wt%. This indicates acceptable compositions of the glasses. More details can be found in Hsieh (2022a).

3.2 Density

This section discusses the results of the glass density measurements obtained using the methods discussed in Section 2.4. The density values ranged from a minimum of 2.60 g/cm^3 to a maximum of 2.75 g/cm^3. The density of these LAW boundary expansion glasses varies little – 60% of the glasses have density values between 2.60 and 2.65 g/cm^3 with the other 40% having densities between 2.74 and 2.75 g/cm^3 and are shown in Table 3.1. Table 3.1 also shows the baseline glass (LAWALG-02, LAWALG-08, LAWALG-10) measurements that these glasses were compared to. These densities increase slightly with spike concentrations. This was expected as these glasses contained several more components of higher molecular weight from the spikes.

Table 3.1. Measured Densities of LAW Boundary Expansion Glasses

Glass ID	Measured Density (g/cm^3)	Glass ID	Measured Density (g/cm^3)
LAWALG-02	2.6217	EMHQ-LBE-06	2.6315
EMHQ-LBE-01	2.6463	LAWALG-10	2.7193
EMHQ-LBE-02	2.6340	EMHQ-LBE-07	2.7524
EMHQ-LBE-03	2.6542	EMHQ-LBE-08	2.7473
EMHQ-LBE-04B	2.5940	EMHQ-LBE-09	2.7529
EMHQ-LBE-04	2.6140	EMHQ-LBE-10	2.7401
EMHQ-LBE-05	2.6013		

Figure 3.5 compares the differences in response of density versus spike concentration for each group of glasses. Overlaid on the plot is the prediction interval (PI) range in difference in density using the model recommended by Vienna et al. (2009). Note: the PI calculation was performed using a model that has not been qualified under NQA-1 and so is for information only. Only small density differences (< 0.04 g cm^{-3}) were observed and the increasing trend with spike concentration is predicted by current models.

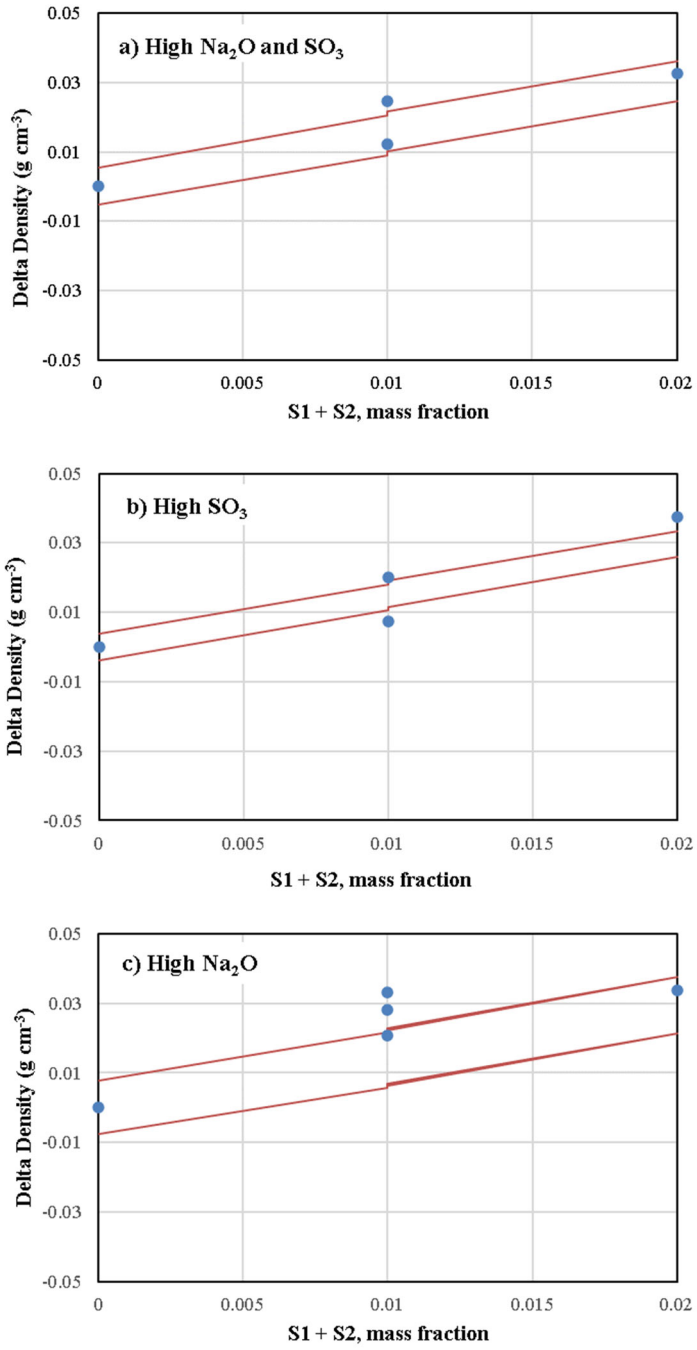

Figure 3.1. Difference in Density versus Spike Concentrations for EMHQ Glasses with a) High Na + S glasses, b) High S glasses, and c) High Na glasses. Red Lines Show 90% Prediction Intervals of Difference in Density Using Vienna et al. 2009 Models. Predicted values for information only.

3.3 Viscosity (η)

This section presents and discusses the viscosity results obtained using the methods discussed in Section 2.5. The results of the viscosity measurements are listed in Appendix D and summarized in Table 3.2.

Table 3.2. Measured ln η (Pa-s) Values versus Temperature (in the sequence of measurement) for the LAW Boundary Expansion Waste Glasses Tested

Point	1	2	3	4	5	6
Glass ID	Target Temp (°C) ln η (Pa-s)	Target Temp (°C) ln η (Pa-s)	Target Temp (°C) ln η (Pa-s)	Target Temp (°C) ln η (Pa-s)	Target Temp (°C) ln η (Pa-s)	Target Temp (°C) ln η (Pa-s)
LAWALG-02	1150	1050	950	1150	1200	1150
	1.15	1.98	3.23	1.11	0.82	1.11
EMHQ-LBE-01	1150	1050	950	1150	1200	1150
	1.05	1.99	3.34	1.04	0.69	1.03
EMHQ-LBE-02	1150	1050	950	1150	1200	1150
	1.10	2.02	3.34	1.06	0.66	1.08
EMHQ-LBE-03	1150	1050	950	1150	1200	1150
	1.03	1.97	3.20	0.98	0.59	1.0
EMHQ-LBE-04B	1150	1050	950	1150	1200	1150
	1.26	2.19	3.51	1.24	0.76	1.24
EMHQ-LBE-04	1150	1050	950	1150	1212	1150
	1.25	2.19	3.50	1.24	0.75	1.27
EMHQ-LBE-05	1150	1050	950	1150	1211	1150
	1.29	2.21	3.52	1.32	0.83	1.30
EMHQ-LBE-06	1150	1050	950	1150	1211	1150
	1.21	2.12	3.41	1.24	0.77	1.23
LAWALG-10	1150	1050	950	1150	1200	1150
	1.61	2.73	4.27	1.59	1.11	1.58
EMHQ-LBE-07	1150	1050	950	1150	1212	1150
	1.32	2.41	3.93	1.33	0.80	1.34
EMHQ-LBE-08	1150	1050	950	1150	1213	1150
	1.34	2.40	3.90	1.32	0.76	1.31
EMHQ-LBE-09	1150	1050	950	1150	1210	1150
	1.36	2.42	3.98	1.31	0.76	1.33
EMHQ-LBE-10	1150	1050	950	1150	1214	1150
	1.38	2.45	3.96	1.34	0.77	1.35

At the melting temperature of 1150 °C, the acceptable viscosity range of LAW glass melts is 2 to 8 Pa·s to avoid processing issues (Vienna et al. 2022). The measured η_{1150} data spanned the range of 2.72 to 4.90 Pa·s.

Two model forms are widely used to fit viscosity-temperature data for each waste glass. The first model form is the Arrhenius equation:

$$\ln(\eta) = A + \frac{B}{T_K} \tag{3.2}$$

where A and B are independent of temperature (T_K), which is in Kelvin (T(°C) + 273.15). The values for the A and B coefficients are shown in Table 3.3 for each glass. The second model is the Vogel-Fulcher-Tamman (VFT) model:

$$\ln(\eta) = E + \frac{F}{T_k - T_0} \tag{3.3}$$

where E, F, and T_0 are temperature independent and potentially composition dependent coefficients and T_K is the temperature in Kelvin (T(°C) + 273.15). This model can be used to estimate the effect of temperature on viscosity over a wide range of temperatures for silicate-based glasses. Therefore, this model was also applied to the data for each glass; the E, F, and T_0 coefficients for each glass are shown in Table 3.3. Table 3.3 also summarizes the viscosity results at 1150 °C (η_{1150}) calculated using the VFT equation [Eq. (3.3)].

Table 3.3. Fitted Coefficients of Arrhenius and VFT Models for Viscosity of LAW Boundary Expansion Waste Glasses Tested

	Arrhenius Coefficients		VFT Coefficients			
Glass ID	A (ln Pa-s)	B (ln Pa-s*K)	E (ln Pa-s)	F (ln Pa-s*K)	T_0 (K)	η_{1150} (Pa-s)
LAWALG-02	11.219	17594	-3.096	2544	821.1	3.093
EMHQ-LBE-01	12.500	19297	-3.929	3150	790.0	2.845
EMHQ-LBE-02	12.461	19272	-5.196	4713	671.1	2.916
EMHQ-LBE-03	12.236	18849	-7.184	7739	477.7	2.724
EMHQ-LBE-04B	12.183	19127	-5.096	4818	663.0	3.461
EMHQ-LBE-04	12.070	18978	-4.476	4411	689.4	3.482
EMHQ-LBE-05	11.823	18690	-4.476	4155	703.0	3.647
EMHQ-LBE-06	11.695	18405	-4.203	3772	727.8	3.391
LAWALG-10	14.397	22766	-6.381	6345	627.1	4.900
EMHQ-LBE-07	13.985	21828	-4.967	4308	739.1	3.782
EMHQ-LBE-08	13.962	21773	-5.795	5348	671.5	3.740
EMHQ-LBE-09	14.429	22435	-5.770	5196	690.0	3.733
EMHQ-LBE-10	14.114	22033	-6.147	5813	647.8	3.858

The 2020 model was used to predict the viscosities (in poise) with measured values at 1150 ºC. The model was developed for the target temperature of 1150 ºC only. It is a reduced partial quadratic model (PQM) with some selected binary terms for a total of 21 terms and the following form:

$$\ln(\eta_{1150},\ P) = \sum_{i=1}^{p} h_i g_i + selected\ \left\{\sum_{i=1}^{p-1}\sum_{j=1}^{p} h_{ij} g_i g_j\ +\ \sum_{i=1}^{p} h_{ii} {g_i}^2\right\} \tag{3.5}$$

where p is the number of components modeled, h_i is the coefficient of the i-th glass component, g_i is the mass fraction of the i-th glass component, h_{ij} is the coefficient of the combined i-th and j-th components, g_j is the mass fraction of the j-th LAW glass component, and h_{ii} is the i-th component quadratic coefficient.

Figure 3.2 compares the differences in response of $\ln[\eta_{1150}]$ versus spike concentration for each group of glasses. P-values for t-tests comparing the measured $\ln[\eta_{1150}]$ between the spiked glasses and their associated baseline were all below the typical threshold for significant differences of 0.05 or 0.10 (minimum being 0.245 for EMHQ-LBE-09), suggesting the differences in $\ln[\eta_{1150}]$ caused by spiking are within measurement uncertainties. The differences in model prediction intervals are also compared to differences in measured values in Figure 3.2, using the model recommended by Vienna et al. (2022). All of the differences in response of the $\ln[\eta_{1150}]$ model fit within the 90% prediction intervals, suggesting the models accurately predict the effect of spiking on $\ln[\eta_{1150}]$. Note that measured values are reported in Pa·s but converted to P for comparison with model predictions according to η_{1150} (P) = 10 η_{1150} (Pa·s).

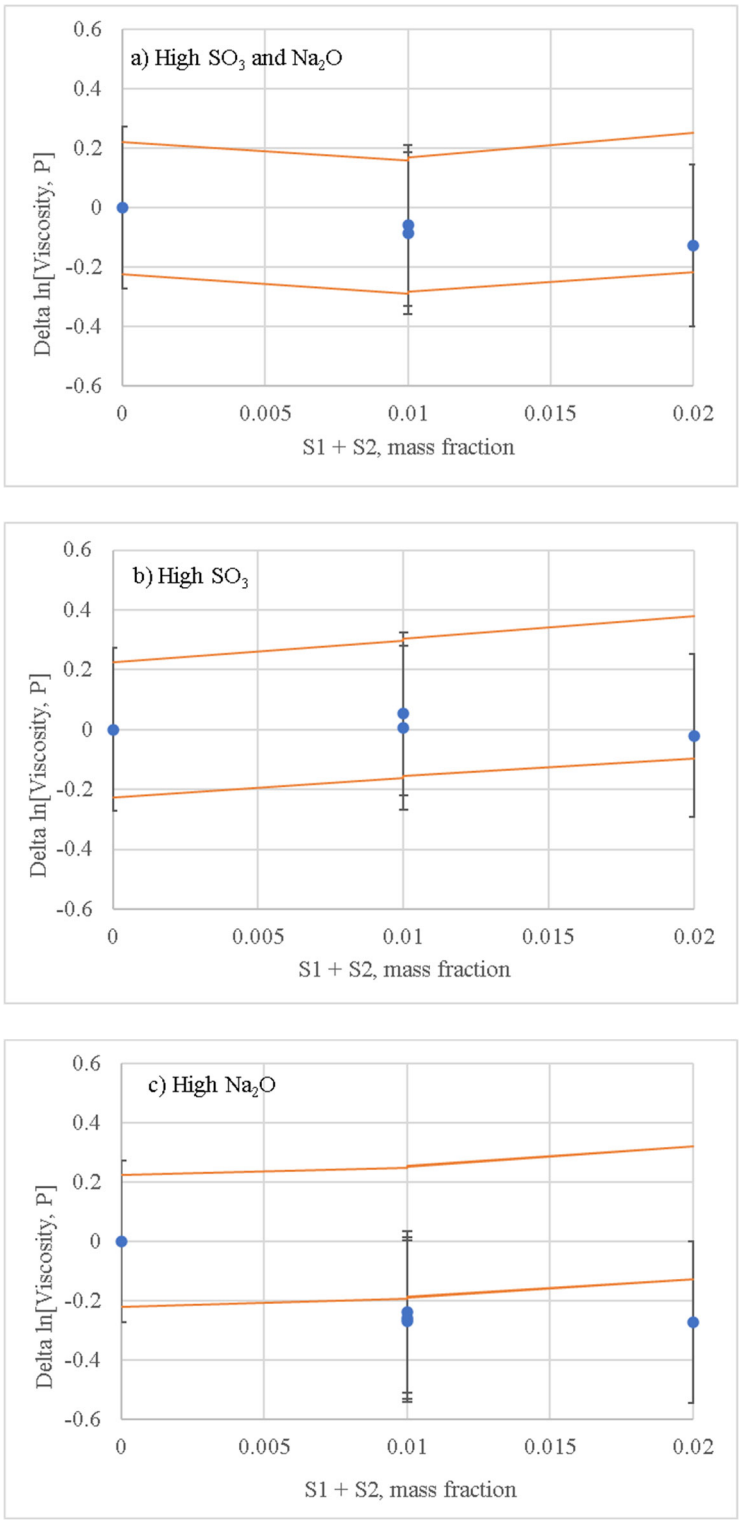

Figure 3.2. Measured Difference in Logarithm Viscosity at 1150°C versus Spike Concentrations for EMHQ Glasses: a) High Na + S glasses, b) High S glasses, and c) High Na glasses. Red Lines Represent 90% Prediction Intervals on Difference in Logarithm Viscosity Using the Vienna et al. 2020 Models.

3.4 Electrical Conductivity

This section presents and discusses the EC results obtained using the methods discussed in Section 2.7. Table 3.4 lists the EC versus temperature data for each of the glasses and Appendix E shows the plots for the EC versus temperature data obtained from the EC experiments.

Table 3.4. Measured Electrical Conductivity (S/m) Values versus Temperatures for the LAW Boundary Expansion Glasses

Target *T*, °C	950	950	1200	1200	1150	1150	1050	1050
Glass ID	Electrical Conductivity (S/m)							
LAWALG-02	19.0	16.4	42.3	36.9	37.9	37.9	28.5	28.4
EMHQ-LBE-01	19.3	19.3	37.6	37.1	31.5	31.5	26.0	26.0
EMHQ-LBE-02	26.1	26.1	53.3	53.4	48.4	48.3	37.9	37.8
EMHQ-LBE-03	20.9	20.9	32.8	--	34.9	35.0	28.6	28.6
EMHQ-LBE-04B	15.0	12.9	51.0	51.7	44.8	44.7	27.7	27.6
EMHQ-LBE-04	18.4	18.3	62.3	62.6	53.7	53.8	34.2	34.1
EMHQ-LBE-05	7.6	10.7	48.9	48.7	41.7	36.7	20.6	22.4
EMHQ-LBE-06	15.5	15.4	60.6	60.6	50.1	47.8	29.1	29.1
LAWALG-10	20.8	20.8	45.6	45.6	40.5	40.5	30.7	30.4
EMHQ-LBE-07	17.5	17.5	33.1	33.0	30.5	30.4	24.6	24.6
EMHQ-LBE-08	16.2	16.2	28.1	28.1	26.5	26.4	21.9	21.8
EMHQ-LBE-09	14.9	15.0	27.6	27.7	25.6	25.6	20.8	20.8
EMHQ-LBE-10	19.8	19.8	29.9	29.8	28.3	28.2	25.0	25.1

The Arrhenius equation was used to fit ε-temperature data for each waste glass:

$$\ln(\varepsilon) = A + \frac{B}{T_K} \tag{3.5}$$

where A and B are temperature-independent and potentially composition-dependent coefficients, and temperature (T_K) is in Kelvin [T(°C) + 273.15]. The values for the A and B coefficients obtained by fitting the equation to the ε-temperature data for each glass (using least squares regression) are shown in Table 3.5 for each glass along with the calculated ε at 1150 °C (ε_{1150}) using Eq. (3.5) fit to each glass measured data.

The 2020 model was used to predict the frequency independent conductivities (in S/cm) with measured values at 1150 ºC. The model was developed for the target temperature of 1150 ºC only. It is a reduced partial quadratic model (PQM) with some selected binary terms for a total of 13 terms and the following form:

$$ln(\varepsilon_{1150}) = \sum_{i=1}^{N} b_i g_i + \text{ Selected } \left\{ \sum_{i=1}^{N} b_{ii} (g_i)^2 + \sum_{i=1}^{N-1} \sum_{<1}^{N} b_{ij}\, g_i g_j \right\} \tag{3.6}$$

where N is the number of components modeled, b_i is the coefficient of the i-th glass component, g_i is the mass fraction of the i-th glass component, b_{ii} and b_{ij} are the coefficients for the selected quadratic terms, and g_j is the mass fraction of j-th glass component.

Table 3.5. Fitted Coefficients of the Arrhenius Model for Electrical Conductivity for the LAW Boundary Expansion Glasses

	Arrhenius Coefficients		
Glass ID	A, ln[S/m]	B, ln[S/m]-K	ε_{1150} (S/m)
LAWALG-02	7.78	-5946	36.5
EMHQ-LBE-01	6.65	-4510	32.5
EMHQ-LBE-02	7.50	-5157	48.1
EMHQ-LBE-03	6.20	-3822	33.6
EMHQ-LBE-04B	10.45	-9518	43.2
EMHQ-LBE-04	10.21	-8898	52.5
EMHQ-LBE-05	12.21	-12189	38.3
EMHQ-LBE-06	10.81	-9865	48.5
LAWALG-10	7.67	-5652	40.3
EMHQ-LBE-07	6.62	-4568	30.2
EMHQ-LBE-08	6.07	-3990	26.2
EMHQ-LBE-09	6.35	-4435	25.4
EMHQ-LBE-10	5.41	-2938	28.3

Figure 3.3 compares the differences in response of $\ln[\varepsilon_{1150}]$ versus spike concentration for each group of glasses. P-values for t-tests comparing the measured $\ln[\varepsilon_{1150}]$ between the spiked glasses and their associated baseline were all below well above the typical threshold for significant differences of 0.05 or 0.10 (minimum being 0.113 for EMHQ-LBE-09), suggesting the differences in $\ln[\varepsilon_{1150}]$ caused by spiking are within measurement uncertainties. The differences in model prediction intervals are also compared to differences in measured values in Figure 3.3, using the model recommended by Vienna et al. (2022). All of the differences in response of the $\ln[\varepsilon_{1150}]$ model fit within the 90% prediction intervals, suggesting the models accurately predict the effect of spiking on $\ln[\varepsilon_{1150}]$. Note that measure values are reported in S/m but converted to S/cm for comparison with model predictions according to ε_{1150} (S/cm) = ε_{1150} (S/m)/100.

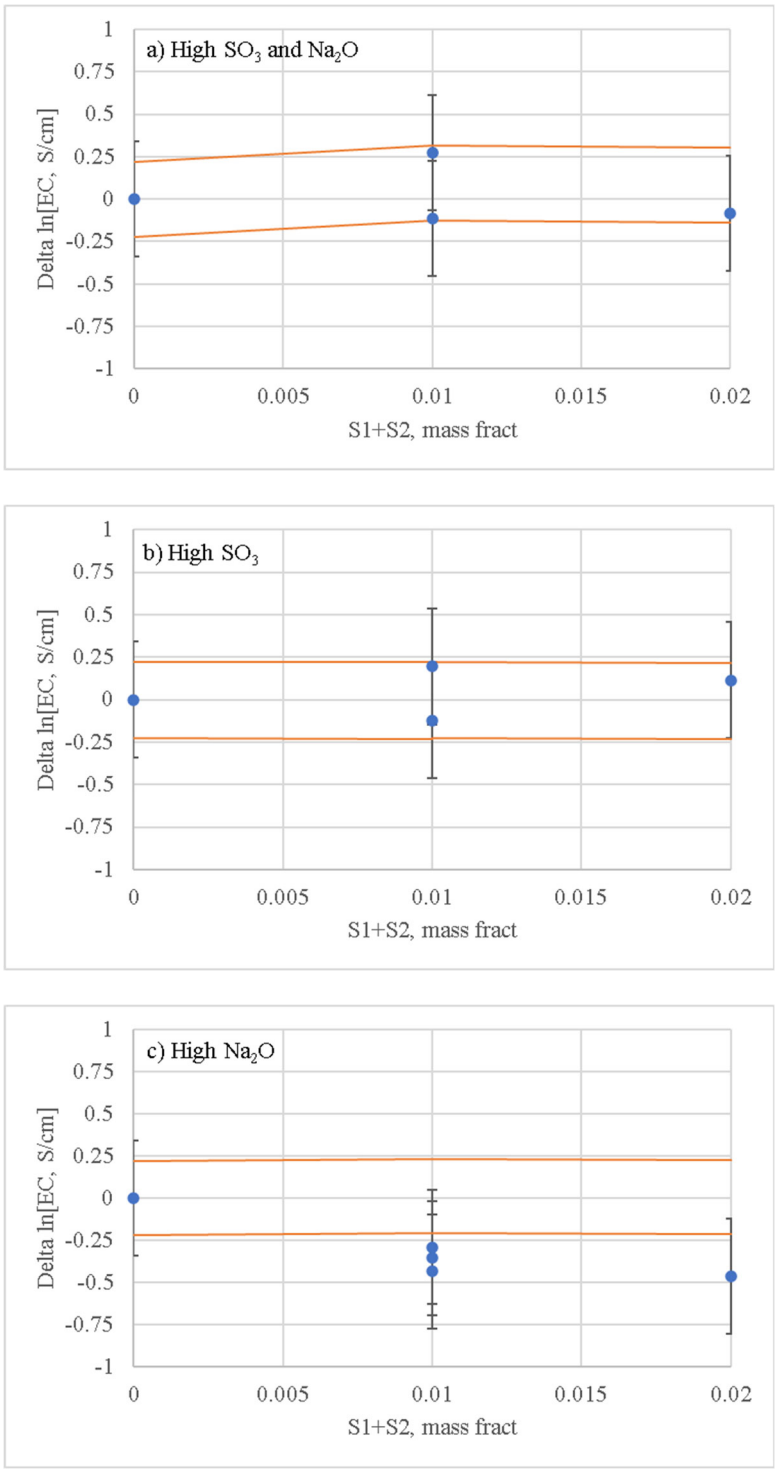

Figure 3.3. Measured Difference in Logarithm Electrical Conductivity at 1150°C versus Spike Concentrations for EMHQ Glasses: a) High Na + S glasses, b) High S glasses, and c) High Na glasses. Red Lines Represent 90% Prediction Intervals on Difference in Logarithm Electrical Conductivity Using the Vienna et al. 2020 Models.

3.5 Crystal Fraction of the Container Centerline Cooled and Isothermally Treated Glass Samples

The CF results from the CCC glasses obtained using the methods discussed in Section 2.5 and tested by XRD did not identify any crystallization in any of the glasses. The baseline glass compositions that were spiked in this study also did not have any crystallization. See Appendix C for photos of CCC-treated glasses.

The CF of the glasses was measured isothermally at 950 °C and 850 °C and the results obtained using the methods discussed in Section 2.8. See Appendix F for photos of CF heat-treated glasses at 950 °C and 850 °C and Appendix G for XRD spectra obtained from them.

All but four glasses had no crystals identified using XRD when treated at 950 °C for 24 h and 850 °C for 48 h. The glasses with crystals contained silicates of either sodium form or zirconium and sodium form or nasicon ($Na_{1+x}Zr_2Si_xP_{3-x}O_{12}$). The total crystallinity ranged from ~0.50 to ~7.6 vol%. These results are summarized in Table 3.6. When compared to the baseline glasses (LAWALG-02, -08, and -10), there were a few more crystals present in the EMHQ glasses that contained 2 wt% spike components. However, in the baseline glasses, when crystals were seen, they were the same form as seen in the EMHQ glasses being Zr-containing silicates. This indicates that the spikes may promote some crystallization in LAW glasses.

The nominal crystallinity requirement for LAW glasses is ≤ 1 vol% of crystal at 950°C. Two glasses exceed this level -- EMHQ-LBE-06 (6.2 vol% Na_2SiO_5) and EMHQ-LBE-10 (1.1 vol% Nasicon). EMHQ-LBE-06 was formed using the high Na_2O and SO_3 base glass and spiked with 1 wt% of both S1 and S2 while EMHQ-LBE-10 was formed using the high Na_2O base glass and spiked with 0.5 wt% of both S1 and S2. Interestingly, EMHQ-LBE-09 formed using the high Na_2O base glass and spiked with 1 wt% of S1 and S2, contained only 0.5 vol% crystal at 950°C.

Table 3.6. Weight Percent Crystallinity and Identification of Crystals by XRD in Heat-Treated EMHQ Waste Glasses

Glass ID	Temp (°C)	Vol% Crystallinity	Wt% Crystallinity	Crystal Phase Identification
LAWALG-02	850	0.0	0.0	None
	950	0.0	0.0	None
EMHQ-LBE-01	850	0.0	0.0	None
	950	0.0	0.0	None
EMHQ-LBE-02	850	0.0	0.0	None
	950	0.0	0.0	None
EMHQ-LBE-03	850	0.0	0.0	None
	950	0.0	0.0	None
LAWALG-08	850	0.0	0.0	None
	950	0.0	0.0	None
EMHQ-LBE-04	850	0.0	0.0	None
	950	0.0	0.0	None
EMHQ-LBE-05	850	0.0	0.0	None
	950	0.0	0.0	None
EMHQ-LBE-06	850	7.6	7.5	Na_2SiO_5
	950	6.2	6.1	Na_2SiO_5
LAWALG-10	850	0.0	0.0	None
	950	0.0	0.0	None

Glass ID	Temp (°C)	Vol% Crystallinity	Wt% Crystallinity	Crystal Phase Identification
EMHQ-LBE-07	850 950	0.0 0.0	0.0 0.0	None None
EMHQ-LBE-08	850 950	2.2 0.92	2.6 1.1	$Na_4Zr_2SiO_{10}$ Nasicon
EMHQ-LBE-09	850 950	2.2 0.50	2.6 0.60	$Na_4Zr_2SiO_{10}$ Nasicon
EMHQ-LBE-10	850 950	0.0 1.1	0.0 1.4	None Nasicon

3.6 Product Consistency Test

This section presents and discusses the PCT results obtained using the methods discussed in Section 2.9. The PCT results are published elsewhere (Hsieh 2022c) and are summarized here in Table 3.7, which includes the results from the baseline glasses they were designed to match. The PCT results were normalized to the target values of the glasses. All the normalized releases of B, Na, Li, and Si were less than the WTP LAW constraint of 2 g/m^2 for all glasses.

Table 3.7. PCT Normalized Concentration Release Results for EMHQ Glasses

Glass ID	Type	NL_B (g/L)	NR_B (g/m^2)	NL_{Na} (g/L)	NR_{Na} (g/m^2)	NL_{Li} (g/L)	NR_{Li} (g/m^2)	NL_{Si} (g/L)	NR_{Si} (g/m^2)
LAWALG-02	Quenched	2.02	1.01	2.42	1.21	NM	NM	0.630	0.315
EMHQ-LBE-01	Quenched	2.46	1.23	2.88	1.44	NM	NM	0.759	0.380
EMHQ-LBE-02	Quenched	3.00	1.50	3.34	1.67	NM	NM	0.842	0.421
EMHQ-LBE-03	Quenched	2.90	1.45	3.28	1.64	NM	NM	0.801	0.401
EMHQ-LBE-04B	Quenched	0.764	0.382	1.12	0.560	1.05	0.525	0.407	0.204
EMHQ-LBE-04	Quenched	0.856	0.428	1.22	0.610	1.19	0.595	0.397	0.199
EMHQ-LBE-05	Quenched	0.737	0.369	1.04	0.520	1.02	0.510	0.342	0.171
EMHQ-LBE-06	Quenched	0.906	0.453	1.29	0.645	1.27	0.635	0.393	0.197
LAWALG-10	Quenched	1.02	0.510	1.58	0.790	NM	NM	0.377	0.189
EMHQ-LBE-07	Quenched	1.25	0.625	1.76	0.880	NM	NM	0.428	0.214
EMHQ-LBE-08	Quenched	1.42	0.710	2.20	1.10	NM	NM	0.484	0.242
EMHQ-LBE-09	Quenched	1.06	0.53	1.56	0.780	NM	NM	0.386	0.193
EMHQ-LBE-10	Quenched	1.09	0.55	1.68	0.840	NM	NM	0.416	0.208

NM = not measured due to no lithium in the glass

Figure 3.4 compares the PCT normalized releases of B (NR_B) with the normalized releases of Na (NR_{Na}) for the quenched glass samples.

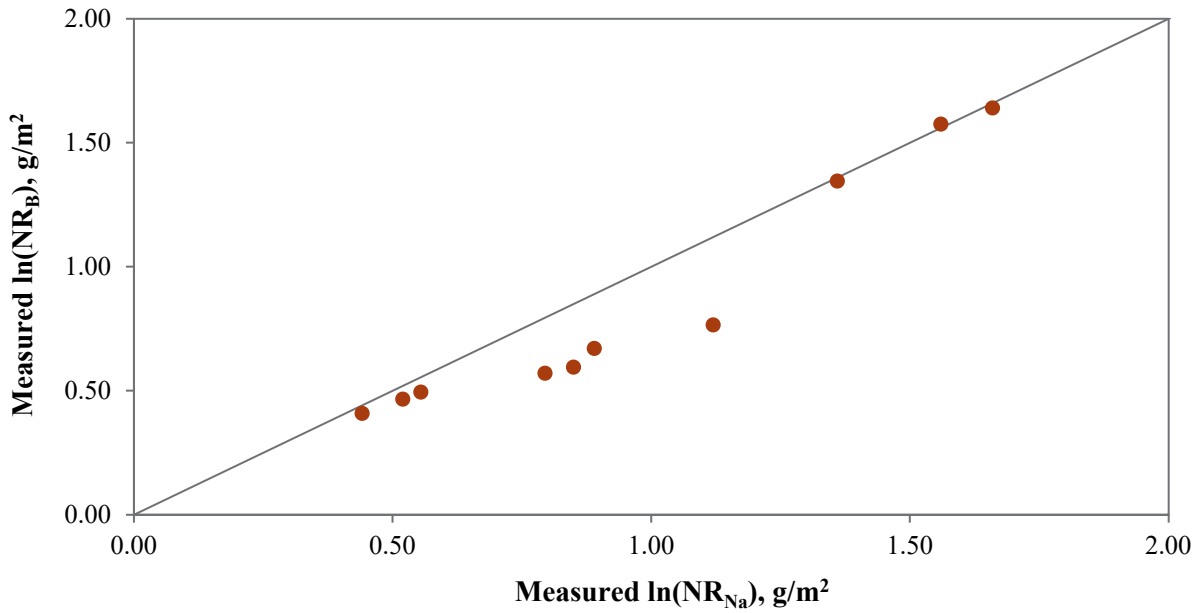

Figure 3.4. Comparison of PCT Normalized Releases of B with Na for Quenched Samples of EMHQ Glasses

Figure 3.5 compares the differences in response of ln[NR_B] versus spike concentration for each group of glasses. P-values for t-tests comparing the measured ln[NR_B] between the spiked glasses and their associated baseline were all below well above the typical threshold for significant differences of 0.05 or 0.10 (minimum being 0.227 for EMHQ-LBE-02), suggesting the differences in ln[NR_B] caused by spiking are within measurement uncertainties. The differences in model prediction intervals are also compared to differences in measured values in Figure 3.5, using the model recommended by Vienna et al. (2022). All of the differences in response of the ln[NR_B] model fit within the 90% prediction intervals, suggesting the models accurately predict the effect of spiking on ln[NR_B].

Figure 3.6 compares the differences in response of ln[NR_{Na}] versus spike concentration for each group of glasses. P-values for t-tests comparing the measured ln[NR_{Na}] between the spiked glasses and their associated baseline were all below well above the typical threshold for significant differences of 0.05 or 0.10 (minimum being 0.205 for EMHQ-LBE-08), suggesting the differences in ln[NR_{Na}] caused by spiking are within measurement uncertainties. The differences in model prediction intervals are also compared to differences in measured values in Figure 3.6, using the model recommended by Vienna et al. (2022). All of the differences in response of the ln[NR_{Na}] model fit within the 90% prediction intervals, suggesting the models accurately predict the effect of spiking on ln[NR_{Na}].

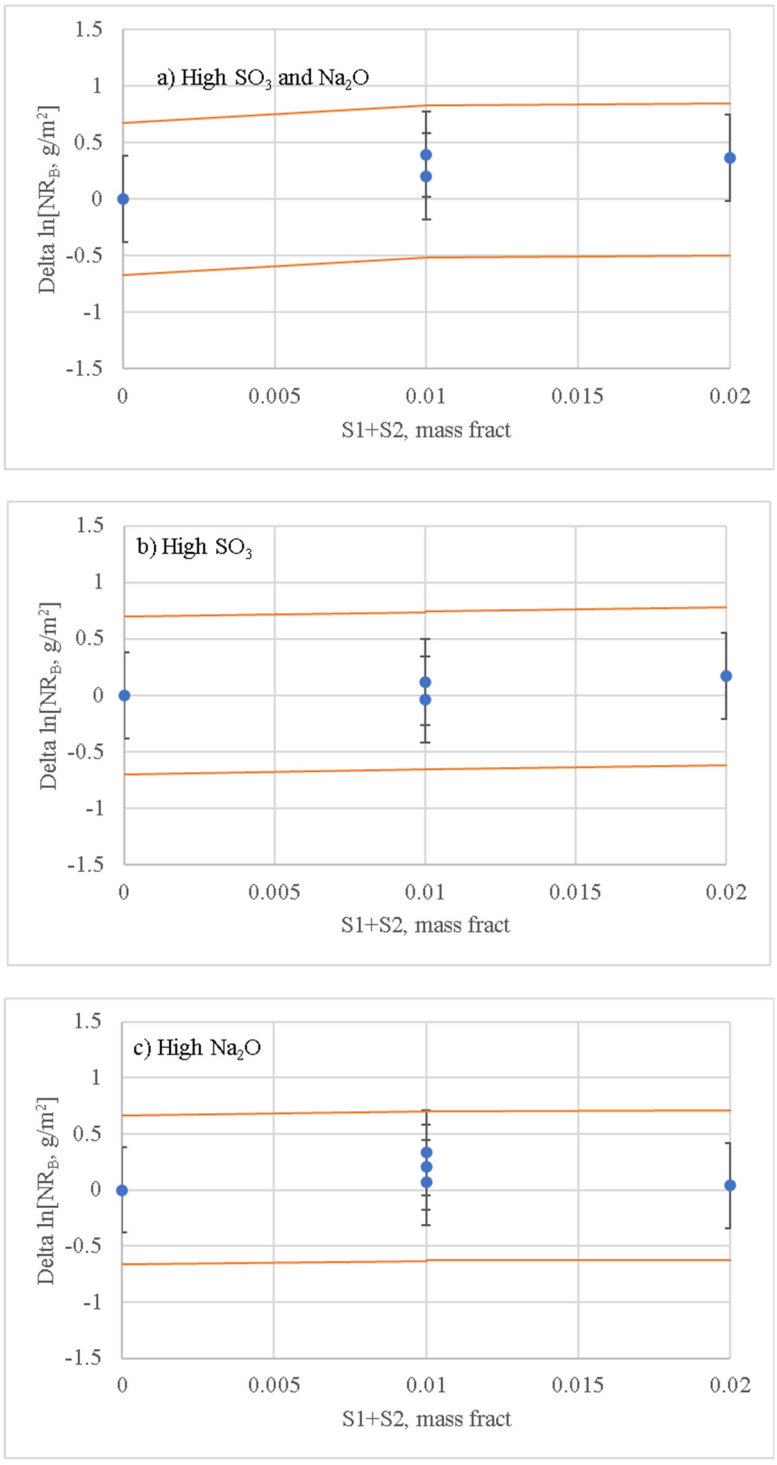

Figure 3.5. Difference in Response of Normalized Release of Boron versus Spike Concentrations for EMHQ Glasses Using the 2020 Model a) High Na + S glasses, b) High S glasses, and c) High Na glasses. Red Lines Represent 90% Prediction Intervals on Difference in Logarithm Normalized Boron Release Using the Vienna et al. 2020 Models.

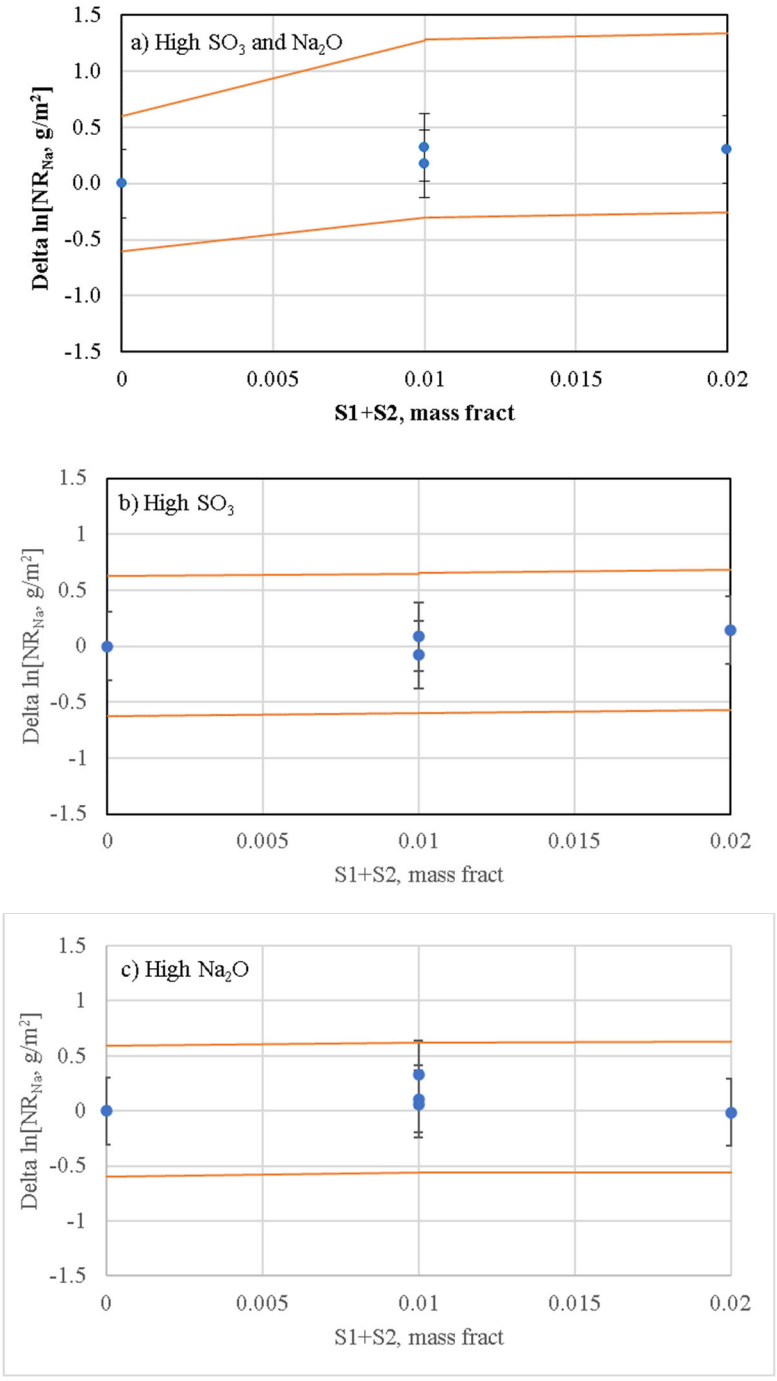

Figure 3.6. Difference in Response of Normalized Releases of Sodium versus Spike Concentrations for EMHQ Glasses Using the 2020 Model a) High Na + S glasses, b) High S glasses, and c) High Na glasses. Red Lines Represent 90% Prediction Intervals on Difference in Logarithm Normalized Sodium Release Using the Vienna et al. 2020 Models.

3.7 Vapor Hydration Test

This section presents and discusses the VHT results obtained using the methods discussed in Section 2.10. The VHT results for the glasses are listed in Table 3.8 and compared to the glasses from the previous test matrix composition they were designed to match.

Table 3.8. VHT Results from the EMHQ Glasses

Sample ID	Alteration Depth (μm)	Alteration Rate ($g/m^2/d$)	Comparison to Limit of 50 $g/m^2/d$
LAWALG-02	187.0	20.65	41%
EMHQ-LBE-01	333.1	35.61	71%
EMHQ-LBE-02	387.4	40.82	82%
EMHQ-LBE-03	301.7	31.79	64%
EMHQ-LBE-04B	50.0	5.03	10%
EMHQ-LBE-04	13.5	1.43	3%
EMHQ-LBE-05	61.5	6.38	13%
EMHQ-LBE-06	24.9	2.65	5%
LAWALG-10	33.5	3.69	7%
EMHQ-LBE-07	31.9	3.51	7%
EMHQ-LBE-08	27.4	2.98	6%
EMHQ-LBE-09	50.4	5.55	11%
EMHQ-LBE-10	48.3	5.29	11%

The Vienna et al. (2022) VHT model is in the form of a PQM logistic regression model on the binary VHT constraint pass/fail. The model is used to calculate the probability that a given glass will fail the VHT:

$$x_b = ln\left[\frac{P(g)}{1-P(g)}\right] = \sum_{i=1}^{q} b_i \cdot g_i \quad (3.7)$$

where x_b = the model predicted logit value for a given glass
g = the composition for a given glass, expanded to match the model form
b = the vector of model coefficients
$P(g)$ = the model predicted "score" or probability that the binary response for a given glass composition (g) is "success" (in this case, suggesting that the glass will fail the VHT)
q = the number of model parameters.

Note that the predicted probability or "score" for a given glass, $P(g)$, is calculated by inverting the logit transformation:

$$P(g) = \frac{e^{x_b}}{1+e^{x_b}} \quad (3.1)$$

As part of the development of the 2020 VHT model, the suggested threshold for predicted model "scores" when classifying a given glass as pass or fail with respect to the VHT was set at 0.19. Thus, a glass

having $P(g) < 0.19$ is predicted to pass the VHT; a glass having $P(g) \geq 0.19$ ($x_b \geq -1.45$) is predicted to fail the VHT.

Figure 3.7 illustrates results comparing VHT model predictions to measured ln[r_a, g m^{-2} d^{-1}]. This shows that all of these glasses passed the VHT and were predicted to do so by the 2020 model. P-values for t-tests comparing the measured ln[r_a] between the spiked glasses and their associated baseline were all below well above the typical threshold for significant differences of 0.05 or 0.10 (minimum being 0.594 for EMHQ-LBE-02), suggesting the differences in ln[r_a] caused by spiking are within measurement uncertainties.

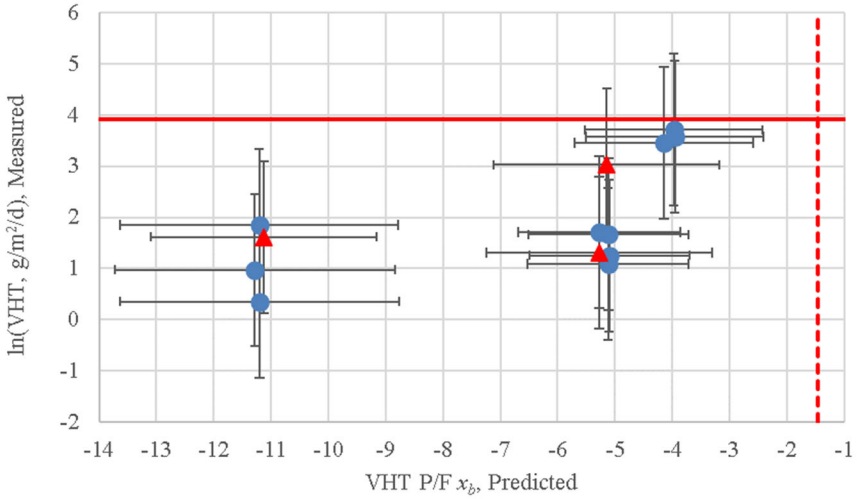

Figure 3.7. Predicted x_b versus Measured ln[r_a] for EMHQ Glasses Using the 2020 Model. Red Triangles Represent the Baseline Glasses, Blue Circles Represent Spiked Glasses, Solid red Line Represents the VHT Limit and Dotted Red Line Represents Prediction Limit)

3.8 Sulfur Solubility Results

Sulfur solubility (i.e., the saturated SO_3 concentrations) of each glass was determined experimentally by measuring SO_3 retention after saturation as discussed in Section 2.11. These results are shown in Table 3.9. The sulfur solubility was between 1.25 and 2.47 wt%.

All measurements for each oxide for each glass were averaged to determine a representative chemical composition for the SSM version of each glass. A sum of oxides was also computed for each glass based on the averaged, measured values. These values are shown in Appendix I. Comparisons of the overall analyzed glass compositions after normalization of the baseline and sulfur-saturated glass samples showed that after the sulfur-saturation, other major glass components only have negligible changes, except for Cl, F, and K_2O. The halides and K_2O can be extracted into the salt and halides may also volatilize from either the melt or the salt.

All measurements for each analyte for each wash solution were averaged to determine a representative chemical composition for each solution; these have been reported by Hsieh (2022b). These values are shown in Appendix I.

Table 3.9. Target and Saturated Concentrations of SO_3 in EMHQ Glasses

	SO_3 wt%		
Sample ID	Target Baseline	Measured Baseline	Sulfur-Saturated
LAWALG-02	1.56	1.37	2.12
EMHQ-LBE-01	1.54	1.38	2.10
EMHQ-LBE-02	1.54	1.41	2.14
EMHQ-LBE-03	1.53	1.40	2.12
EMHQ-LBE-04B	1.68	1.39	2.50
EMHQ-LBE-04	1.69	1.35	2.38
EMHQ-LBE-05	1.69	1.37	2.47
EMHQ-LBE-06	1.67	1.35	2.31
LAWALG-10	0.192	0.182	1.33
EMHQ-LBE-07	0.190	0.193	1.32
EMHQ-LBE-08	0.190	0.196	1.30
EMHQ-LBE-09	0.188	0.190	1.25
EMHQ-LBE-10	0.190	0.188	1.30

The 2020 model was used to predict the sulfur solubilities with measured values. It is a reduced PQM with a selected binary term for a total of 11 terms and the following generalized form:

$$w_{SO_3}^{Pred} = \sum_{i=1}^{q} s_i n_i + \text{selected}\left\{ \sum_{i=1}^{q} s_{ii} n_i^2 + \sum_{j=1}^{q-1} \sum_{k=j+1}^{q} s_{jk} n_j n_k \right\} \quad (3.2)$$

where $w_{SO_3}^{Pred}$ = the predicted SO_3 solubility (in wt%)
q = the number of components in the waste glass except for SO_3
n_i = normalized (after removing SO_3) mass fraction of the i-th component
s_i = coefficient of the i-th component
s_{ii} = coefficient for the i-th component squared
s_{jk} = coefficient for the j-th and k-th components cross-product

In this model, there are no squared terms (s_{ii}) and only one cross-product term (s_{jk}).

Figure 3. compares the differences in response of SO_3 solubility versus spike concentration for each group of glasses using the model recommended by Vienna et al. (2022). The SO_3 solubility of spiked glasses were within experimental uncertainty of the unspiked glass (with p-values for t-tests all ≥ 0.895).

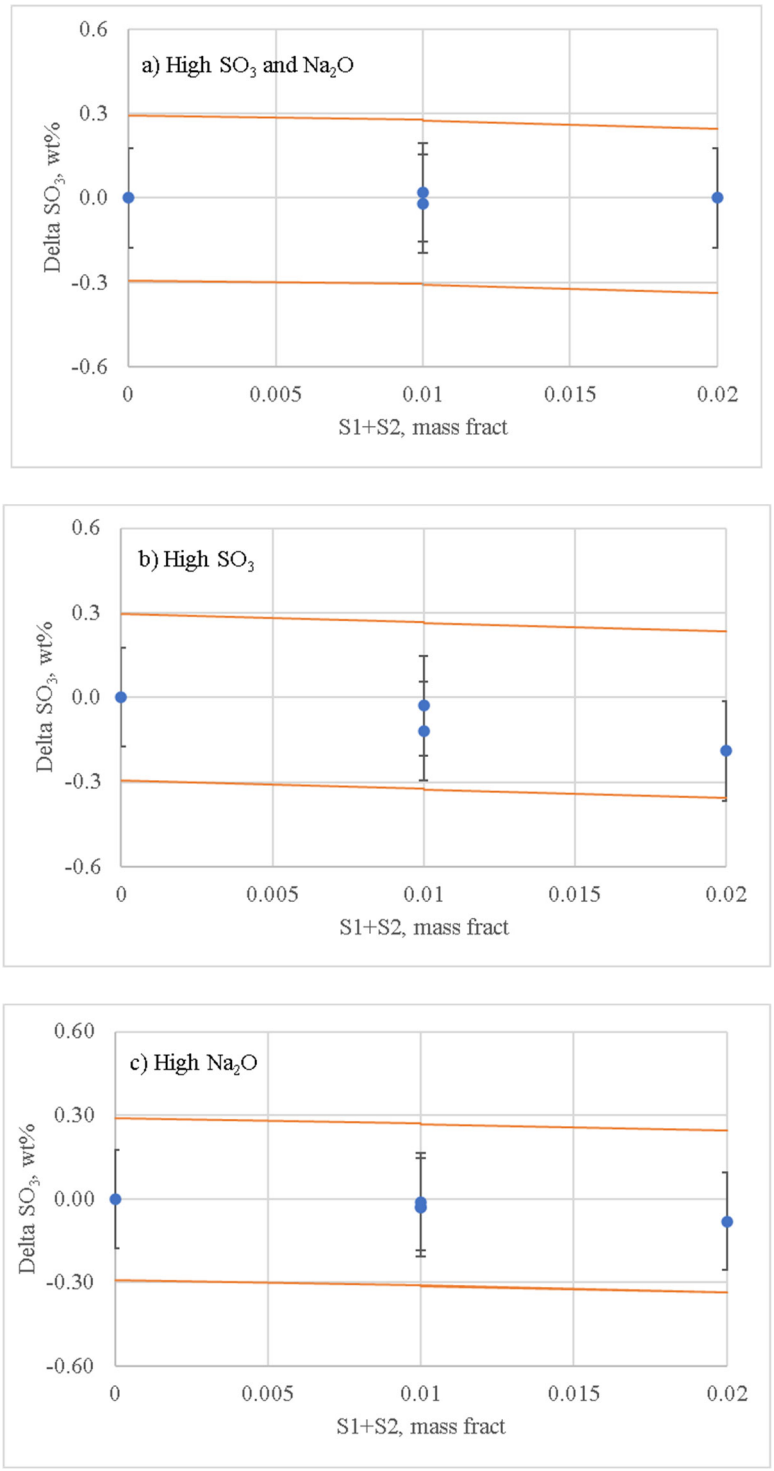

Figure 3.9. Difference in wt% SO_3 Solubility versus Spike Concentrations for EMHQ Glasses Using the 2020 Model a) High Na + S glasses, b) High S glasses, and c) High Na glasses. Red Lines Represent 90% Prediction Intervals on Difference in SO_3 Saturation Using the Vienna et al. 2020 Models.

4.0 Additional Data Evaluation

Forty glasses excluded from modeling glass properties based on component concentrations exceeding the model validity (MV) limits are listed in Table 4.1. Of those 40 glasses, 21 exceed the range for SOM (> 0.0033 to 0.016). The predicted properties with PI are compared to measured properties with confidence interval (CI) to evaluate the performance of current models for the extended composition regions with particular focus on expanding the SOM.

Table 4.1. List of Database Glasses Excluded from Modeling due to Model Validity Ranges with Which Properties Have Measured Data (Vienna et al. 2022)

#	GlassID	Reason (Comment)	PCT	VHT	Visc	EC	SO_3	K3
12	LAWA46	Others > 0.0033 (= 0.03103) mf (0.03 Ga_2O_3)	1	1	1	1	0	0
13	LAWA47	Others > 0.0033 (= 0.03103) mf (0.03 Y_2O_3)	1	1	1	1	0	0
14	LAWA48	Others > 0.0033 (= 0.03103) mf (0.03 La_2O_3)	1	1	1	1	0	0
20	LAWA64	Others > 0.0033 (= 0.07985) mf (0.079 SrO)	1	1	1	1	0	0
25	LAWA85	Others > 0.0033 (= 0.02096) mf (0.02 SrO)	1	0	1	1	0	0
26	LAWA86	Others > 0.0054 (= 0.02096) mf (0.02 SrO)	1	0	0	0	0	0
43	LAWABP1	Others ≥ 0.0033 (= 0.020001) mf (0.02 La_2O_3)	1	1	1	1	0	0
67	LAWC14	V_2O_5 > 0.0033 (= 0.057118) mf	1	0	1	1	0	0
80	LAWC25	K_2O > 0.06 (= 0.080927) mf	0	0	1	1	0	0
81	LAWC25S	K_2O > 0.07 (= 0.080670) mf	0	0	0	0	1	1
90	LAWA54	Others > 0.0044(= 0.078579) mf (0.078 SrO)	0	1	0	0	1	0
91	LAWA55	Others > 0.0044 (=0.078630) mf (0.078 BaO)	0	1	0	0	1	0
94	LAWA58	Others > 0.0044 (=0.049942) mf (0.049 Bi_2O_3)	0	1	0	0	1	0
95	LAWA59	Others > 0.0044 (=0.029906) mf (0.0295 Sb_2O_3)	0	1	0	0	1	0
96	LAWA61	Others > 0.0027 (0.024981) mf (0.0245 MnO)	0	0	0	0	1	0
97	LAWA62	Others > 0.0027 (0.030415) mf (0.03 CoO)	0	0	0	0	1	0
98	LAWA63	Others > 0.0027 (0.030430) mf (0.03 CuO)	0	0	0	0	1	0
99	LAWA65	MgO > 0.06 (0.060380) mf	0	0	0	0	1	0
106	LAWA72	Others > 0.0027 (0.078721) mf (0.0777 SrO)	0	0	0	0	1	0
115	LAWABPS	Others > 0.0027 (0.019928) mf (0.0197 La_2O_3)	0	0	0	0	1	0
118	LAWA91	Others > 0.0027 (0.078713) mf (0.0777 La_2O_3)	0	0	0	0	1	0
119	LAWA92	Others > 0.0027 (0.078709) mf (0.0777 Gd_2O_3)	0	0	0	0	1	0
167	LAWA120S1	K_2O > 0.07 (0.082850) mf	0	0	0	0	1	0
168	LAWA120S2	K_2O > 0.07 (0.082775) mf	0	0	0	0	1	0
169	LAWA121S1	K_2O > 0.07 (0.082841) mf	0	0	0	0	1	0
170	LAWA121S2	K_2O > 0.07 (0.082742) mf	0	0	0	0	1	0
450	DWV-G-51B	F > 0.0091 (= 0.013) mf	0	0	1	1	0	0
453	BWV-G-142B	F > 0.0091 (= 0.013006) mf	0	0	1	1	0	0
626	FWV-G-108B	F > 0.0091 (= 0.012001) mf	0	0	1	1	0	0
628	GWV-G-36D	F > 0.0091 (= 0.009306) mf	0	0	1	1	0	0
629	GWV-G-65A	F > 0.0091 (= 0.009303) mf	0	0	1	1	0	0
727	ORPLG9CrS4	Cr_2O_3 > 0.008 (0.009864) mf	0	0	0	0	1	0
739	ORPLA28	MgO>0.06 (=0.07015) mf	1	1	0	0	1	0
740	ORPLA29	MgO > 0.06 (0.100218) mf	1	1	0	0	1	0
742	ORPLA31	MgO>0.06 (=0.07015) mf	1	1	0	0	1	0
743	ORPLA32	MgO > 0.06 (0.100218) mf	1	1	0	0	1	0
k022	AY102D2-01	Others > 0.016 (= 0.0332) mf (0.02 MnO, 0.005 PbO)	0	0	0	0	0	1
k023	AY102D2-05	Others > 0.016 (= 0.0332) mf (0.02 MnO, 0.005 Pb)	0	0	0	0	0	1
k024	AY102D2-06	Others > 0.016 (= 0.0279) mf (0.017 MnO, 0.004 PbO)	0	0	0	0	0	1
k255	ORPLA20HV	V_2O_5 > 0.04 (= 0.05) mf	0	0	0	0	0	1
Total		40	18	18	13	13	22	4

Figure 4.1 shows an example predicted versus measured plot with measurement CIs and prediction PIs depicted for several hypothetical glasses. The figure also includes confidence rectangles for two hypothetical glasses; one confidence rectangle intersects the 45° line, the other does not. Again, for model extrapolation performance purposes, if any part of a given confidence rectangle intercepts the 45° line, then the measured and predicted values are in agreement for the corresponding glass from the set.

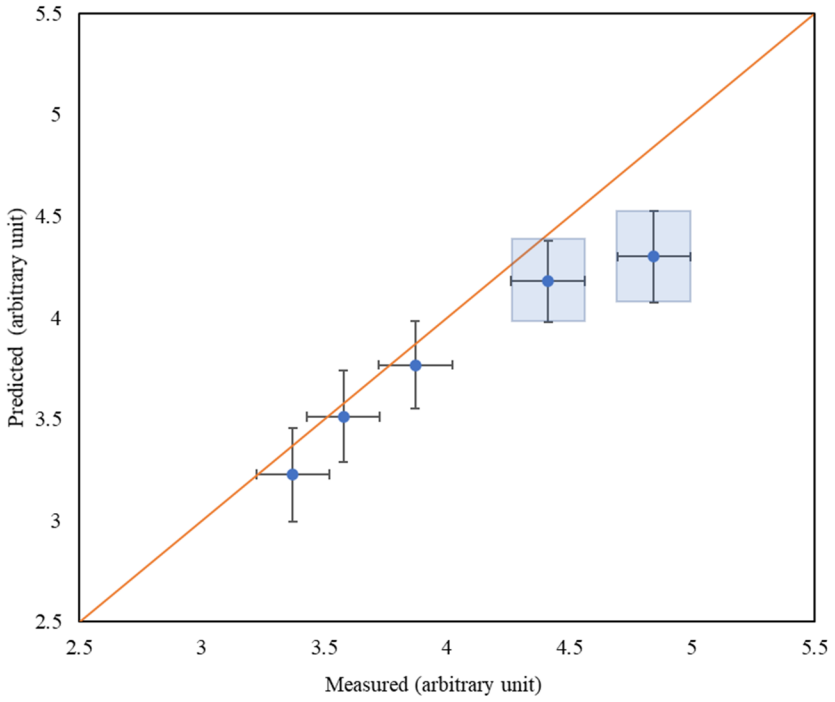

Figure 4.1. Visualization of the 90% Probability Area Represented by the Blue Shaded Rectangular Shapes

A different approach was used to evaluate the VHT response model because it was a logit function (x_b) of probability to pass or fail the VHT limit. For VHT response the predicted x_b with PI is plotted versus the measured $\ln[r_a]$ with CI. The plot is divided into quadrants using the prediction pass threshold of $x_b \leq -1.45$ and the measured contract requirement of $\ln[r_a] \leq 3.91$ ($\ln[g/m^2/d]$). Points with confidence rectangles intercepting the appropriate quadrant represent adequate model performance while points located in the appropriate quadrant represent good model performance.

For these analyses, 90% confidence is assumed to be adequate.

4.1 Viscosity and Electrical Conductivity

A total of 13 glasses were excluded from viscosity and EC model fitting for being outside of the MV limits (Tables 5.1 and 6.1 in Vienna et al. 2022). Six of these glasses were excluded due to SOM > 0.0033. The predicted vs measured logarithm viscosity plot is given in Figure 4.2. Twelve of the 13 datapoints have confidence rectangles intersecting the 45° line. The exception being LAWA64 containing 7.9 wt% SrO. The two glasses with elevated SrO (LAWA64 and LAWA85) are shown as open blue circles on the plot. Both are over predicted suggesting that the model predicts “others” increase viscosity more than SrO does by a factor of roughly 11.6. The differences in component effects slopes between CaO and Others and between MgO and Others for the logarithm viscosity model (in Table 9.3 of Vienna et al. 2022) are 16.1 and 11.5, respectively. This suggests that the viscosity of high SrO LAW

glasses can be accomplished by adding SrO to MgO (on an equal mass basis) rather than including it in the Others pseudo component.

The predicted vs measured logarithm EC plot is given in Figure 4.3. All 13 datapoints have confidence rectangles intersecting the 45° line.

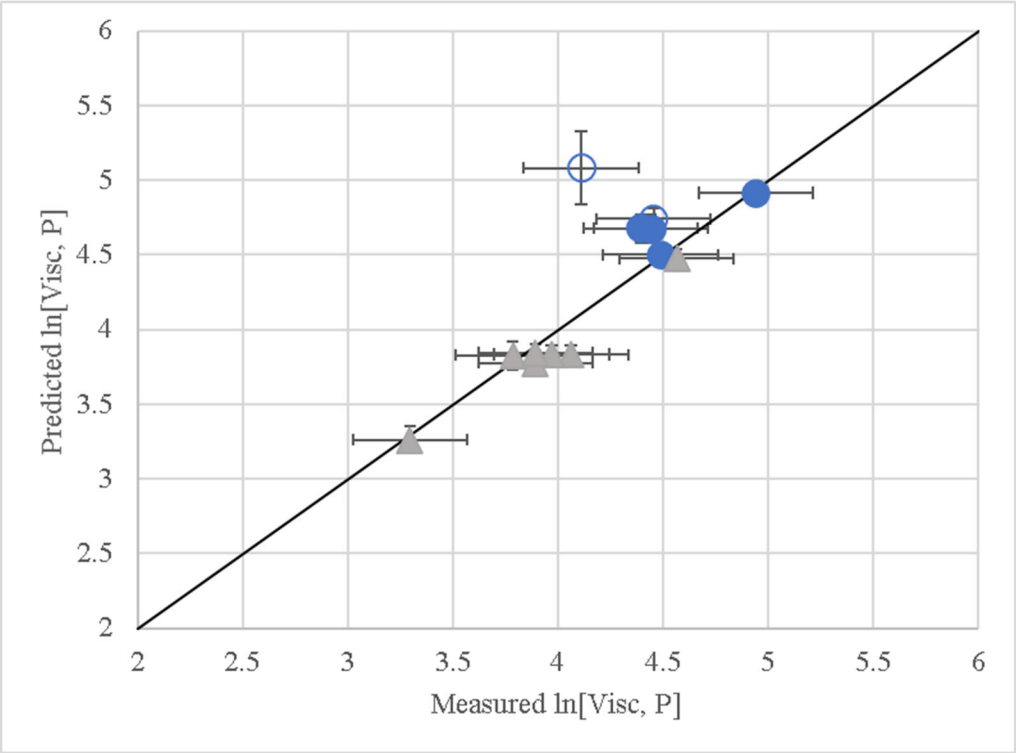

Figure 4.2. Predicted versus Measured ln[η_{1150}, P] of Database Glasses outside of Current MV Limits. Blue Circles Represent High SOM Data and Grey Triangles Represent Other Glasses.

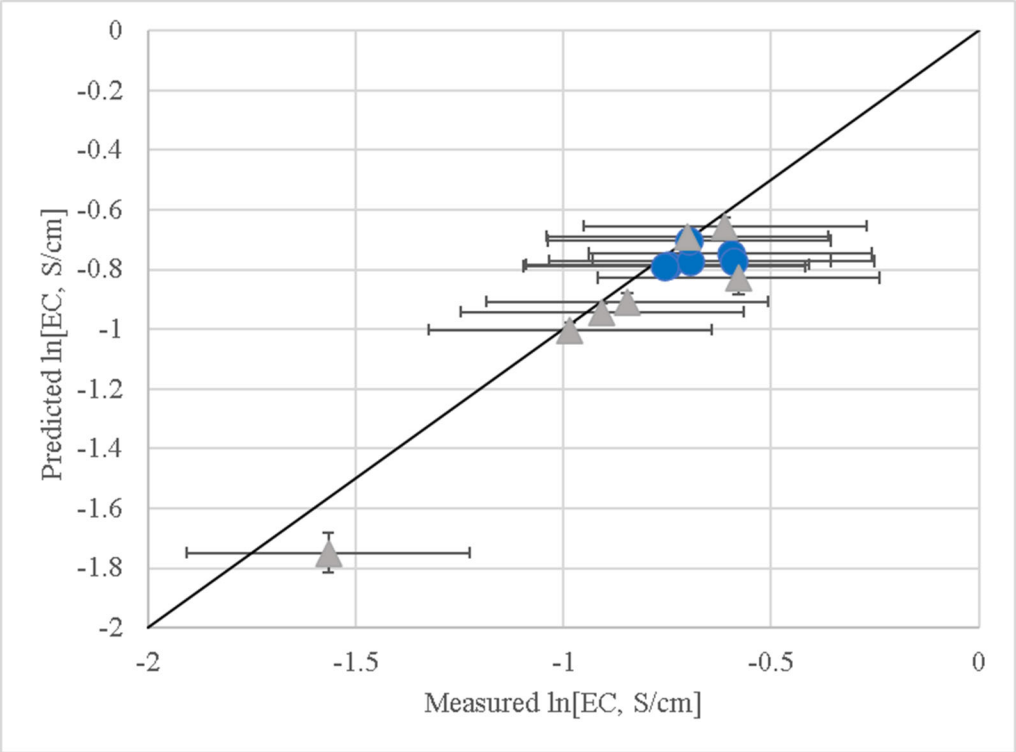

Figure 4.3. Predicted versus Measured ln[EC, S/cm] of Database Glasses outside of Current MV Limits. Blue Circles Represent High SOM Data and Grey Triangles Represent Other Glasses.

4.2 Product Consistency Test

A total of 18 glasses were excluded from PCT model fitting for being outside of the MV limits (Tables 3.1 in Vienna et al. 2022). One of those glasses (LAWC14) was also excluded from ln[NR_{Na}] response modeling for significant incongruence. Seven of these glasses were excluded due to SOM > 0.0054. The predicted vs measured ln[NR_B] and ln[NR_{Na}] plots are given in Figure 4.4 and Figure 4.5, respectively. The confidence rectangles intersecting the 45° line for all but the highest MgO concentration glasses (ORPLA29 and ORPLA32 with 10.0 wt% MgO). The four glasses with elevated MgO (also including ORPLA28 and ORPLA31 with 7.0 wt% MgO) are shown as open grey triangles on the plot. The residuals (predicted – measured) are shown in Figure 4.6. The PCT responses of all four high MgO glasses are under predicted suggesting that the model does not account for a nonlinear effect of MgO on PCT responses. These models will need to be refitted to allow for higher than 6 wt% MgO to be adequately predicted. As all other glasses are adequately represented by the models, SOM expansion is not excluded.

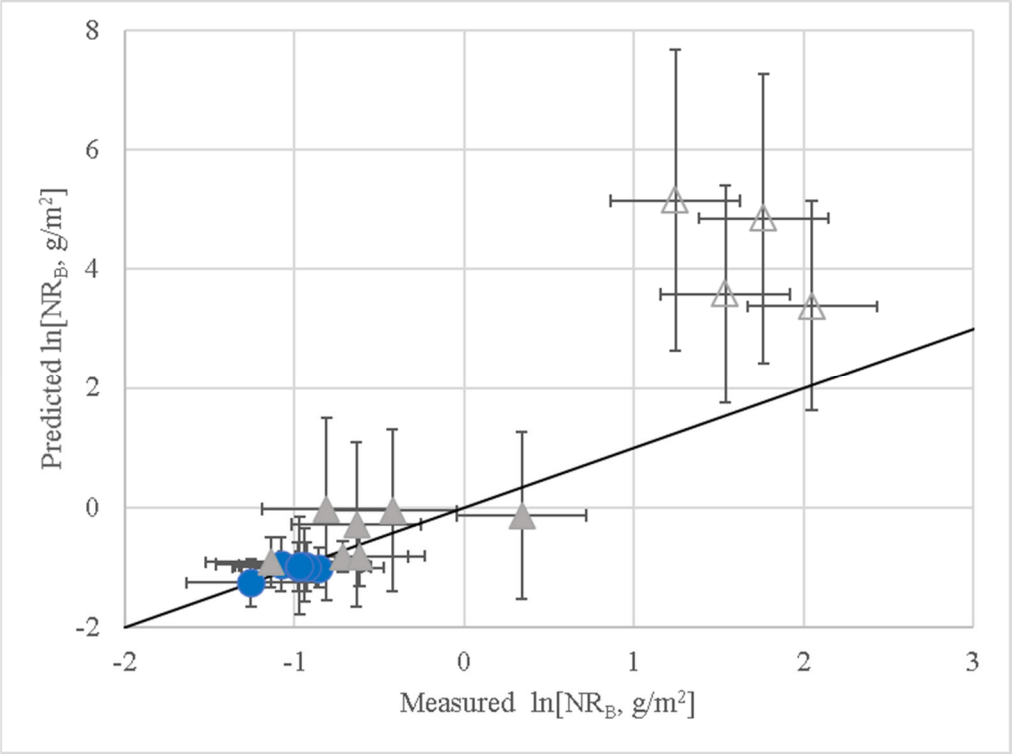

Figure 4.4. Predicted versus Measured ln[NR_B, g/m^2] of Database Glasses outside of Current MV Limits. Blue Circles Represent High SOM Data and Grey Triangles Represent Other Glasses.

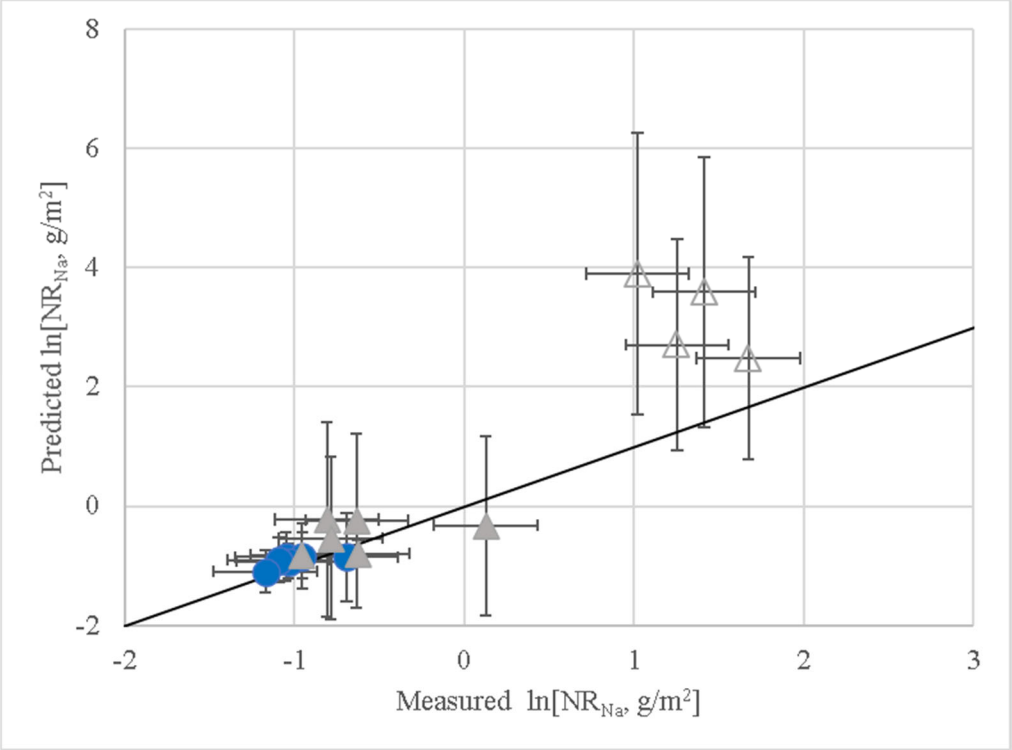

Figure 4.5. Predicted versus Measured ln[NR_{Na}, g/m^2] of Database Glasses outside of Current MV Limits. Blue Circles Represent High SOM Data and Grey Triangles Represent Other Glasses.

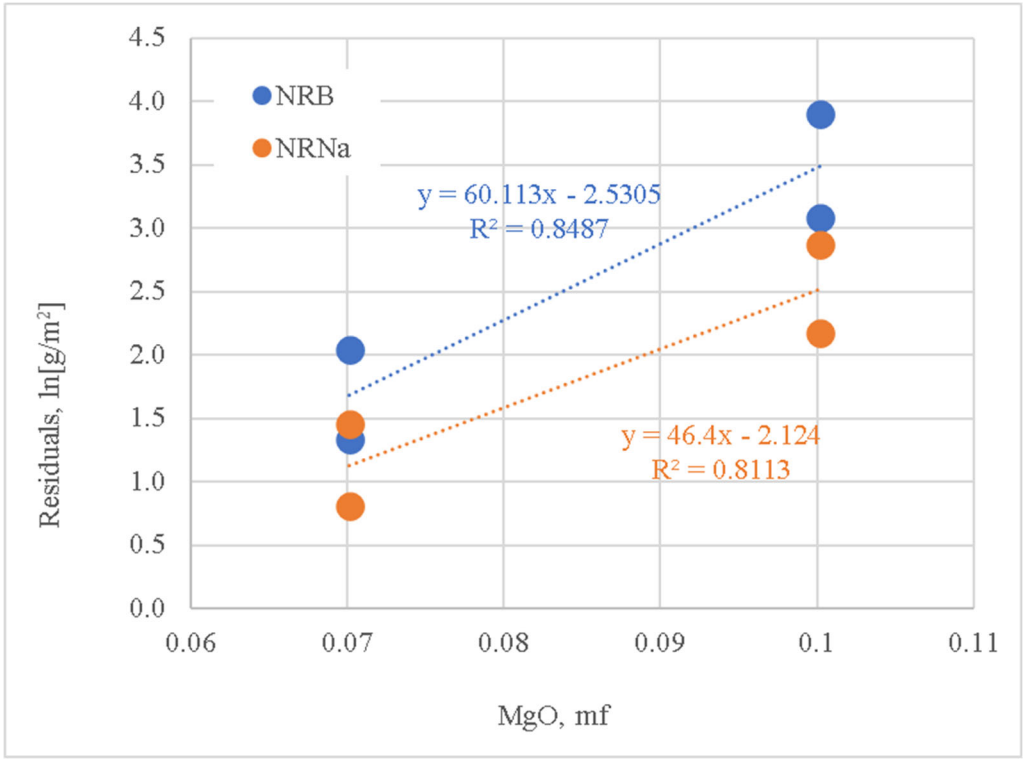

Figure 4.6. Residual ln[NR_α, g/m^2] vs MgO Concentrations

4.3 Vapor Hydration Test

A total of 18 glasses were excluded from VHT model fitting for being outside of the MV limits (Tables 4.1 in Vienna et al. 2022). Nine of these glasses were excluded due to SOM > 0.0044. The predicted x_b vs measured ln[r_a] plot is given in Figure 4.7. Four quadrants are formed by the predicted threshold of $x_b \leq -1.45$ and measured contract limit of ln[r_a] ≤ 3.91 (ln[g/m^2/d]).

I. Predicted to fail yet measured to pass
II. Predicted to fail and measured to fail
III. Predicted to pass and measured to pass
IV. Predicted to pass yet measured to fail

The datapoints for all but two glasses (GWV-G-65A and DWV-G-51B both with elevated F concentrations) fall within the appropriate quadrants (4 points in II and 12 points in III). The misclassified points fall in quadrant I however their confidence rectangles intersect quadrant III. The misclassification rate of 2:18 or 89% accuracy is consistent with model fit and model validation accuracy rates reported by Vienna et al. 2022 (Table 4.4) of 79.7% and 80.8%, respectively.

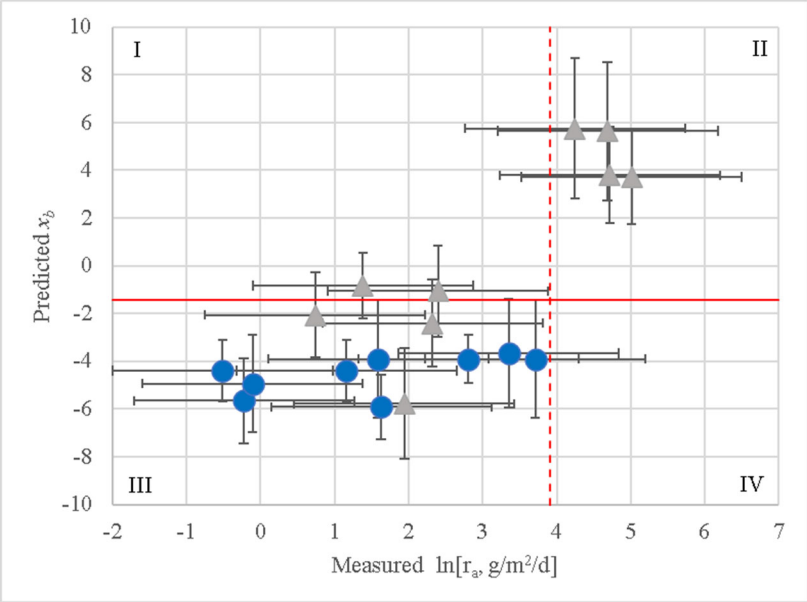

Figure 4.7. Predicted x_b vs Measured ln[r_a, g/m^2/d] of Database Glasses outside of Current MV Limits. Blue Circles Represent High SOM Data and Grey Triangles Represent Other Glasses.

4.4 SO_3 Solubility

A total of 22 glasses were excluded from SO_3 solubility model fitting for being outside of the MV limits (Tables 7.1 in Vienna et al. 2022). Eleven of these glasses were excluded due to SOM > 0.0027. The predicted vs measured SO_3 solubility plot is given in Figure 4.8. Eighteen of the 22 datapoints have confidence rectangles intersecting the 45° line. The exceptions being: ORPLA29 (with 10.0 wt% MgO), LAWA121S1 (with 8.29 wt% K_2O), LAWA55 (with 7.8 wt% BaO), and LAWA54 (with 7.8 wt% SrO). The two glasses with high concentrations of SOM are underpredicted by the model suggesting the model is conservative. This is not surprising since the effects of BaO and SrO on sulfur solubility are expected to be higher than the Others pseudo-component.

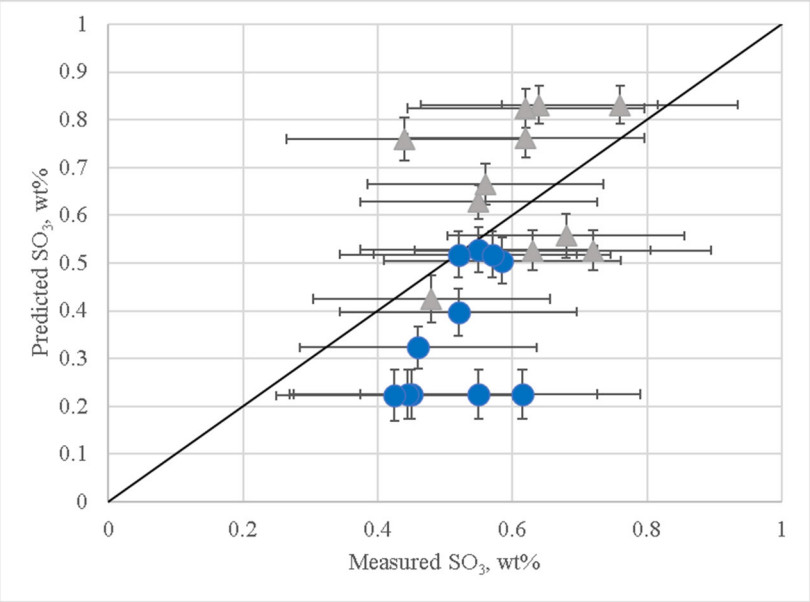

Figure 4.8. Predicted versus Measured SO_3 Solubility of Database Glasses outside of Current MV Limits. Blue Circles Represent High SOM Data and Grey Triangles Represent Other Glasses.

4.5 K-3 Refractory Neck Corrosion

A total of 4 glasses were excluded from Monofrax® K-3 refractory neck corrosion (logarithm of neck corrosion depth in inches) model fitting for being outside of the MV limits (Tables 8.1 in Vienna et al. 2022). Three of these glasses were excluded due to Others > 0.016. The predicted vs measured ln[K3, in] plot is given in Figure 4.8. Half (2) of the datapoints have confidence rectangles intersecting the 45° line. The exceptions being: AY102D2-05 (with 2 wt% MnO and 0.5 wt% PbO) and ORPLA20HV (with 5.71 wt% V_2O_5). The high SOM glass with the confidence rectangle not intersecting the 45° line was over predicted suggesting a conservative response. It should be noted that Vienna et al. (2022) concluded that the current K-3 model is not based on sufficient data to be used in LAW glass formulation and will need to be revised once additional data become available.

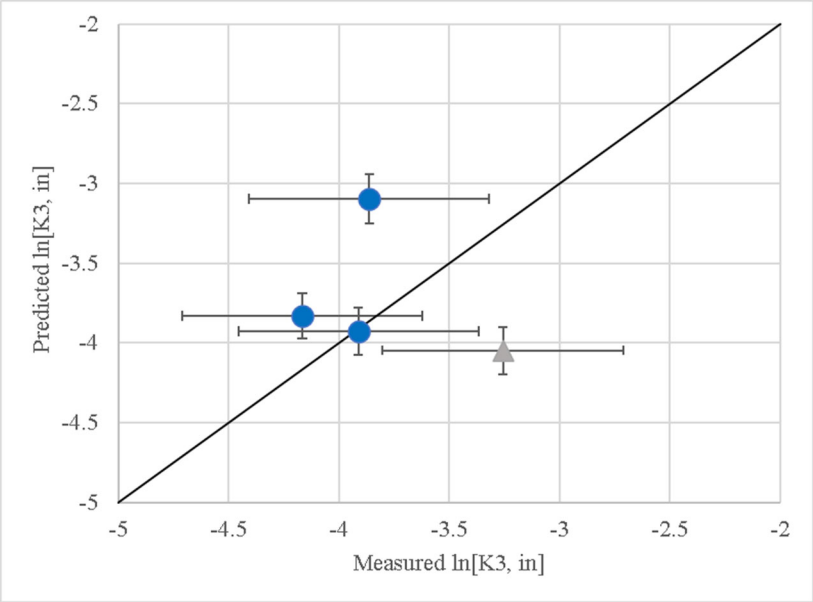

Figure 4.9. Predicted versus Measured K-3 Refractory Corrosion of Database Glasses outside of Current MV Limits. Blue Circles Represent High SOM Data and Grey Triangles Represent Other Glasses.

5.0 Discussion and Recommendations

This report presented the glass compositions and glass property data of the expanded minor component concentrations. These results can be used to establish a model validity boundary for SOM pseudo-component for Hanford LAW glass property-composition models reported by Vienna et al. (2022).

Three representative baseline glasses, previously formulated and tested, were tested with different concentrations of two representative spike compositions containing 17 groups of minor components. Concentrations up to a total of 2 wt% of combined minor component spikes were evaluated using ten new glasses based on the three original baseline formulations.

The following properties were measured and evaluated against the current model predictions: crystal formation after CCC, isothermal crystallinity as a function of temperature, density, viscosity, EC, PCT, VHT, and sulfur solubility.

The XRD scans of CCC glass samples did not identify any crystals present for any of the 10 glasses. The baseline compositions that the spiked glasses were designed to match did not have any crystallization either, indicating that the element spikes present in these glasses did not change the CCC crystallization properties of the glass.

The isothermal CF measurements of the glass showed that only four glasses had crystals identified in the XRD analysis when treated at both 950 °C for 24 ± 1 h and 850 °C for 48 ± 2 h. The glasses with crystals contained silicates of either sodium form or zirconium and sodium form or nasicon. The total crystallinity ranged from ~0. 50 to ~7.6 vol%. When compared to the baseline glasses, the EMHQ glasses contained more crystals in the spiked glasses with 2 wt% spike components. However, when crystals were seen in the baseline glasses, they were the same form as seen in the spiked glasses, being Zr-containing silicates. This indicates that the spikes may be pushing the solubility limit of these elements.

The measured viscosity and electrical conductivity at 1150 °C, PCT normalized sodium and boron releases, and VHT alteration rate of the spiked glasses were all found to be within experimental uncertainty of the associated unspiked baseline glasses. All of the differences in property responses were found to be within the 90% prediction intervals, suggesting the models accurately predict the effect of spiking on all modelled properties. These results strongly suggest that an expansion of SOM component concentration range to 2 wt% is justified.

To confirm this suggestion the data that were removed from model fitting due to higher concentrations of SOM were also evaluated. For each property, each of the glasses excluded due to high concentration of SOM (≥2 wt%, depending on the property) were found to match prediction within 90% confidence. That is, the 90% confidence rectangle defined by the measurement uncertainty range and the prediction interval, crossed the 45° line. This result further justifies an expansion of the SOM component concentration range to 2 wt% and above.

Based on these results, we recommend increasing the validity range of SOM to 2 wt% for the Vienna et al. (2022) LAW glass property models.

6.0 References

10 CFR 830, Subpart A, *Quality Assurance Requirements*. Code of Federal Regulations.

ASTM C1663, *Standard Test Method for Measuring Waste Glass or Glass Ceramic Durability by Vapor Hydration Test*. ASTM International, West Conshohocken, PA.

ASTM C1285, *Standard Test Methods for Determining Chemical Durability of Nuclear, Hazardous, and Mixed Waste Glasses and Multiphase Glass Ceramics: The Product Consistency Test (PCT)*. ASTM International, West Conshohocken, PA.

ASTM C1720, *Standard Test Method for Determining Liquidus Temperature of Immobilized Waste Glasses and Simulated Waste Glasses*. ASTM International, West Conshohocken, PA.

Crum JV, TB Edwards, RL Russell, PJ Workman, MJ Schweiger, RF Schumacher, DE Smith, DK Peeler, and JD Vienna. 2012. "DWPF Startup Frit Viscosity Measurement Round Robin Results." *Journal of the American Ceramic Society* 95(7):2196-2205.

DOE Order 414.1D, *Quality Assurance*. U.S. Department of Energy, Washington, D.C.

Ebert, WL and SF Wolfe. 1999. Round-robin Testing of a Reference Glass for Low-Activity Waste Forms. ANL-99/22, Argonne National Laboratory, Argonne, IL.

Gervasio, V, JD Vienna, SK Cooley, SM Baird, DL Bellofatto, BE Westman, DS Kim, X Lu, JB Lang, DA Cutforth, EL Rivers, and NA Lumetta. 2022. Experimental Verification of the Preliminary Enhanced LAW Glass Formulation Algorithm, Pacific Northwest National Laboratory, Richland, WA.

Hsieh M. 2022a. *Composition Measurements of the Environmental Management Headquarters (EMHQ) Low-Activity Waste (LAW) Glasses*. SRNL-STI-2021-00678, Rev. 0, Savannah River National Laboratory, Aiken, SC.

Hsieh M. 2022b. *Characterization of the Sulfur-Saturated Melt Versions of the EMHQ LAW Glasses*. SRNL-STI-2022-00003, Rev. 0, Savannah River National Laboratory, Aiken, SC.

Hsieh M. 2022c. *Product Consistency Test Results for the Environmental Management Headquarters (EMHQ) Low-Activity Waste (LAW) Glasses*. SRNL-STI-2021-00682, Rev. 0, Savannah River National Laboratory, Aiken, SC.

Jin T, DS Kim, LP Darnell, BL Weese, NL Canfield, M Bliss, MJ Schweiger, JD Vienna, and AA Kruger. 2019. "A Crucible Salt Saturation Method for Determining Sulfur Solubility in Glass Melt." *International Journal of Applied Glass Science* 10:92-102.

Kim DS, D Peeler, and P Hrma. 1995. "Effect of Crystallization on the Chemical Durability of Simulated Nuclear Waste Glasses." *Environmental Issues and Waste Management Technologies in the Ceramic and Nuclear Industries* 177-186.

Kim DS and JD Vienna. 2012. *Preliminary ILAW Formulation Algorithm Description*, 24590-LAW-RPT-RT-04-0003, Rev. 1, ORP-56321, River Protection Project, Hanford Tank Waste Treatment and Immobilization Plant, Richland, WA.

Lonergan CE, E Rivers, D Bellofatto, DS Kim, and JD Vienna. 2021a. *Crystallization Constraints for WTP LAW Operations: Assessment of CCC Impacts on VHT and PCT*. PNNL-31138, Rev. 0, EWG-RPT-032, Pacific Northwest National Laboratory, Richland, WA.

Lonergan CE, E Rivers, SM Baird, SE Sannoh, DS Kim, and JD Vienna. 2021b. *Glass Crystallization Constraints for WTP LAW Operations: Assessment of Isothermal Treatments on Crystal Formation*. PNNL-31334, Rev. 1, EWG-RPT-033, Rev. 1, Pacific Northwest National Laboratory, Richland, WA.

Lu, X, DS Kim, and JD Vienna. 2021. "Impacts of constraints and uncertainties on projected amount of Hanford low-activity waste glasses." *Journal of Nuclear Materials* (to be published).

Mellinger GB and JL Daniel. 1984. *Approved Reference and Testing Materials for Use in Nuclear Waste Management Research and Development Programs*. PNL-4955-2, Pacific Northwest Laboratory, Richland, WA.

Muller, IS, K Gilbo, I Joseph, and IL Pegg. 2014. Enhanced LAW Glass Property-Composition Models—Phase 1. VSL-13R2940-1, Vitreous State Laboratory, The Catholic University of America, Washington, DC.

NQA-1-2012, *Quality Assurance Requirements for Nuclear Facility Application*. American Society of Mechanical Engineers, New York, NY.

Piepel GF, SK Cooley, IS Muller, H Gan, I Joseph, and IL Pegg. 2007. ILAW PCT, VHT, Viscosity, and Electrical Conductivity Model Development. VSL-07R1230-1, Rev. 0, Vitreous State Laboratory, The Catholic University of America, Washington, D.C.

Shannon, R.D. 1976. "Revised Effective Ionic-Radii and Systematic Studies of Interatomic Distances in Halides and Chalcogenides," *Acta Crystallographica Section A*, **32**(1):751-767, DOI: 10.1107/S0567739476001551.

Smith GL. 1993. *Characterization of Analytical Reference Glass-1 (ARG-1)*. PNL-8992, Pacific Northwest Laboratory, Richland, WA.

Vienna, JD, P Hrma, A Jiricka, DE Smith, TH Lorier, IA Reamer, and RL Schultz. 2001. Hanford Immobilized LAW Product Acceptance Testing: Tanks Focus Area Results. PNNL-13744, Pacific Northwest National Laboratory, Richland, WA.

Vienna, JD, A Heredia-Langner, SK Cooley, E Holmes, DS Kim, and NA Lumetta. 2022. *Glass Property-Composition Models for Support of Hanford WTP LAW Facility Operation*. PNNL-30932, Rev. 2, Pacific Northwest National Laboratory, Richland, WA.

Appendix A – Morphology/Color of Each Quenched Glass

The photos in this appendix show each glass after melting in a Pt-alloy crucible twice at the specified melt temperature.

Figure A.1. Photo of Glass EMHQ-LBE-01 Morphology of Second Melt at 1150 °C for 1 h

Figure A.2. Photo of Glass EMHQ-LBE-02 Morphology of Second Melt at 1150 °C for 1 h

Figure A.3. Photo of Glass EMHQ-LBE-03 Morphology of Second Melt at 1150 °C for 1 h

Figure A.4. Photo of Glass EMHQ-LBE-04 Morphology of Second Melt at 1150 °C for 1 h

Figure A.5. Photo of Glass EMHQ-LBE-05 Morphology of Second Melt at 1150 °C for 1 h

Figure A.6. Photo of Glass EMHQ-LBE-06 Morphology of Second Melt at 1250 °C for 1 h

Figure A.7. Photo of Glass EMHQ-LBE-07 Morphology of Third Melt at 1250 °C for 1 h

Figure A.8. Photo of Glass EMHQ-LBE-08 Morphology of Third Melt at 1250 °C for 1 h

Figure A.9. Photo of Glass EMHQ-LBE-09 Morphology of Second Melt at 1250 °C for 1 h

Figure A.10. Photo of Glass EMHQ-LBE-10 Morphology of Third Melt at 1250 °C for 1 h

Appendix B – Analyzed LAW Boundary Expansion Glass Compositions

The data in this section compares the targeted glass compositions with the analyzed glass compositions and their percent differences. There appeared to be overall agreement in all samples, and the targeted compositions are adequate for use in future work to develop property-composition models.

Table B.1. Comparison of Targeted and Analyzed LAW Boundary Expansion Glass Compositions for Glass EMHQ-LBE-01

Glass ID	EMHQ-LBE-01		
Component	Targeted (wt%)	Analyzed (wt%)	% Diff
Al_2O_3	5.286	5.410	2.35
B_2O_3	12.717	11.800	-7.21
CaO	9.535	9.340	-2.05
Cl	0.122	0.104	-14.48
Cr_2O_3	0.056	0.048	-15.06
F	0.113	0.094	-16.89
Fe_2O_3	0.131	0.118	-9.83
K_2O	0.125	0.100	-20.31
Li_2O	0.000	<0.215	--
MgO	0.142	0.165	15.85
Na_2O	20.376	20.500	0.61
P_2O_5	0.301	0.274	-9.10
SiO_2	40.787	40.100	-1.68
SnO_2	0.000	<0.127	--
SO_3	1.524	1.380	-9.46
TiO_2	0.125	0.137	9.70
V_2O_5	3.957	3.990	0.84
ZnO	0.000	--	--
ZrO_2	3.699	3.690	-0.25
Sum	99.0	97.6	-1.42

Table B.2. Comparison of Targeted and Analyzed LAW Boundary Expansion Glass Compositions for Glass EMHQ-LBE-02

Glass ID	EMHQ-LBE-02		
Component	Targeted (wt%)	Analyzed (wt%)	% Diff
Al_2O_3	5.279	5.320	0.77
B_2O_3	12.701	11.800	-7.10
CaO	9.523	9.310	-2.24
Cl	0.121	0.101	-16.84
Cr_2O_3	0.056	0.048	-13.70
F	0.112	0.086	-23.63
Fe_2O_3	0.131	0.125	-4.36
K_2O	0.125	0.098	-21.49
Li_2O	0.000	<0.215	--
MgO	0.142	0.161	13.18
Na_2O	20.351	20.100	-1.23
P_2O_5	0.301	0.275	-8.66
SiO_2	40.736	39.800	-2.30
SnO_2	0.000	<0.127	--
SO_3	1.522	1.410	-7.38
TiO_2	0.125	0.111	-11.01
V_2O_5	3.952	3.990	0.96
ZnO	0.000	--	--
ZrO_2	3.695	3.630	-1.75
Sum	99.5	97.3	-2.25

Table B.3. Comparison of Targeted and Analyzed LAW Boundary Expansion Glass Compositions for Glass EMHQ-LBE-03

Glass ID	EMHQ-LBE-03		
Component	Targeted (wt%)	Analyzed (wt%)	% Diff
Al_2O_3	5.227	5.360	2.54
B_2O_3	12.575	11.700	-6.96
CaO	9.428	9.250	-1.89
Cl	0.121	0.107	-11.87
Cr_2O_3	0.056	0.048	-13.48
F	0.111	0.091	-17.53
Fe_2O_3	0.129	0.118	-8.81
K_2O	0.124	0.094	-23.68
Li_2O	0.000	<0.215	--
MgO	0.141	0.159	12.91
Na_2O	20.146	20.200	0.27
P_2O_5	0.297	0.271	-8.74
SiO_2	40.328	39.700	-1.56
SnO_2	0.000	<0.127	--
SO_3	1.507	1.400	-7.10
TiO_2	0.123	0.109	-11.73
V_2O_5	3.913	3.940	0.69
ZnO	0.000	--	--
ZrO_2	3.659	3.640	-0.51
Sum	98.6	97.0	-1.57

Table B.4. Comparison of Targeted and Analyzed LAW Boundary Expansion Glass Compositions for Glass EMHQ-LBE-04

Glass ID	EMHQ-LBE-04		
Component	Targeted (wt%)	Analyzed (wt%)	% Diff
Al_2O_3	3.490	3.580	2.57
B_2O_3	13.354	12.400	-7.15
CaO	12.072	11.600	-3.91
Cl	0.077	0.068	-12.10
Cr_2O_3	0.025	0.022	-11.39
F	0.094	0.071	-24.45
Fe_2O_3	0.129	0.120	-7.07
K_2O	0.087	0.056	-35.75
Li_2O	1.632	1.850	13.38
MgO	0.178	0.197	10.52
Na_2O	11.035	11.500	4.21
P_2O_5	0.156	0.144	--
SiO_2	48.967	47.800	-2.38
SnO_2	0.000	<0.127	--
SO_3	1.663	1.350	-18.84
TiO_2	0.090	0.075	-16.68
V_2O_5	3.977	4.020	1.09
ZnO	0.000	--	--
ZrO_2	1.971	1.960	-0.54
Sum	99.010	96.900	-2.13

Table B.5. Comparison of Targeted and Analyzed LAW Boundary Expansion Glass Compositions for Glass EMHQ-LBE-04B

Glass ID	EMHQ-LBE-04B		
Component	Targeted (wt%)	Analyzed (wt%)	% Diff
Al_2O_3	3.525	3.62	-2.62
B_2O_3	13.488	12.7	6.20
CaO	12.193	12.7	-4.00
Cl	0.078	0.0704	10.82
Cr_2O_3	0.025	<0.0365	--
F	0.095	0.0707	33.88
Fe_2O_3	0.130	0.119	9.59
K_2O	0.088	0.0592	47.89
Li_2O	1.648	1.96	-15.92
MgO	0.180	0.203	-11.32
Na_2O	11.145	11.6	-3.92
P_2O_5	0.158	<0.229	--
SiO_2	49.456	48.8	1.34
SnO_2	0.000	--	--
SO_3	1.680	1.39	20.87
TiO_2	0.090	0.0799	13.18
V_2O_5	4.016	4.27	-5.94
ZnO	0.000	--	--
ZrO_2	1.990	1.88	5.87
Sum	99.998	99.8	0.20

Table B.6. Comparison of Targeted and Analyzed LAW Boundary Expansion Glass Compositions for Glass EMHQ-LBE-05

Glass ID	EMHQ-LBE-05		
Component	Targeted (wt%)	Analyzed (wt%)	% Diff
Al_2O_3	3.486	3.510	0.69
B_2O_3	13.338	12.200	-8.53
CaO	12.057	11.600	-3.79
Cl	0.077	0.063	-18.47
Cr_2O_3	0.025	0.026	2.25
F	0.094	0.068	-27.14
Fe_2O_3	0.129	0.139	7.78
K_2O	0.087	0.054	-38.09
Li_2O	1.630	1.810	11.06
MgO	0.178	0.200	12.35
Na_2O	11.021	11.500	4.34
P_2O_5	0.156	0.146	-6.45
SiO_2	48.906	47.300	-3.28
SnO_2	0.000	<0.127	--
SO_3	1.661	1.370	-17.54
TiO_2	0.089	0.109	21.89
V_2O_5	3.972	4.020	1.22
ZnO	0.000	--	--
ZrO_2	1.968	2.000	1.61
Sum	99.543	96.800	-2.76

Table B.7. Comparison of Targeted and Analyzed LAW Boundary Expansion Glass Compositions for Glass EMHQ-LBE-06

Glass ID	EMHQ-LBE-06		
Component	Targeted (wt%)	Analyzed (wt%)	% Diff
Al_2O_3	3.451	3.520	2.01
B_2O_3	13.205	12.300	-6.86
CaO	11.937	11.500	-3.66
Cl	0.076	0.070	-8.47
Cr_2O_3	0.025	0.024	-4.46
F	0.093	0.071	-23.32
Fe_2O_3	0.128	0.128	0.25
K_2O	0.085	0.053	-37.78
Li_2O	1.614	1.810	12.14
MgO	0.176	0.198	12.34
Na_2O	10.911	11.300	3.56
P_2O_5	0.155	0.141	-8.85
SiO_2	48.418	47.600	-1.69
SnO_2	0.000	<0.127	--
SO_3	1.645	1.350	-17.93
TiO_2	0.089	0.075	-15.74
V_2O_5	3.931	3.980	1.25
ZnO	0.000	--	--
ZrO_2	1.949	1.940	-0.46
Sum	98.555	96.800	-1.78

Table B.8. Comparison of Targeted and Analyzed LAW Boundary Expansion Glass Compositions for Glass EMHQ-LBE-07

Glass ID	EMHQ-LBE-07		
Component	Targeted (wt%)	Analyzed (wt%)	% Diff
Al_2O_3	8.666	8.820	1.78
B_2O_3	8.610	8.020	-6.85
CaO	7.610	7.550	-0.78
Cl	0.083	0.066	-20.62
Cr_2O_3	0.170	0.153	-9.89
F	0.067	0.065	-3.08
Fe_2O_3	0.124	0.117	-5.95
K_2O	0.072	0.052	-27.19
Li_2O	0.000	<0.215	--
MgO	0.115	0.130	12.78
Na_2O	23.463	22.900	-2.40
P_2O_5	0.310	0.297	-4.18
SiO_2	39.241	38.600	-1.63
SnO_2	4.324	4.300	-0.56
SO_3	0.194	0.193	-0.45
TiO_2	0.139	0.133	-4.11
V_2O_5	0.000	<0.179	--
ZnO	0.000	--	--
ZrO_2	5.802	5.730	-1.24
Sum	98.997	97.500	-1.51

Table B.9. Comparison of Targeted and Analyzed LAW Boundary Expansion Glass Compositions for Glass EMHQ-LBE-08

Glass ID	EMHQ-LBE-08		
Component	Targeted (wt%)	Analyzed (wt%)	% Diff
Al_2O_3	8.655	8.860	2.37
B_2O_3	8.599	8.020	-6.73
CaO	7.600	7.450	-1.97
Cl	0.083	0.064	-23.18
Cr_2O_3	0.170	0.157	-7.41
F	0.067	0.062	-6.41
Fe_2O_3	0.124	0.131	5.43
K_2O	0.071	0.051	-28.08
Li_2O	0.000	<0.215	--
MgO	0.115	0.133	15.52
Na_2O	23.434	22.700	-3.13
P_2O_5	0.310	0.294	-5.03
SiO_2	39.192	38.900	-0.75
SnO_2	4.319	4.280	-0.90
SO_3	0.194	0.196	1.23
TiO_2	0.139	0.131	-5.44
V_2O_5	0.000	<0.179	--
ZnO	0.000	--	--
ZrO_2	5.794	5.690	-1.80
Sum	99.535	98.000	-1.54

Table B.10. Comparison of Targeted and Analyzed LAW Boundary Expansion Glass Compositions for Glass EMHQ-LBE-09

Glass ID	EMHQ-LBE-09		
Component	Targeted (wt%)	Analyzed (wt%)	% Diff
Al_2O_3	8.568	8.840	3.17
B_2O_3	8.512	7.940	-6.72
CaO	7.523	7.510	-0.18
Cl	0.083	0.069	-16.47
Cr_2O_3	0.168	0.153	-8.69
F	0.066	0.068	3.08
Fe_2O_3	0.123	0.107	-13.01
K_2O	0.071	0.052	-26.32
Li_2O	0.000	<0.215	--
MgO	0.114	0.128	12.32
Na_2O	23.199	22.600	-2.58
P_2O_5	0.305	0.289	-5.37
SiO_2	38.796	38.600	-0.51
SnO_2	4.275	4.270	-0.12
SO_3	0.191	0.190	-0.70
TiO_2	0.137	0.136	-0.84
V_2O_5	0.000	<0.179	--
ZnO	0.000	--	--
ZrO_2	5.736	5.720	-0.27
Sum	98.538	97.700	-0.85

Table B.11. Comparison of Targeted and Analyzed LAW Boundary Expansion Glass Compositions for Glass EMHQ-LBE-10

Glass ID	EMHQ-LBE-10		
Component	Targeted (wt%)	Analyzed (wt%)	% Diff
Al_2O_3	8.660	8.840	2.07
B_2O_3	8.604	7.970	-7.37
CaO	7.605	7.550	-0.72
Cl	0.083	0.066	-20.45
Cr_2O_3	0.170	0.153	-9.83
F	0.067	0.066	-0.77
Fe_2O_3	0.124	0.108	-13.13
K_2O	0.072	0.048	-33.44
Li_2O	0.000	<0.215	--
MgO	0.115	0.129	11.98
Na_2O	23.448	22.900	-2.34
P_2O_5	0.310	0.293	-5.41
SiO_2	39.216	38.600	-1.57
SnO_2	4.321	4.300	-0.49
SO_3	0.194	0.188	-2.96
TiO_2	0.139	0.134	-3.33
V_2O_5	0.000	<0.179	--
ZnO	0.000	--	--
ZrO_2	5.798	5.740	-1.00
Sum	99.265	97.700	-1.58

Appendix C – Container Centerline Cooling (CCC) Glass Photographs

This appendix contains photos of glasses after they were CCC treated beginning at the glass melting temperature of 1150 °C.

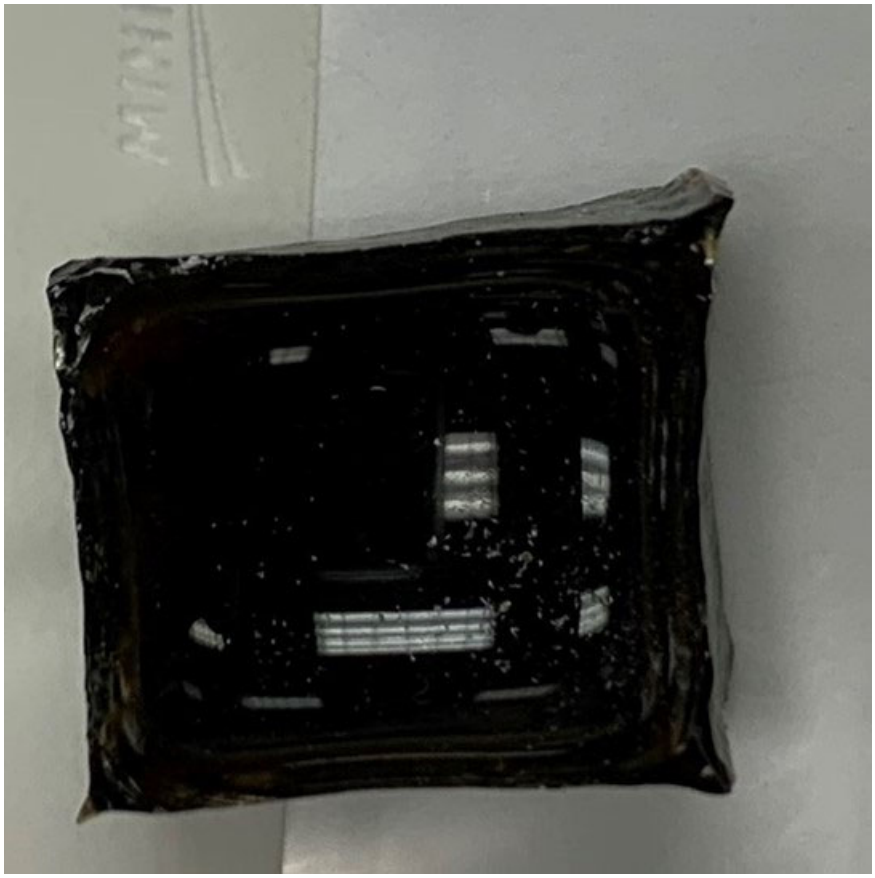

Figure C.1. Glass EMHQ-LBE-01 after CCC

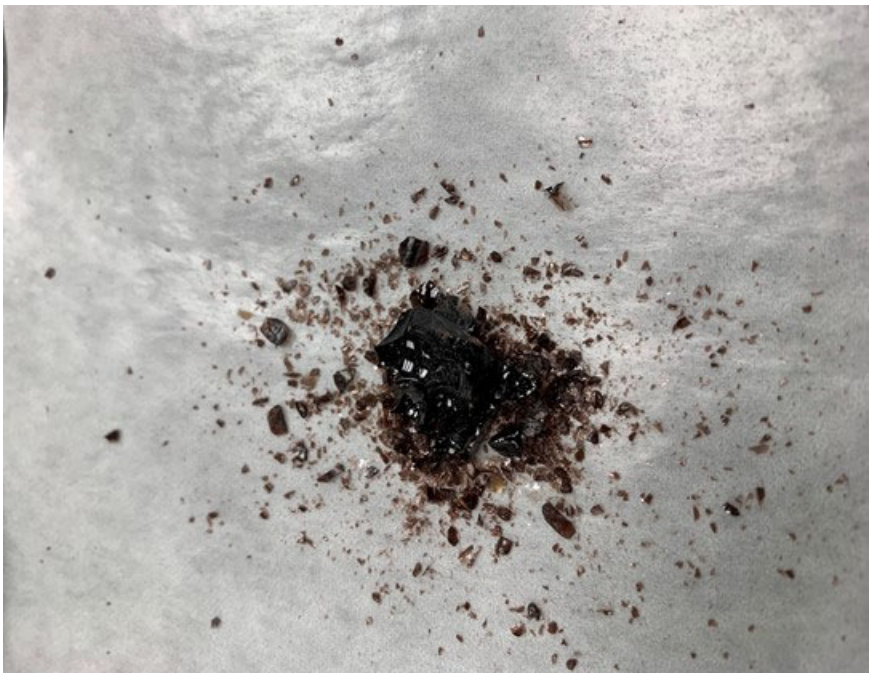

Figure C.2. Glass EMHQ-LBE-02 after CCC

Figure C.3. Glass EMHQ-LBE-03 after CCC

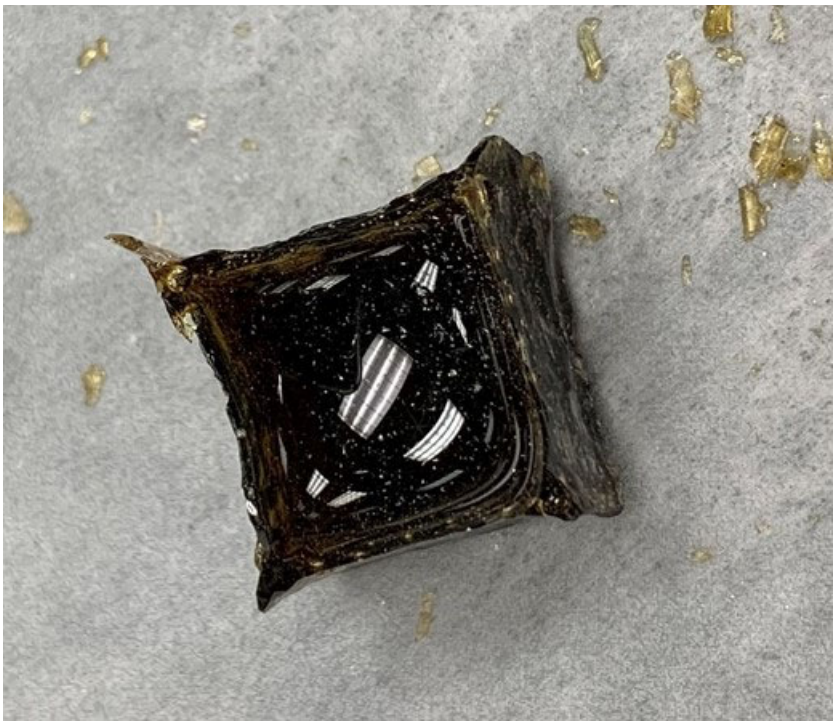

Figure C.4. Glass EMHQ-LBE-04 after CCC

Figure C.5. Glass EMHQ-LBE-05 after CCC

Figure C.6. Glass EMHQ-LBE-06 after CCC

Figure C.7. Glass EMHQ-LBE-07 after CCC

Figure C.8. Glass EMHQ-LBE-08 after CCC

Figure C.9. Glass EMHQ-LBE-09 after CCC

Figure C.10. Glass EMHQ-LBE-10 CCC

Appendix D – Viscosity Data

This appendix contains the measured viscosity data for each of the glasses in this matrix. The plots shown in this appendix are fitted to the Arrhenius equation:

$$\ln(\eta) = A + \frac{B}{T_K} \quad \text{(D.1)}$$

where A and B are independent of temperature and temperature (T_K) is in K (T(°C) + 273.15). If the plots showed curvature, they would be better fit to the Vogel- Fulcher-Tamman (VFT) model:

$$\ln(\eta) = E + \frac{F}{T_k - T_0} \quad \text{(D.2)}$$

where E, F, and T_0 are temperature independent and composition dependent coefficients, and T_K is the temperature in K (T(°C) + 273.15). The intent of the figures and Arrhenius equation fits shown in this appendix is mainly to assess trends of the data and provide some observations about whether there may be sufficient curvature in the data to consider VFT fits in the subsequent work that will decide between fitting the viscosity-temperature data to the Arrhenius or VFT equations. All the glasses in this matrix appear to have very good fits to the Arrhenius equation and do not show a need for fitting to the VFT model.

D.1 Glass EMHQ-LBE-01 Viscosity Data

Table D.1. Viscosity Data for Glass EMHQ-LBE-01

Measured Temp., °C	Viscosity, Pa-s	1/T x10000, K^{-1}	ln η, Pa-s
1150	2.857	7.027	1.050
1050	7.294	7.558	1.987
950	28.247	8.176	3.341
1150	2.827	7.027	1.039
1200	1.999	6.788	0.692
1150	2.801	7.027	1.030

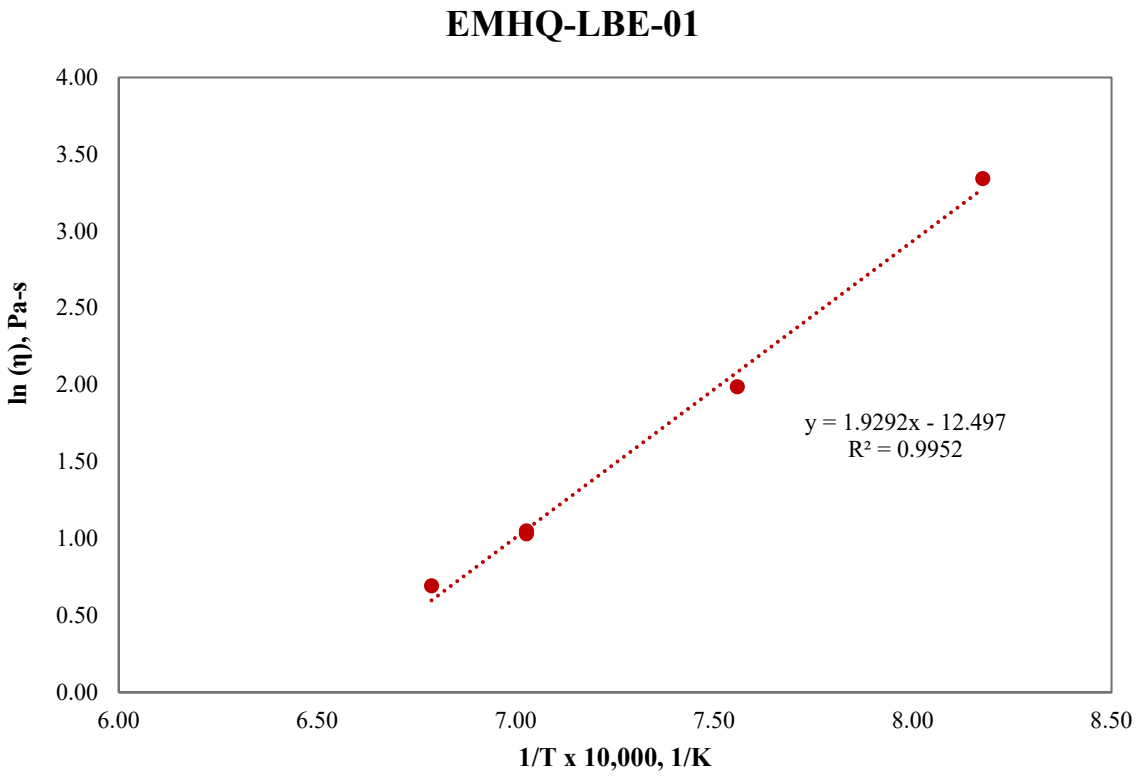

Figure D.1. Viscosity-Temperature Data and Arrhenius Equation Fit for Glass EMHQ-LBE-01

D.2 Glass EMHQ-LBE-02 Viscosity Data

Table D.2. Viscosity Data for Glass EMHQ-LBE-02

Measured Temp., °C	Viscosity, Pa-s	1/T x10000, K^{-1}	ln η, Pa-s
1150	3.009	7.027	1.101
1050	7.521	7.558	2.018
950	28.325	8.176	3.344
1150	2.883	7.027	1.059
1200	1.941	6.788	0.663
1150	2.939	7.027	1.078

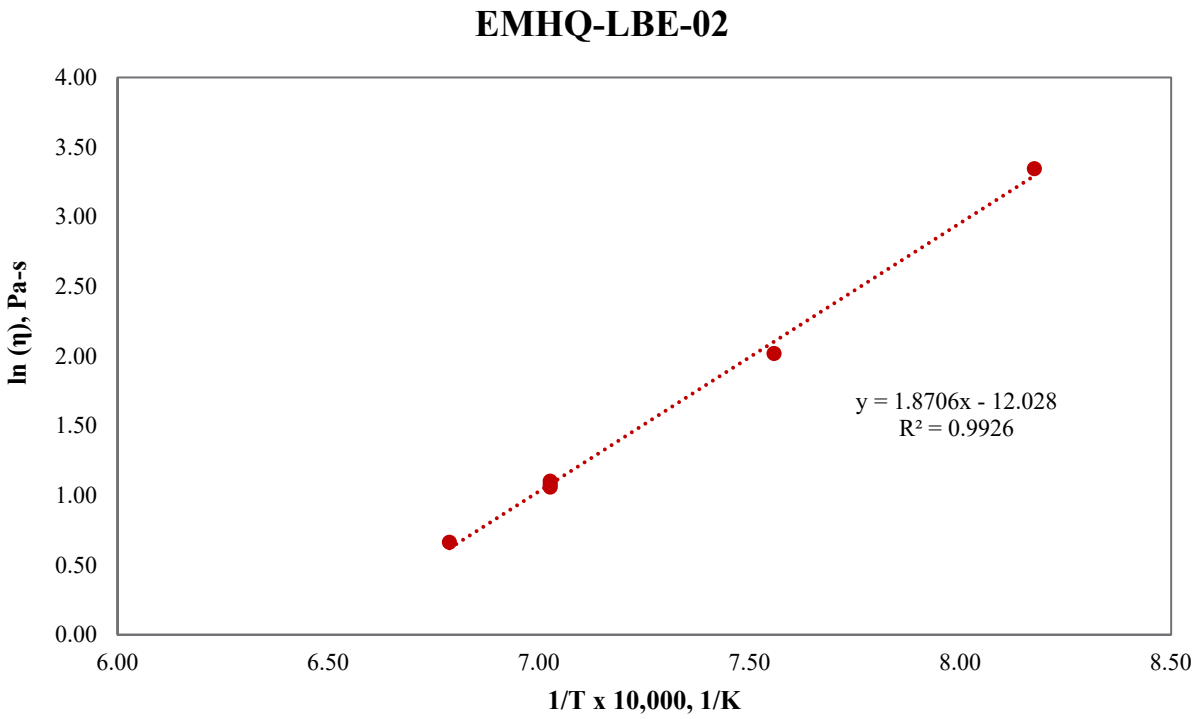

Figure D.2. Viscosity-Temperature Data and Arrhenius Equation Fit for Glass EMHQ-LBE-02

D.3 Glass EMHQ-LBE-03 Viscosity Data

Table D.3. Viscosity Data for Glass EMHQ-LBE-03

Measured Temp., °C	Viscosity, Pa-s	1/T x10000, K^{-1}	ln η, Pa-s
1150	2.797	7.027	1.028
1050	7.177	7.558	1.971
950	24.494	8.176	3.198
1150	2.666	7.027	0.981
1200	1.807	6.788	0.591
1150	2.710	7.027	0.997

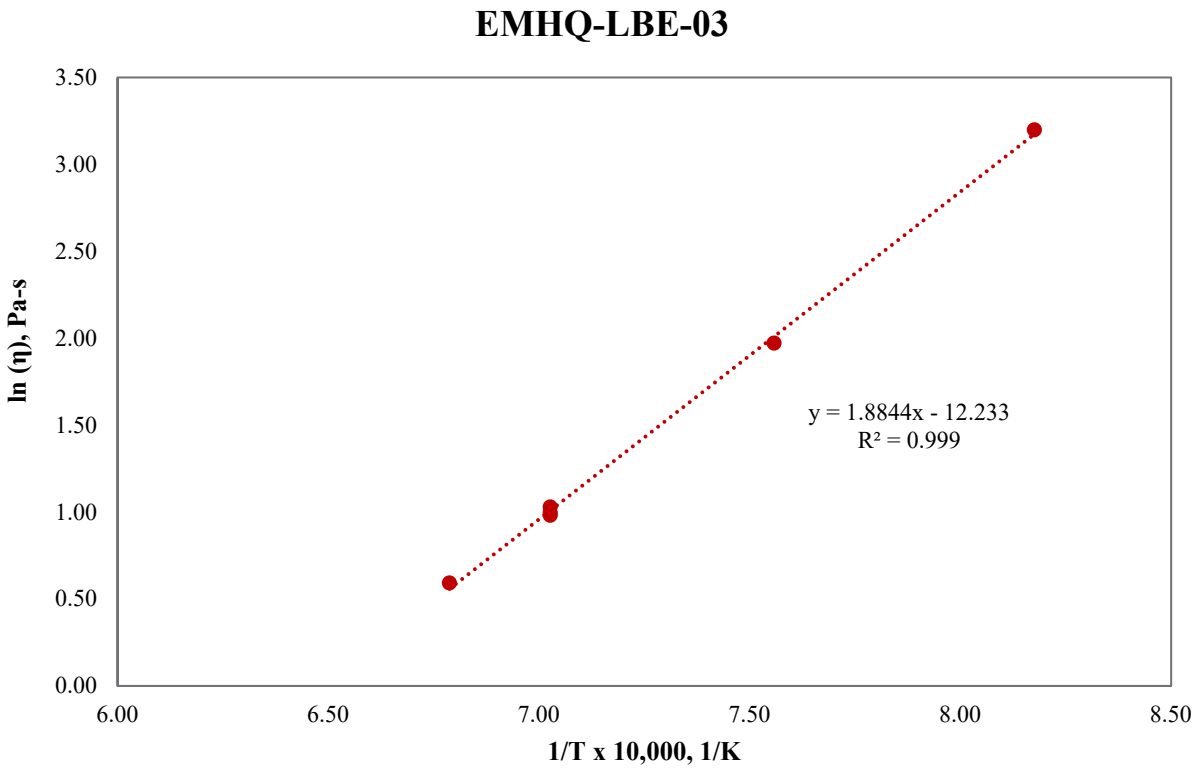

Figure D.3. Viscosity-Temperature Data and Arrhenius Equation Fit for Glass EMHQ-LBE-03

D.4 Glass EMHQ-LBE-04 Viscosity Data

Table D.4. Viscosity Data for Glass EMHQ-LBE-04

Measured Temp., °C	Viscosity, Pa-s	1/T x10000, K-1	ln η, Pa-s
1150	3.506	7.027	1.254
1050	8.888	7.558	2.185
950	33.221	8.176	3.503
1150	3.456	7.027	1.240
1200	2.125	6.735	0.754
1150	3.556	7.027	1.269

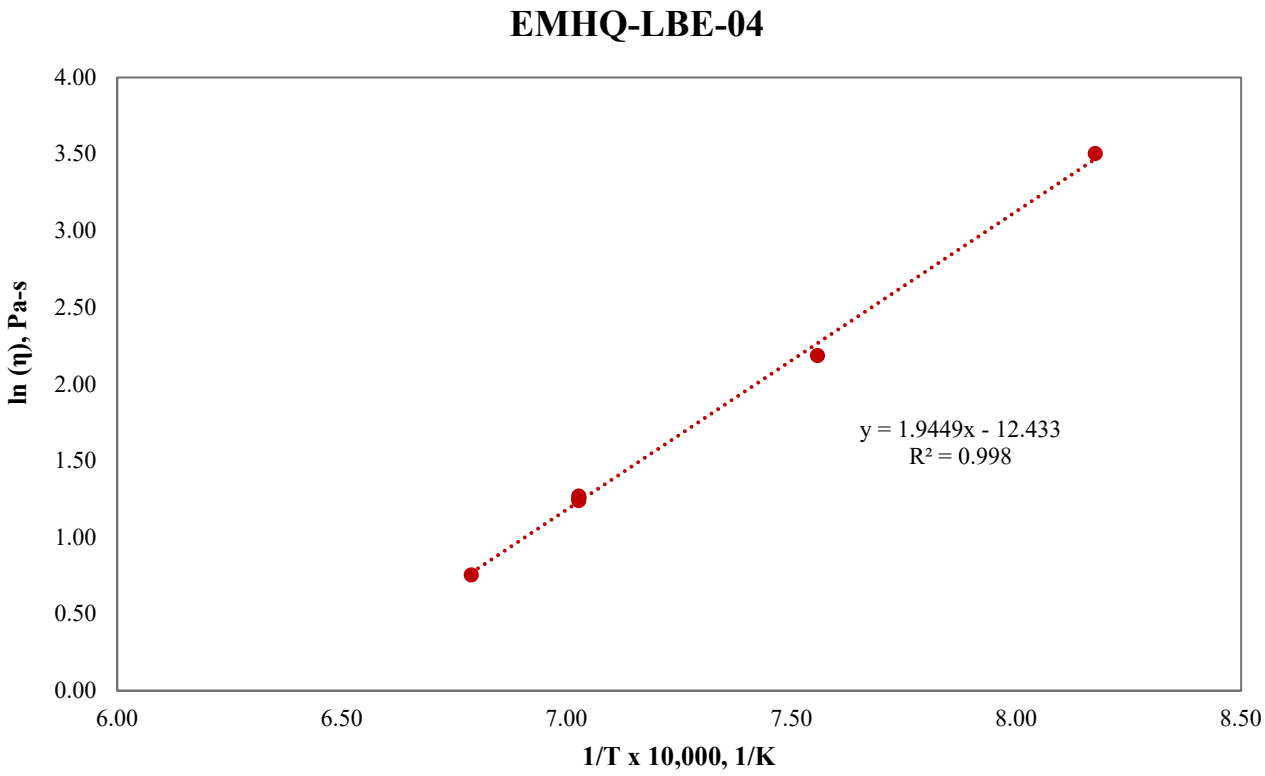

Figure D.4. Viscosity-Temperature Data and Arrhenius Equation Fit for Glass EMHQ-LBE-04

D.5 Glass EMHQ-LBE-04B Viscosity Data

Table D.5. Viscosity Data for Glass EMHQ-LBE-04B

Measured Temp., °C	Viscosity, Pa-s	1/T x10000, K^{-1}	ln η, Pa-s
1150	3.534	7.027	1.262
1050	8.963	7.558	2.193
950	33.318	8.176	3.506
1150	3.445	7.027	1.237
1212	2.135	6.788	0.758
1150	3.454	7.027	1.239

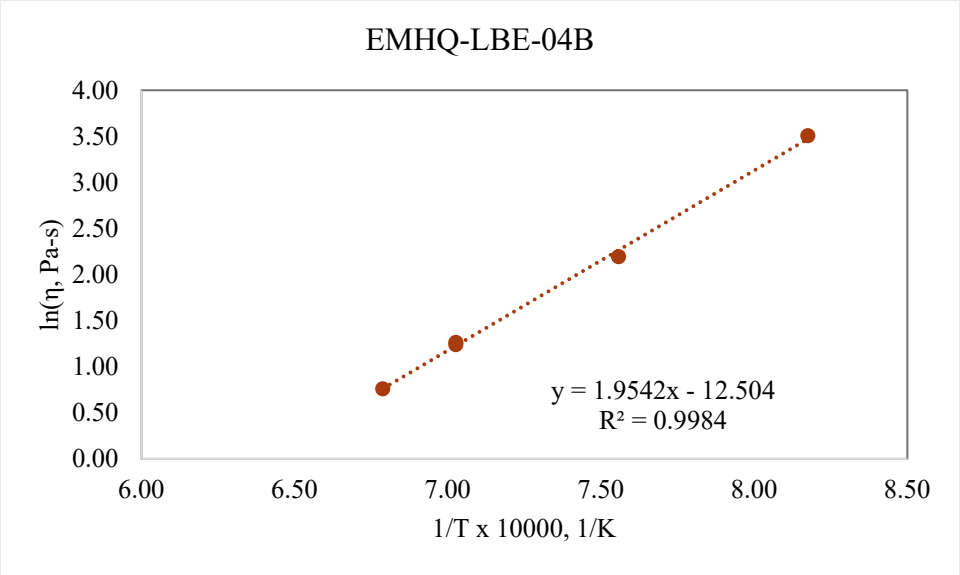

Figure D.5. Viscosity-Temperature Data and Arrhenius Equation Fit for Glass EMHQ-LBE-04B

D.6 Glass EMHQ-LBE-05 Viscosity Data

Table D.6. Viscosity Data for Glass EMHQ-LBE-05

Measured Temp., °C	Viscosity, Pa-s	1/T x10000, K^{-1}	ln η, Pa-s
1150	3.642	7.027	1.293
1050	9.096	7.558	2.208
950	33.656	8.176	3.516
1150	3.729	7.027	1.316
1211	2.282	6.737	0.825
1150	3.679	7.027	1.303

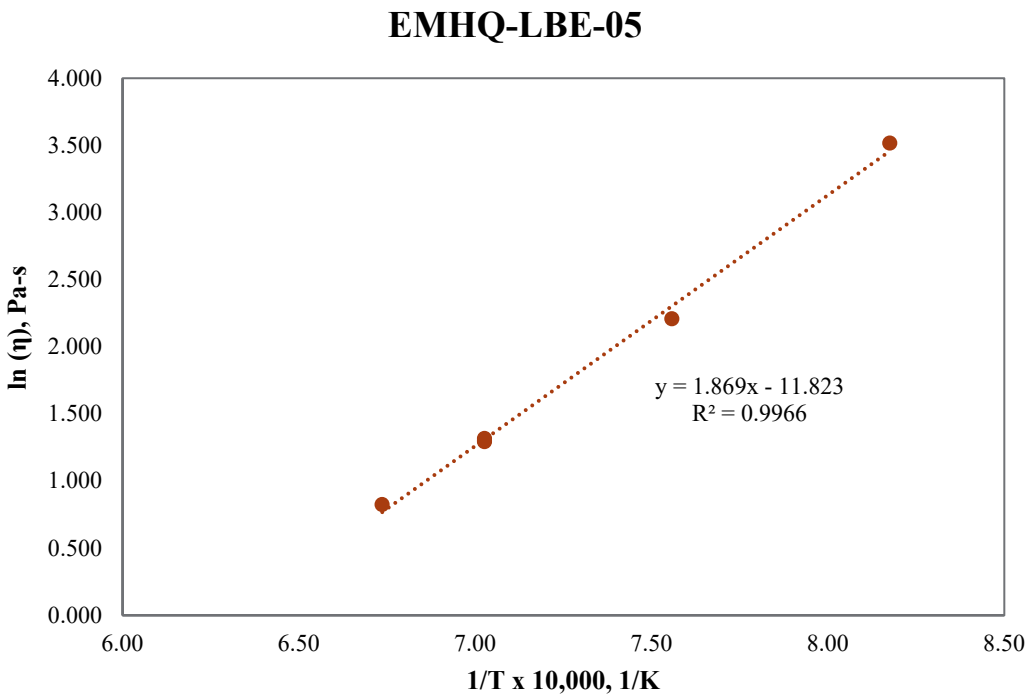

Figure D.6. Viscosity-Temperature Data and Arrhenius Equation Fit for Glass EMHQ-LBE-05

D.7 Glass EMHQ-LBE-06 Viscosity Data

Table D.7. Viscosity Data for Glass EMHQ-LBE-06

Measured Temp., °C	Viscosity, Pa-s	1/T x10000, K^{-1}	ln η, Pa-s
1150	3.364	7.027	1.213
1050	8.343	7.558	2.121
950	30.372	8.176	3.414
1150	3.449	7.027	1.238
1211	2.160	6.736	0.770
1150	3.426	7.027	1.231

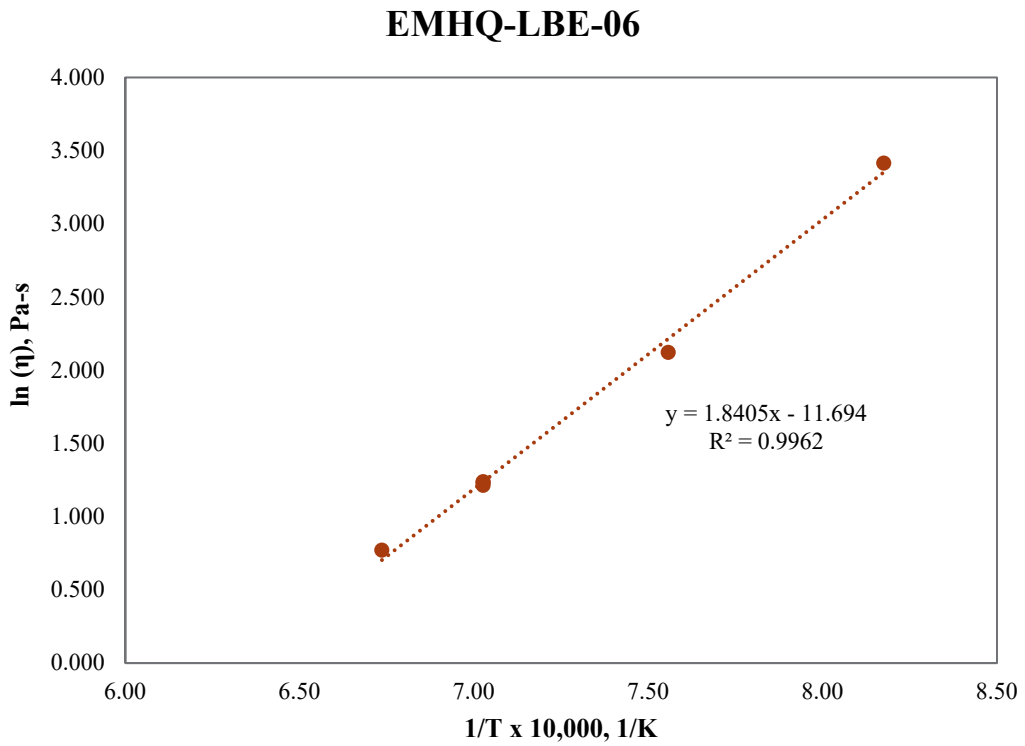

Figure D.7. Viscosity-Temperature Data and Arrhenius Equation Fit for Glass EMHQ-LBE-06

D.8 Glass EMHQ-LBE-07 Viscosity Data

Table D.8. Viscosity Data for Glass EMHQ-LBE-07

Measured Temp., °C	Viscosity, Pa-s	1/T x10000, K^{-1}	ln η, Pa-s
1150	3.737	7.027	1.318
1050	11.087	7.558	2.406
950	51.049	8.176	3.933
1150	3.795	7.027	1.334
1212	2.227	6.731	0.800
1150	3.832	7.027	1.343

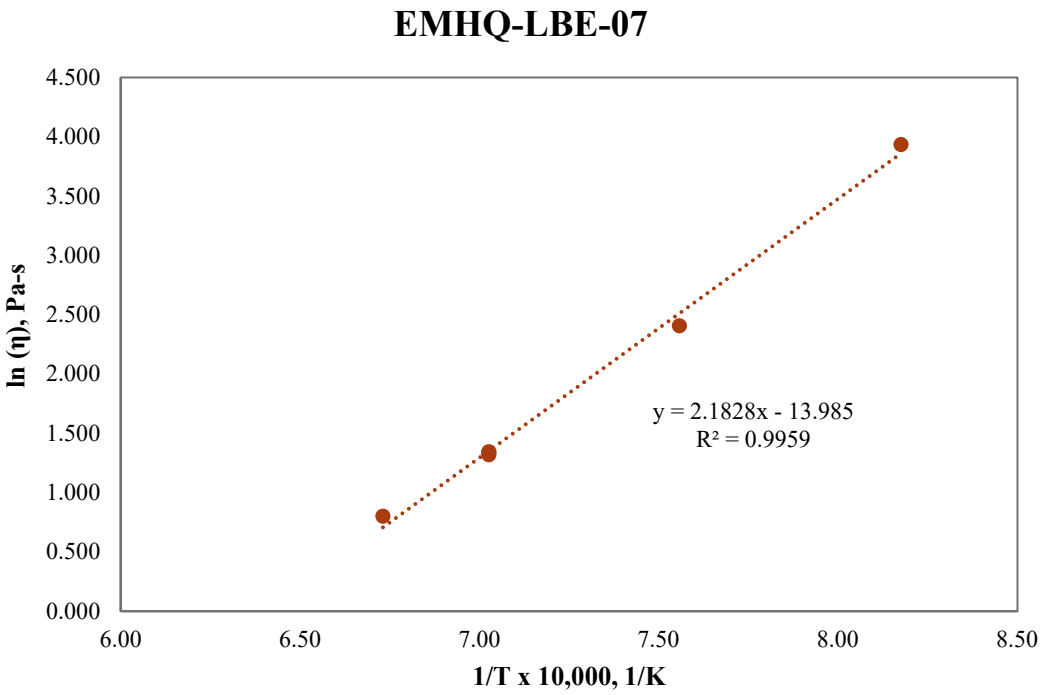

Figure D.8. Viscosity-Temperature Data and Arrhenius Equation Fit for Glass EMHQ-LBE-07

D.9 Glass EMHQ-LBE-08 Viscosity Data

Table D.9. Viscosity Data for Glass EMHQ-LBE-08

Measured Temp., °C	Viscosity, Pa-s	1/T x10000, K^{-1}	ln η, Pa-s
1150	3.820	7.027	1.340
1050	11.054	7.558	2.403
950	49.403	8.176	3.900
1139	3.730	7.027	1.316
1170	2.144	6.729	0.763
1150	3.722	7.027	1.314

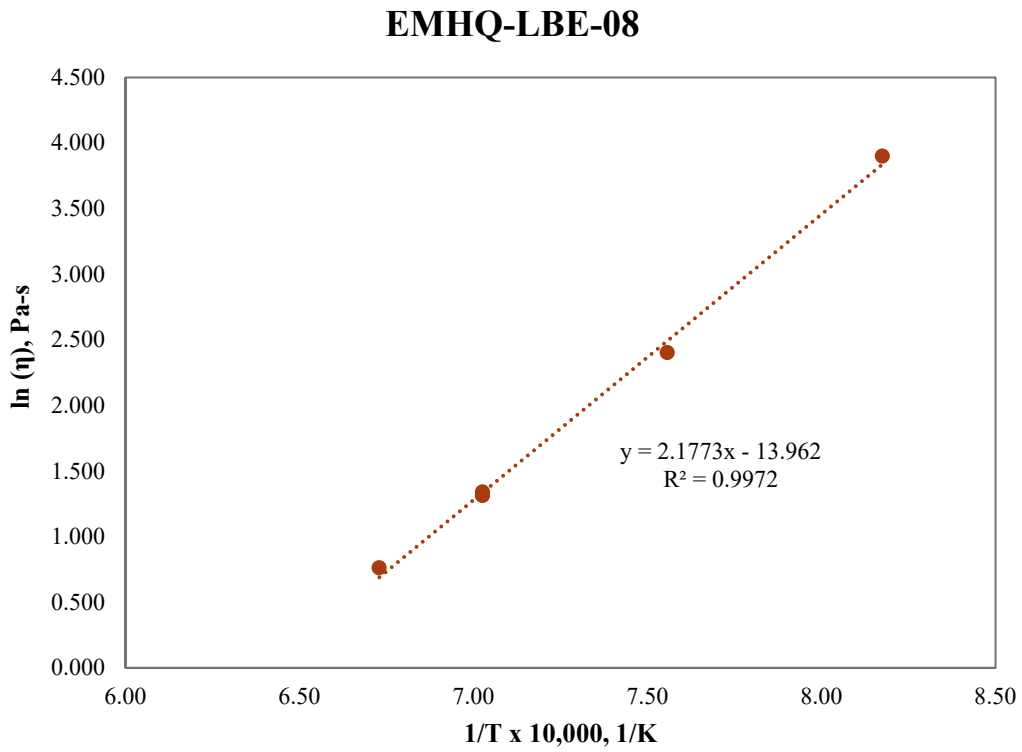

Figure D.9. Viscosity-Temperature Data and Arrhenius Equation Fit for Glass EMHQ-LBE-08

D.10 Glass EMHQ-LBE-09 Viscosity Data

Table D.10. Viscosity Data for Glass EMHQ-LBE-09

Measured Temp., °C	Viscosity, Pa-s	1/T x10000, K^{-1}	ln η, Pa-s
1150	3.876	7.027	1.355
1050	11.205	7.558	2.416
950	53.507	8.176	3.980
1140	3.686	7.027	1.305
1170	2.142	6.743	0.762
1150	3.774	7.027	1.328

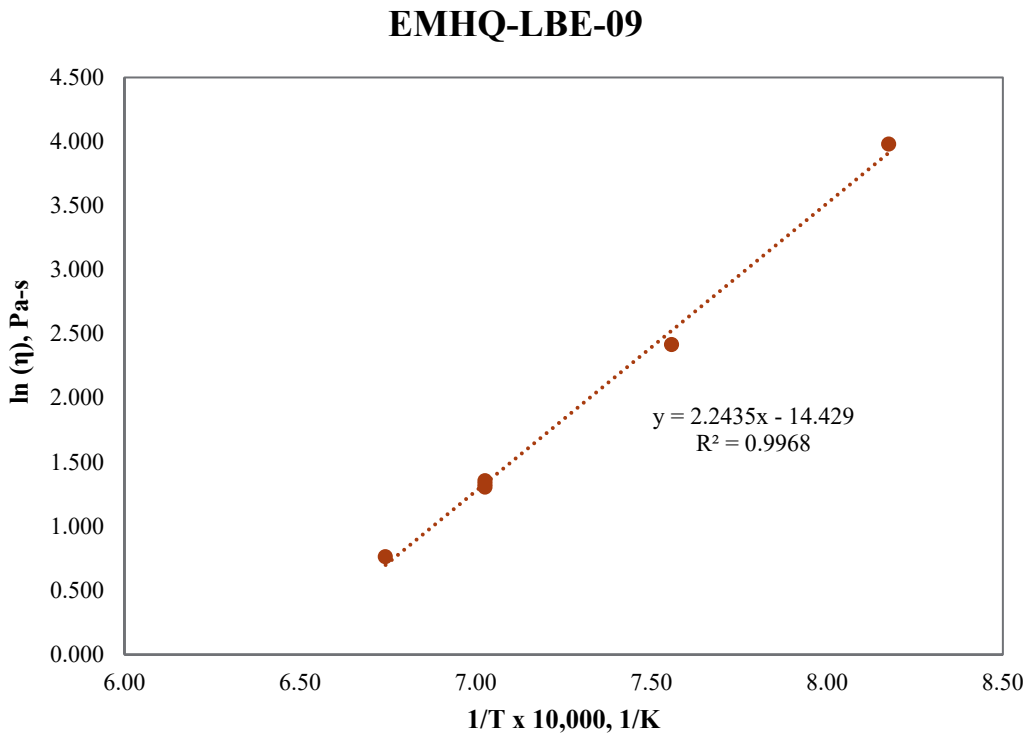

Figure D.10. Viscosity-Temperature Data and Arrhenius Equation Fit for Glass EMHQ-LBE-09

D.11 Glass EMHQ-LBE-10 Viscosity Data

Table D.11. Viscosity Data for Glass EMHQ-LBE-10

Measured Temp., °C	Viscosity, Pa-s	1/T x10000, K^{-1}	ln η, Pa-s
1150	3.977	7.027	1.380
1050	11.562	7.558	2.448
950	52.401	8.176	3.959
1150	3.823	7.027	1.341
1214	2.153	6.724	0.767
1150	3.858	7.027	1.350

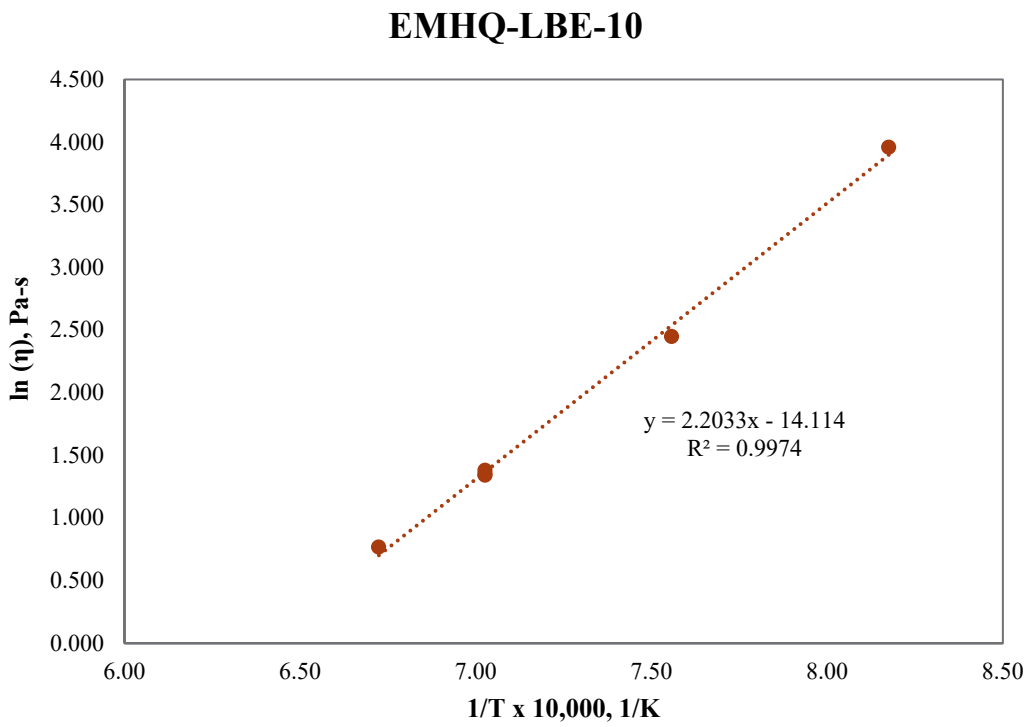

Figure D.11. Viscosity-Temperature Data and Arrhenius Equation Fit for Glass EMHQ-LBE-10

Appendix E – Electrical Conductivity Data

This appendix contains the measured electrical conductivity data for each of the glasses in this matrix.

The plots shown in this appendix are fitted to the Arrhenius equation, which is shown below:

$$\ln(\varepsilon) = A + \frac{B}{T_K} \quad \text{(E.1)}$$

where A and B are independent of temperature (T_K) is in K (T(°C) + 273.15)**.**

The intent of the figures and Arrhenius equation fits shown in this appendix is mainly to assess trends of the data and provide some observations about whether there may be sufficient curvature in the data to consider VFT fits in the subsequent work that will decide between fitting the data to the Arrhenius or VFT equations for the electrical conductivity-temperature data for each glass that is being made.

E.1 Glass EMHQ-LBE-01 Electrical Conductivity Data

Table E.1. Electrical Conductivity Data for Glass EMHQ-LBE-01

Temperature, °C	Conductivity, S/m	1/T, K^{-1}	ln ε (S/m)
950	19.298	0.000818	2.960
950	19.312	0.000818	2.961
1200	36.643	0.000679	3.601
1200	37.145	0.000679	3.615
1150	31.543	0.000703	3.451
1150	31.532	0.000703	3.451
1050	26.030	0.000756	3.259
1050	25.952	0.000756	3.256

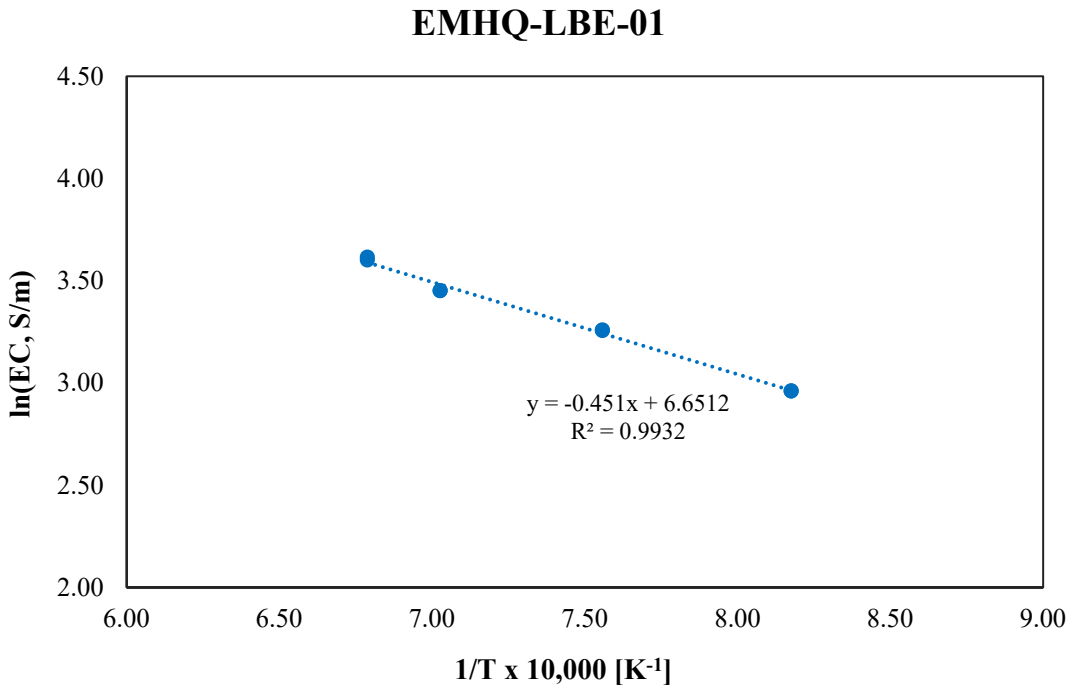

Figure E.1. Electrical Conductivity-Temperature Data and Arrhenius Equation Fit for Glass EMHQ-LBE-01

E.2 Glass EMHQ-LBE-02 Electrical Conductivity Data

Table E.2. Electrical Conductivity Data for Glass EMHQ-LBE-02

Temperature, °C	Conductivity, S/m	1/T, K^{-1}	ln ε, S/m
950	26.05	0.000818	3.260
950	26.08	0.000818	3.261
1200	53.32	0.000679	3.976
1200	53.36	0.000679	3.977
1150	48.38	0.000703	3.879
1150	48.27	0.000703	3.877
1050	37.86	0.000756	3.634
1050	37.82	0.000756	3.633

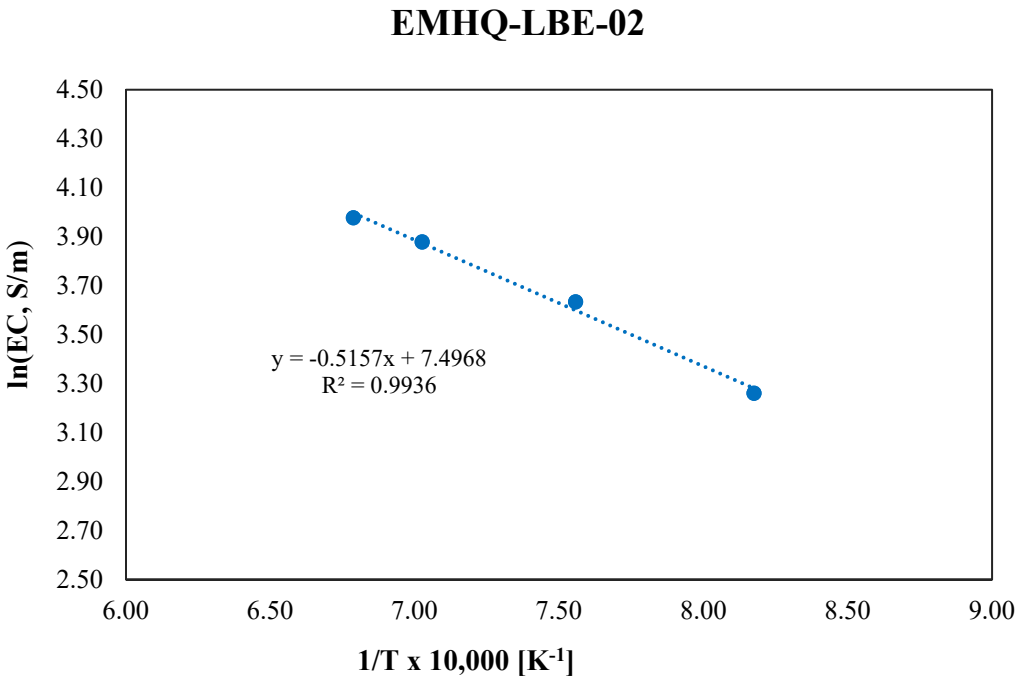

Figure E.2. Electrical Conductivity-Temperature Data and Arrhenius Equation Fit for Glass EMHQ-LBE-02

E.3 Glass EMHQ-LBE-03 Electrical Conductivity Data

Table E.3. Electrical Conductivity Data for Glass EMHQ-LBE-03

Temperature, °C	Conductivity, S/m	1/T, K^{-1}	ln ε, S/m
950	20.88	0.000818	3.039
950	20.89	0.000818	3.039
1200	32.76	0.000679	3.489
1150	34.92	0.000703	3.553
1150	34.98	0.000703	3.555
1050	28.56	0.000756	3.352
1050	28.57	0.000756	3.352

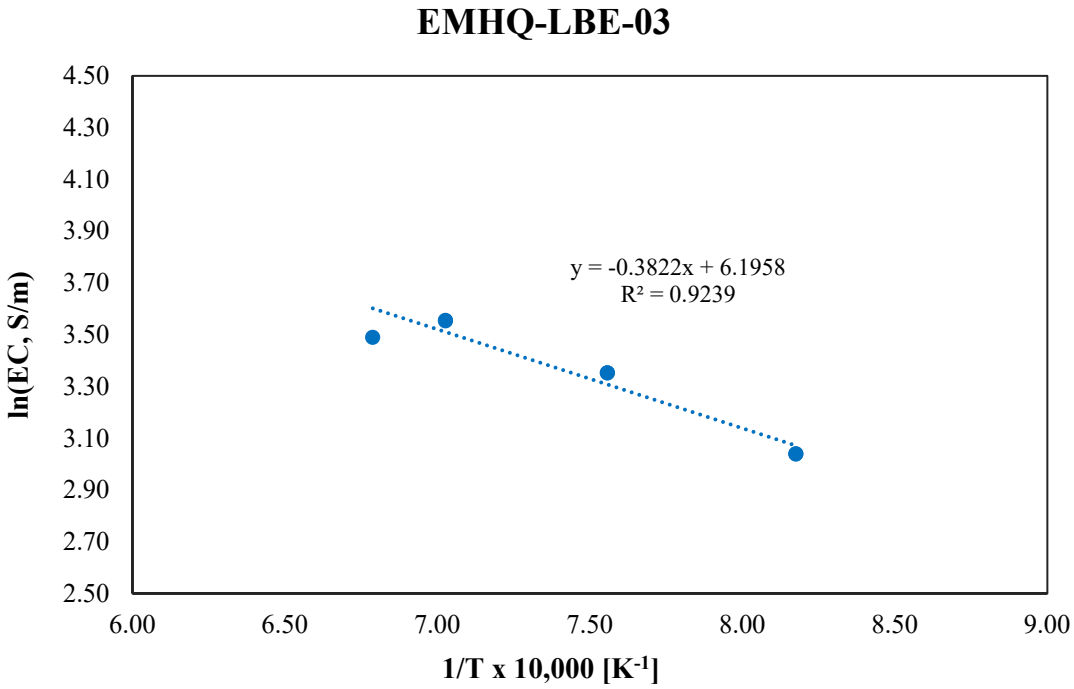

Figure E.3. Electrical Conductivity-Temperature Data and Arrhenius Equation Fit for Glass EMHQ-LBE-03

E.4 Glass EMHQ-LBE-04 Electrical Conductivity Data

Table E.4. Electrical Conductivity Data for Glass EMHQ-LBE-04

Temperature, °C	Conductivity, S/m	1/T, K^{-1}	ln ε, S/m
950	18.40	0.000818	2.912
950	18.35	0.000818	2.909
1200	62.34	0.000679	4.133
1200	62.63	0.000679	4.137
1150	53.66	0.000703	3.983
1150	53.80	0.000703	3.985
1050	34.22	0.000756	3.533
1050	34.13	0.000756	3.530

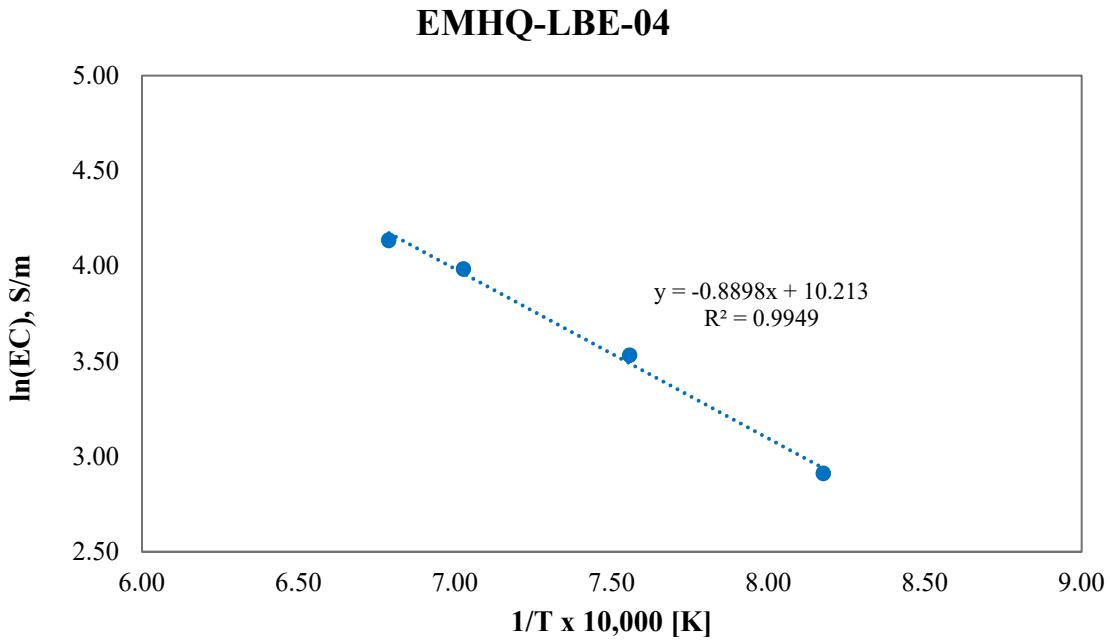

Figure E.4. Electrical Conductivity-Temperature Data and Arrhenius Equation Fit for Glass EMHQ-LBE-04

E.5 Glass EMHQ-LBE-04B Electrical Conductivity Data

Table E.5. Electrical Conductivity Data for Glass EMHQ-LBE-04B

Temperature, °C	Conductivity, S/m	1/T, K^{-1}	ln ε, S/m
950	15.03	0.000818	2.710
950	12.89	0.000818	2.557
1050	27.69	0.000756	3.321
1050	27.64	0.000756	3.319
1150	44.76	0.000703	3.801
1150	44.66	0.000703	3.799
1200	51.00	0.000679	3.932
1200	51.65	0.000679	3.944

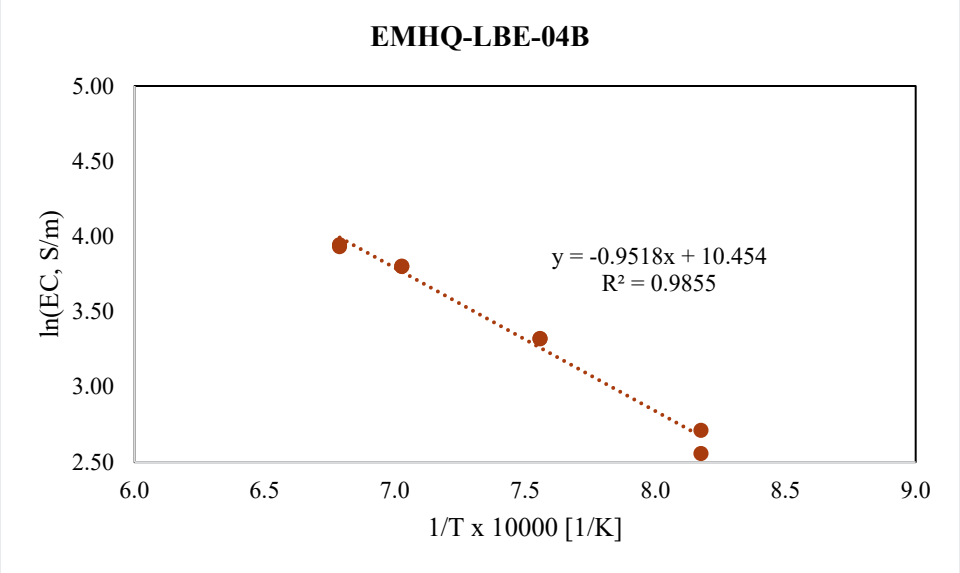

Figure E.5. Electrical Conductivity-Temperature Data and Arrhenius Equation Fit for Glass EMHQ-LBE-04B

E.6 Glass EMHQ-LBE-05 Electrical Conductivity Data

Table E.6. Electrical Conductivity Data for Glass EMHQ-LBE-05

Temperature, °C	Conductivity, S/m	1/T, K^{-1}	ln ε, S/m
950	7.64	0.000818	2.033
950	10.71	0.000818	2.372
1200	48.88	0.000679	3.889
1200	48.67	0.000679	3.885
1150	41.67	0.000703	3.730
1150	36.69	0.000703	3.602
1050	20.56	0.000756	3.023
1050	22.41	0.000756	3.110

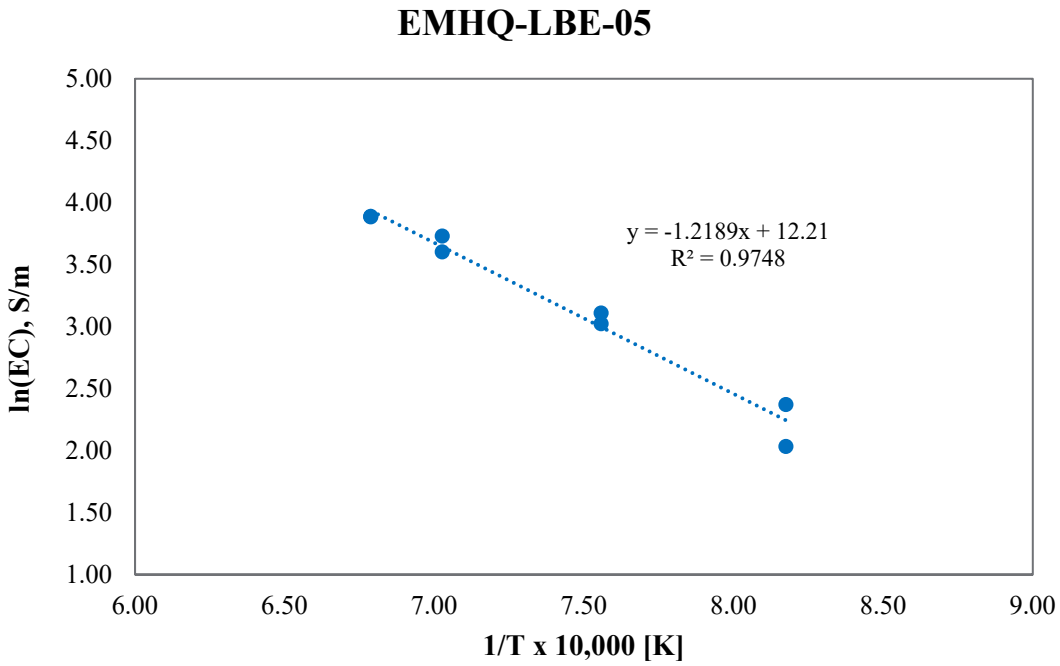

Figure E.6. Electrical Conductivity-Temperature Data and Arrhenius Equation Fit for Glass EMHQ-LBE-05

E.7 Glass EMHQ-LBE-06 Electrical Conductivity Data

Table E.7. Electrical Conductivity Data for Glass EMHQ-LBE-06

Temperature, °C	Conductivity, S/m	1/T, K^{-1}	ln ε, S/m
950	15.54	0.000818	2.743
950	15.42	0.000818	2.735
1200	60.57	0.000679	4.104
1200	60.57	0.000679	4.104
1150	50.10	0.000703	3.914
1150	47.79	0.000703	3.867
1050	29.09	0.000756	3.370
1050	29.13	0.000756	3.372

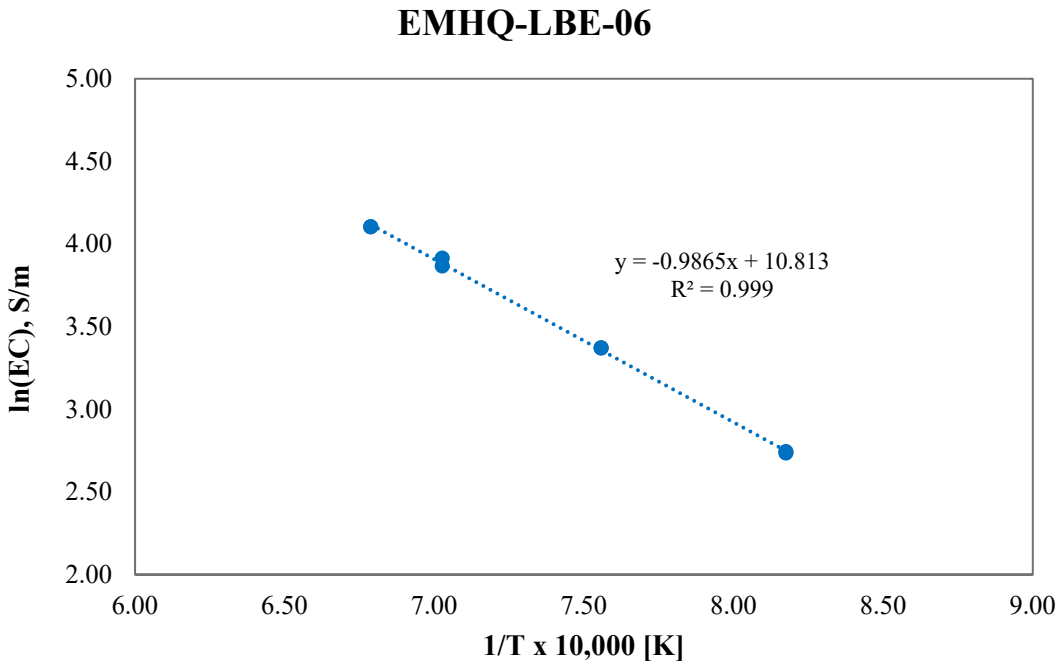

Figure E.7. Electrical Conductivity-Temperature Data and Arrhenius Equation Fit for Glass EMHQ-LBE-06

E.8 Glass EMHQ-LBE-07 Electrical Conductivity Data

Table E.8. Electrical Conductivity Data for Glass EMHQ-LBE-07

Temperature, °C	Conductivity, S/m	1/T, K^{-1}	ln ε, S/m
950	17.54	0.000818	2.864
950	17.53	0.000818	2.864
1200	33.08	0.000679	3.499
1200	32.96	0.000679	3.495
1150	30.47	0.000703	3.417
1150	30.44	0.000703	3.416
1050	24.56	0.000756	3.201
1050	24.56	0.000756	3.201

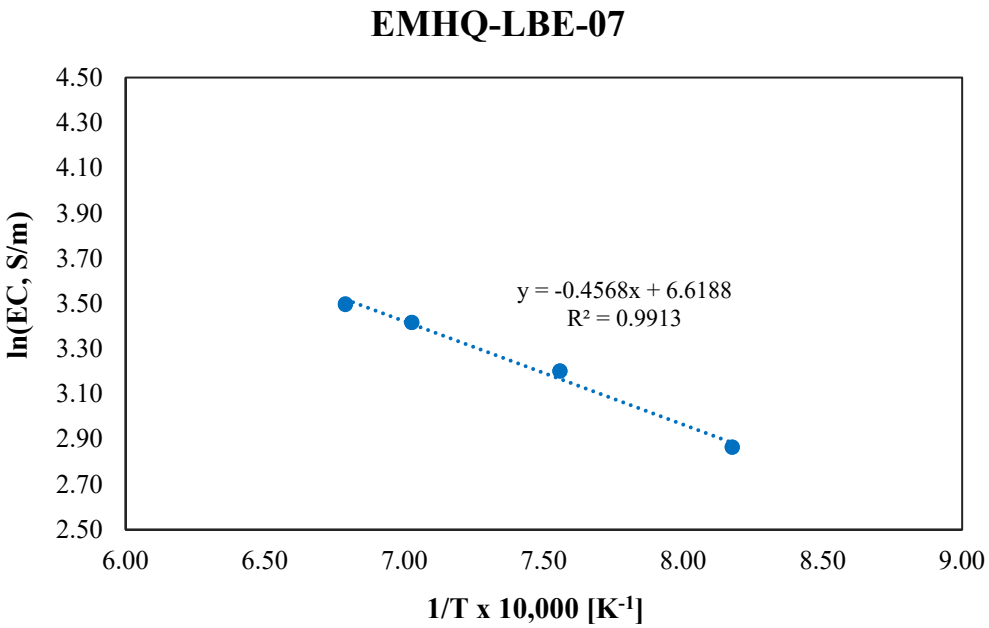

Figure E.8. Electrical Conductivity-Temperature Data and Arrhenius Equation Fit for Glass EMHQ-LBE-07

E.9 Glass EMHQ-LBE-08 Electrical Conductivity Data

Table E.9. Electrical Conductivity Data for Glass EMHQ-LBE-08

Temperature, °C	Conductivity, S/m	1/T, K^{-1}	ln ε, S/m
950	16.23	0.000818	2.787
950	16.22	0.000818	2.786
1200	28.12	0.000679	3.336
1200	28.11	0.000679	3.336
1150	26.48	0.000703	3.276
1150	26.43	0.000703	3.275
1050	21.87	0.000756	3.033
1050	21.85	0.000756	3.033

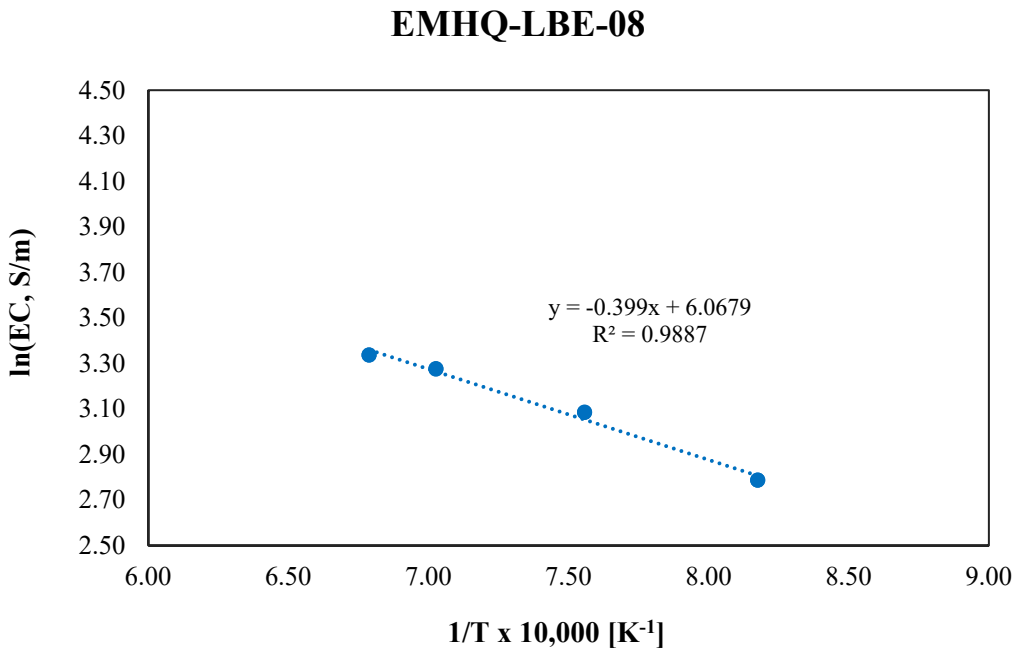

Figure E.9. Electrical Conductivity-Temperature Data and Arrhenius Equation Fit for Glass EMHQ-LBE-08

E.10 Glass EMHQ-LBE-09 Electrical Conductivity Data

Table E.10. Electrical Conductivity Data for Glass EMHQ-LBE-09

Temperature, °C	Conductivity, S/m	1/T, K^{-1}	ln ε, S/m
950	14.95	0.000818	2.705
950	14.96	0.000818	2.706
1200	27.63	0.000679	3.319
1200	27.66	0.000679	3.320
1150	25.59	0.000703	3.242
1150	25.57	0.000703	3.242
1050	20.77	0.000756	3.033
1050	20.76	0.000756	3.033

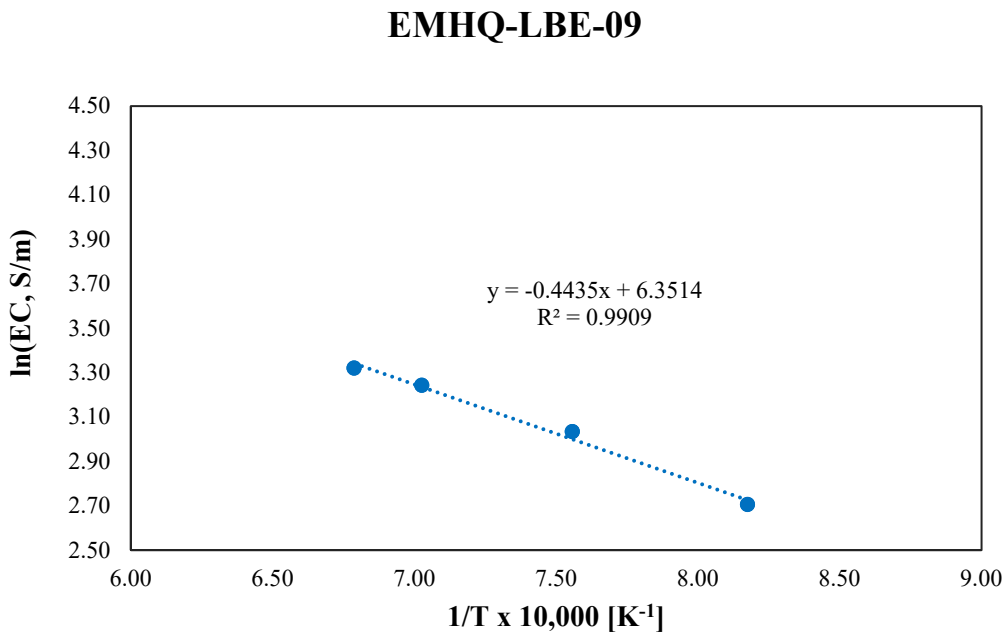

Figure E.10. Electrical Conductivity-Temperature Data and Arrhenius Equation Fit for Glass EMHQ-LBE-09

E.11 Glass EMHQ-LBE-10 Electrical Conductivity Data

Table E.11. Electrical Conductivity Data for Glass EMHQ-LBE-10

Temperature, °C	Conductivity, S/m	1/T, K^{-1}	ln ε, S/m
950	19.82	0.000818	2.987
950	19.76	0.000818	2.984
1200	29.90	0.000679	3.398
1200	29.82	0.000679	3.395
1150	28.35	0.000703	3.345
1150	28.24	0.000703	3.341
1050	25.04	0.000756	3.221
1050	25.12	0.000756	3.223

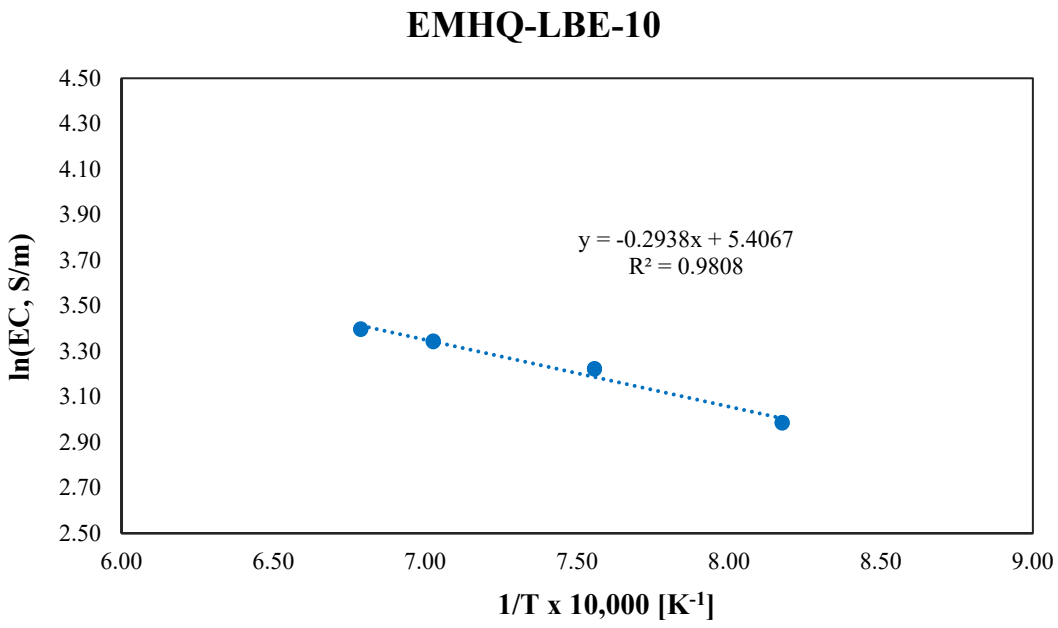

Figure E.11. Electrical Conductivity-Temperature Data and Arrhenius Equation Fit for Glass EMHQ-LBE-10

Appendix F – Crystal Fraction (CF) of Heat-Treated Glasses Photographs

This appendix contains photos of glasses after they were heat-treated at 950 °C for 24 h and 850 °C for 48 h.

Figure F.1. Glass EMHQ-LBE-01 after CF Heat Treatment at 950 °C for 24 h

Figure F.2. Glass EMHQ-LBE-01 after CF Heat Treatment at 850 °C for 48 h

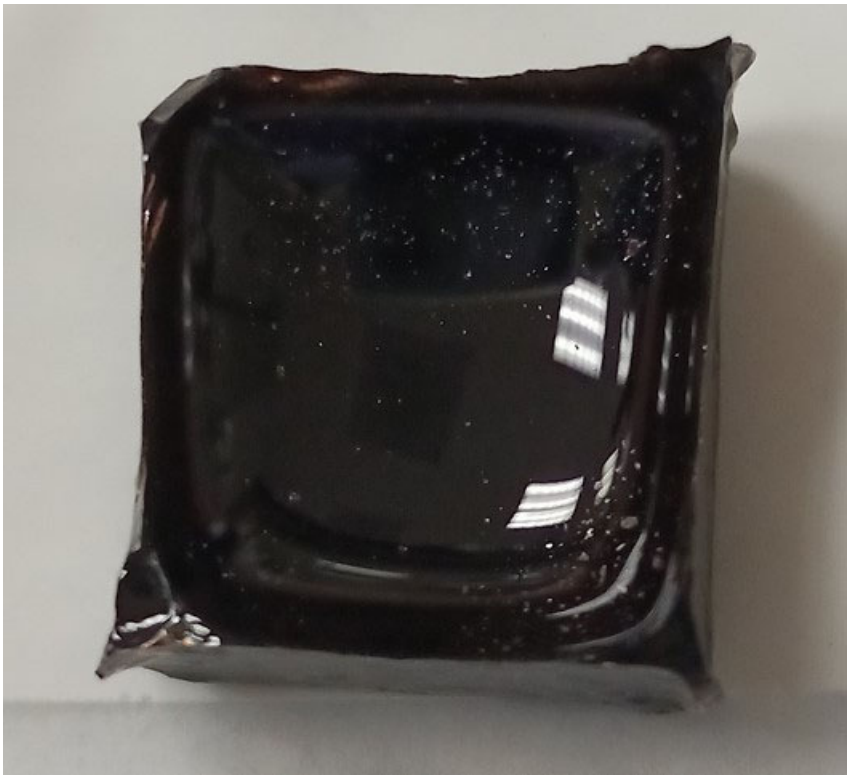

Figure F.3. Glass EMHQ-LBE-02 after CF Heat Treatment at 950 °C for 24 h

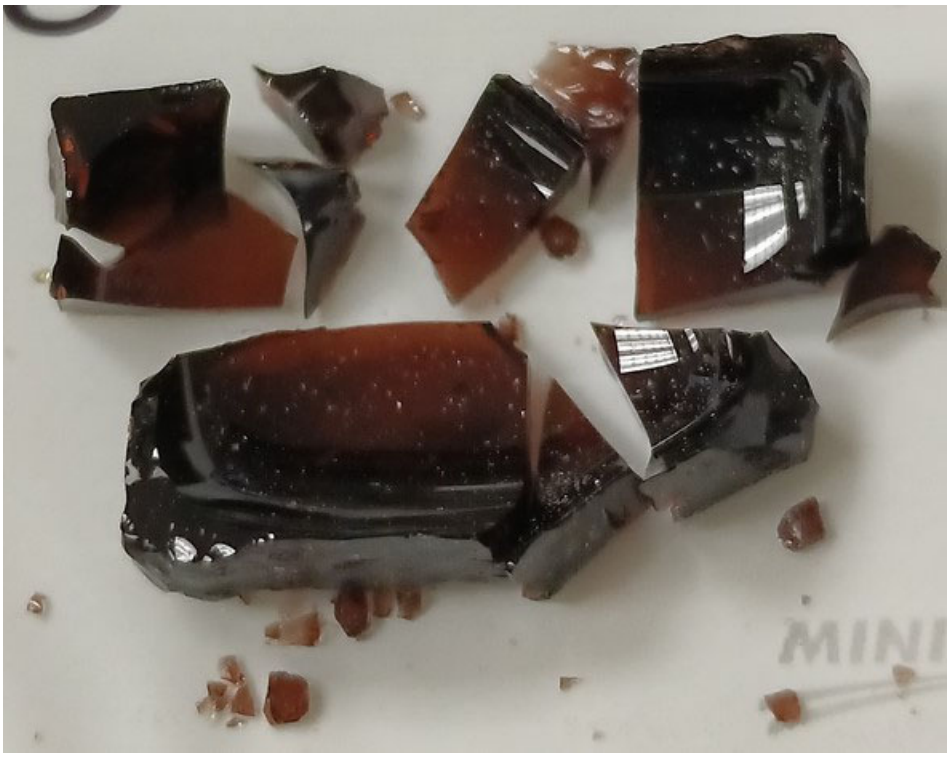

Figure F.4. Glass EMHQ-LBE-02 after CF Heat Treatment at 850 °C for 48 h

Figure F.5. Glass EMHQ-LBE-03 after CF Heat Treatment at 950 °C for 24 h

Figure F.6. Glass EMHQ-LBE-03 after CF Heat Treatment at 850 °C for 48 h

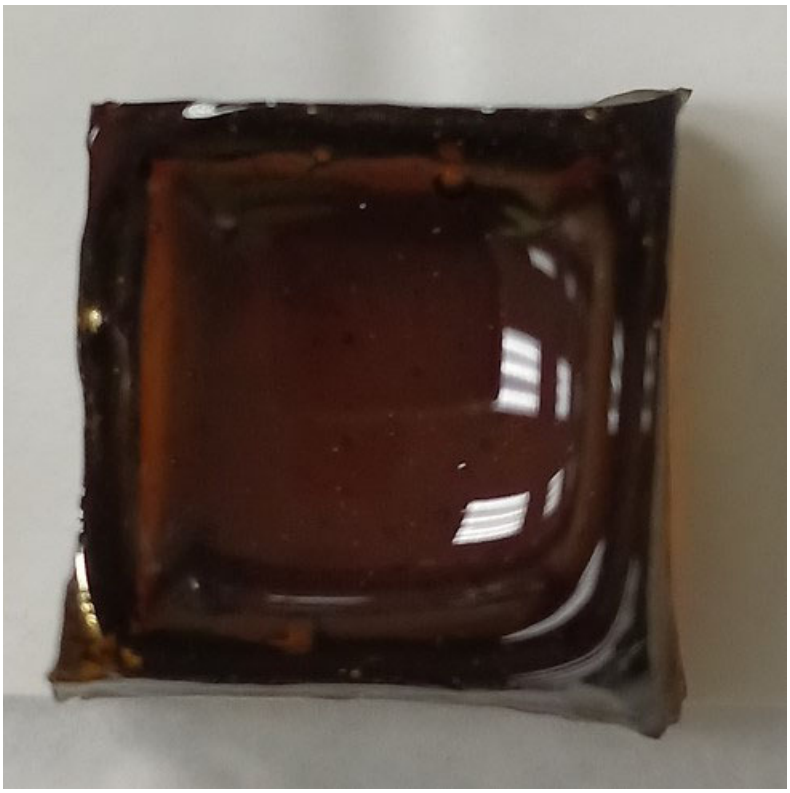

Figure F.7. Glass EMHQ-LBE-04 after CF Heat Treatment at 950 °C for 24 h

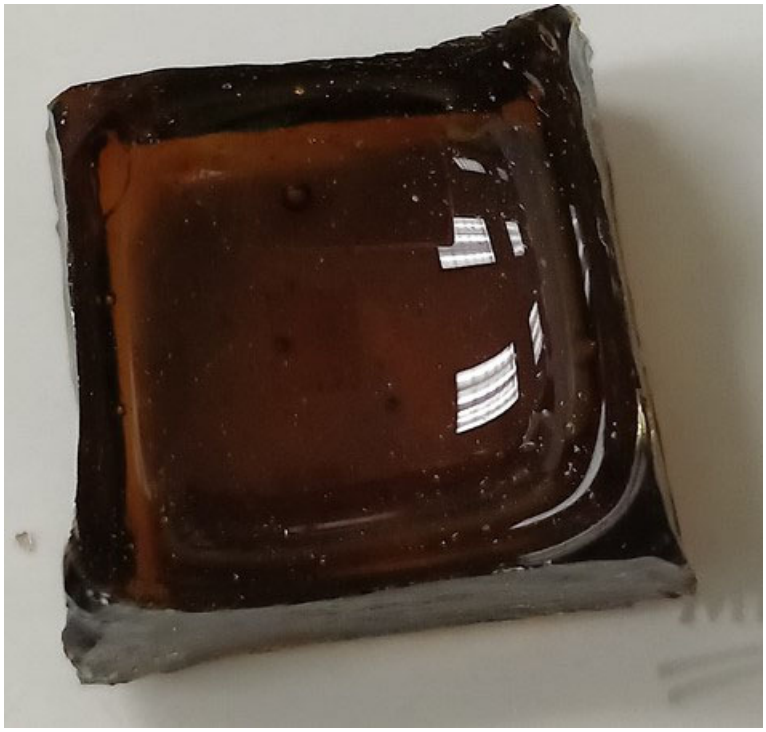

Figure F.8. Glass EMHQ-LBE-04 after CF Heat Treatment at 850 °C for 48 h

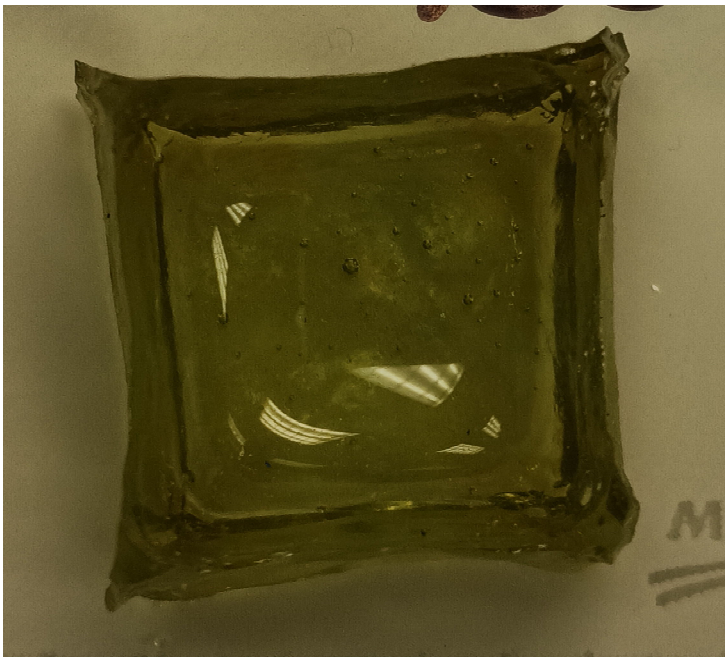

Figure F.9. Glass EMHQ-LBE-04B after CF Heat Treatment at 950 °C for 24 h

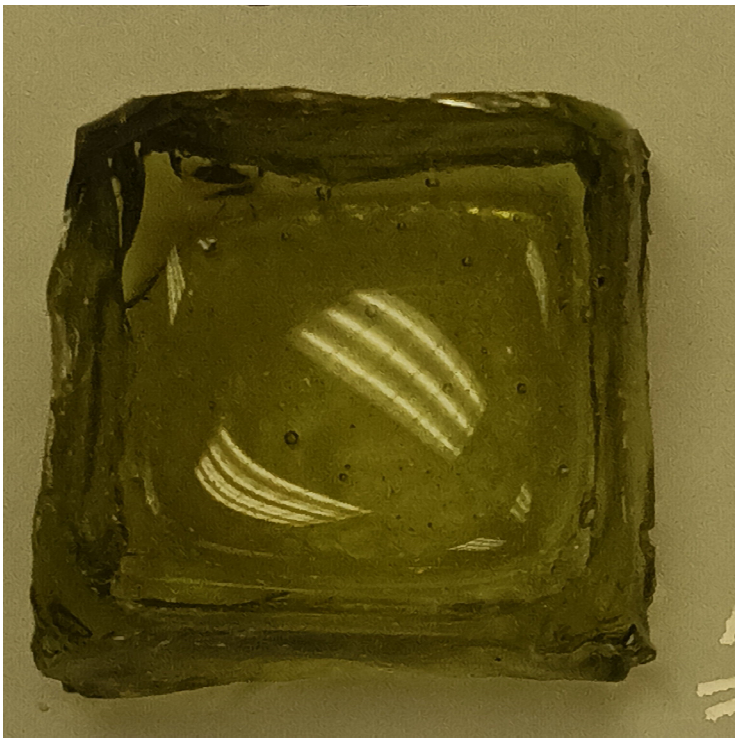

Figure F.10. Glass EMHQ-LBE-04B after CF Heat Treatment at 850 °C for 48 h

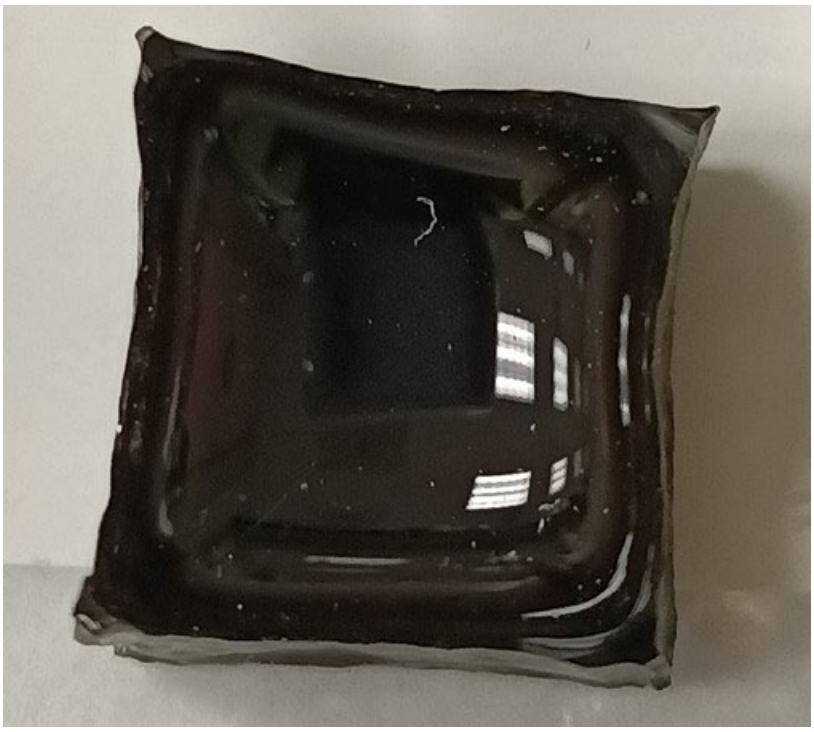

Figure F.11. Glass EMHQ-LBE-05 after CF Heat Treatment at 950 °C for 24 h

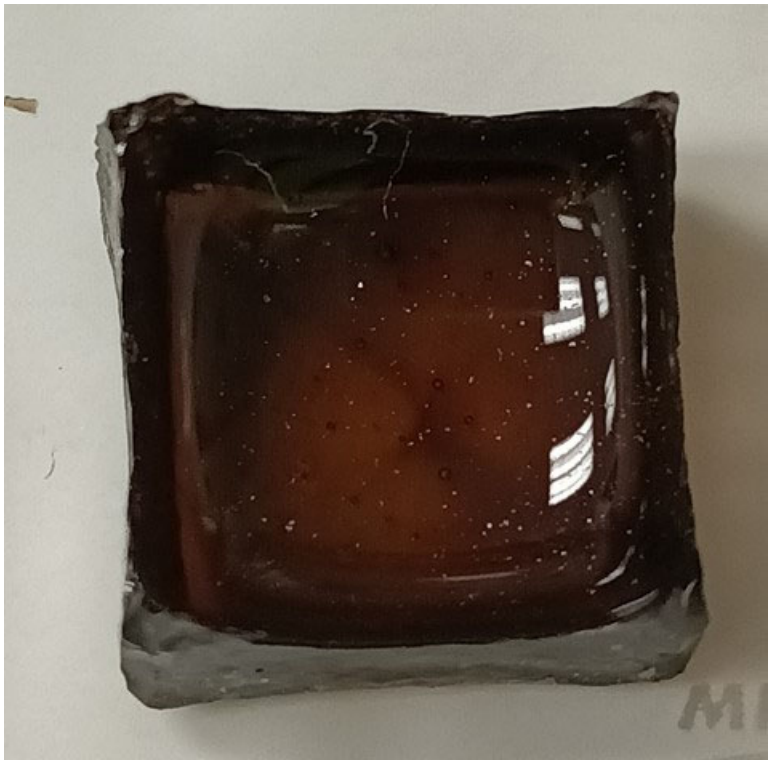

Figure F.12. Glass EMHQ-LBE-05 after CF Heat Treatment at 850 °C for 48 h

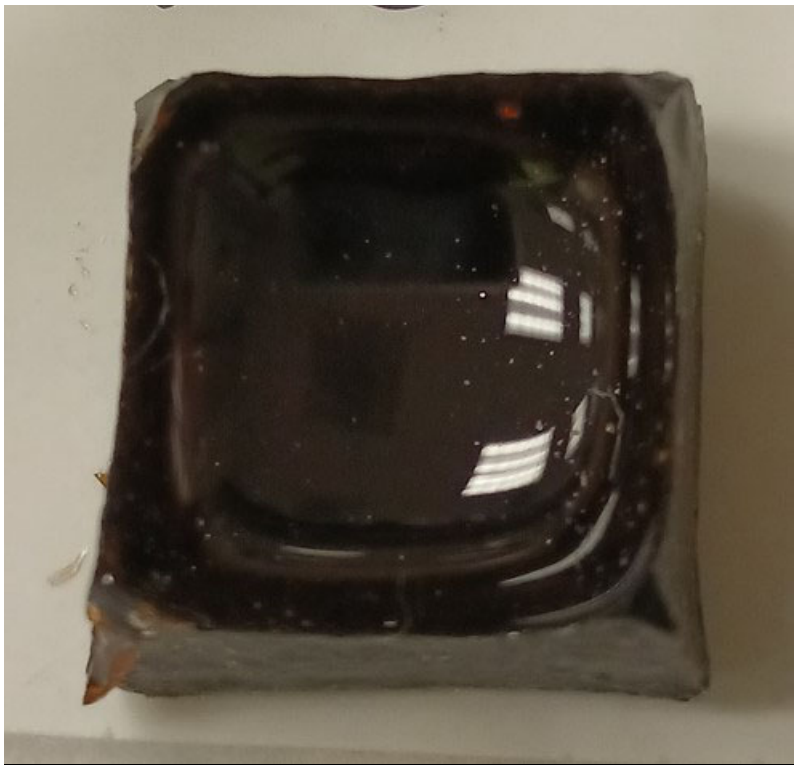

Figure F.13. Glass EMHQ-LBE-06 after CF Heat Treatment at 950 °C for 24 h

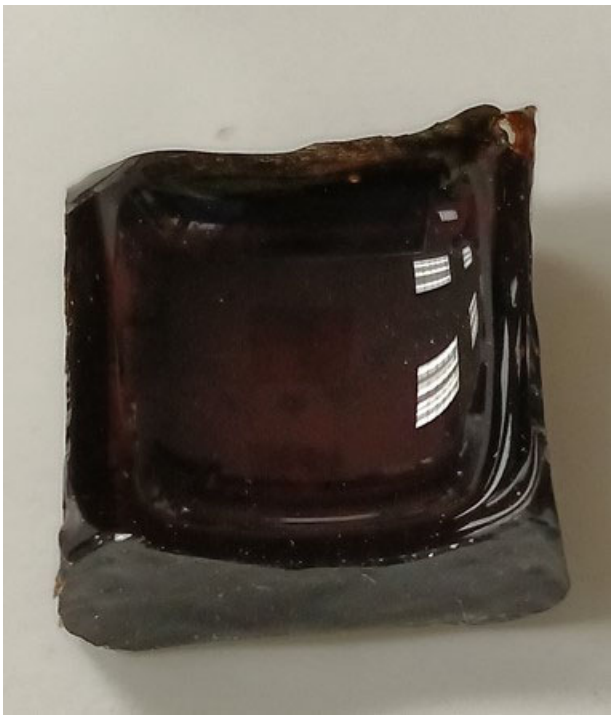

Figure F.14. Glass EMHQ-LBE-06 after CF Heat Treatment at 850 °C for 48 h

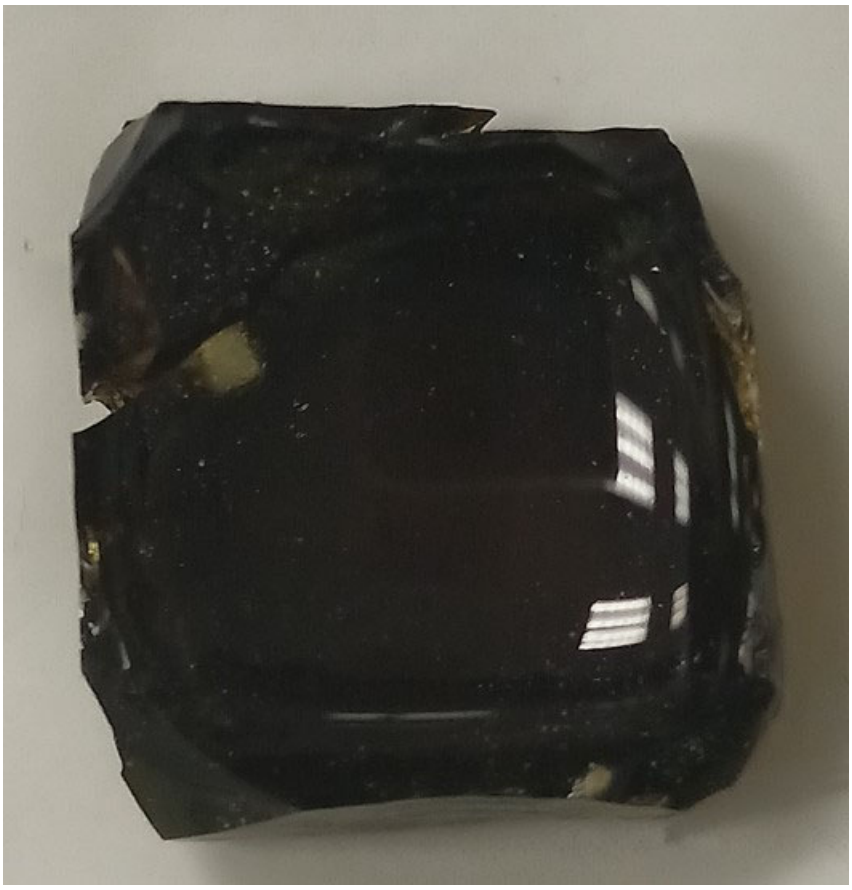

Figure F.15. Glass EMHQ-LBE-07 after CF Heat Treatment at 950 °C for 24 h

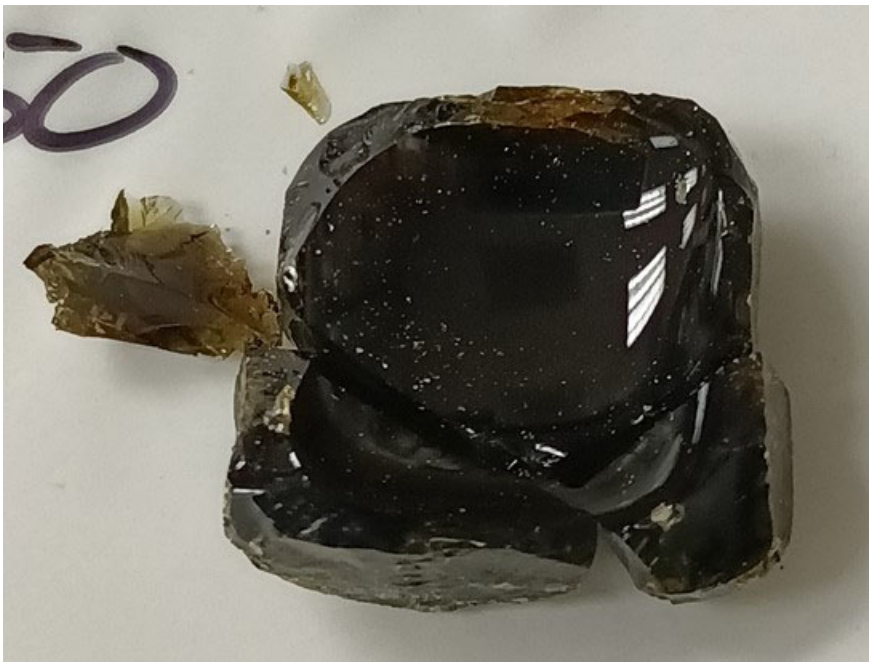

Figure F.16. Glass EMHQ-LBE-07 after CF Heat Treatment at 850 °C for 48 h

Figure F.17. Glass EMHQ-LBE-08 after CF Heat Treatment at 950 °C for 24 h

Figure F.18. Glass EMHQ-LBE-08 after CF Heat Treatment at 850 °C for 48 h

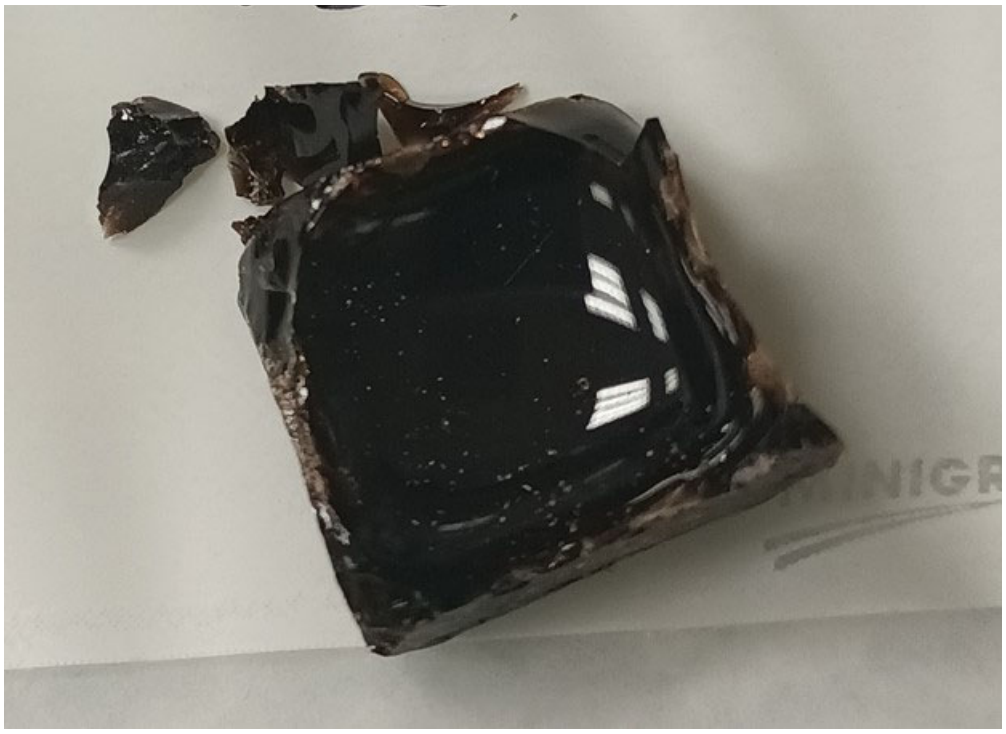

Figure F.19. Glass EMHQ-LBE-09 after CF Heat Treatment at 950 °C for 24 h

Figure F.20. Glass EMHQ-LBE-09 after CF Heat Treatment at 850 °C for 48 h

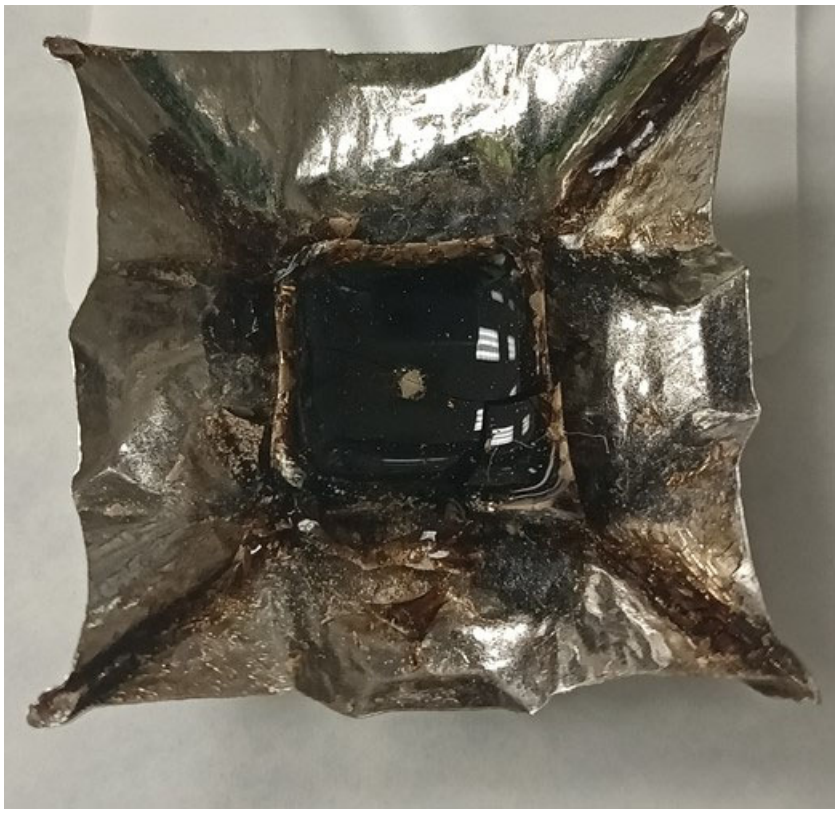

Figure F.21. Glass EMHQ-LBE-10 after CF Heat Treatment at 950 °C for 24 h

Figure F.22. Glass EMHQ-LBE-10 after CF Heat Treatment at 850 °C for 48 h

Appendix G – XRD Isothermal Crystal Fraction Glasses

This appendix shows the X-ray diffraction (XRD) plots of several glasses after isothermal crystal fraction (CF) heat-treating at 950 °C and at 850 °C. Most of the glasses remained amorphous, with only four glasses developing crystals. These crystals were mainly a Zr-containing crystal or a silicate.

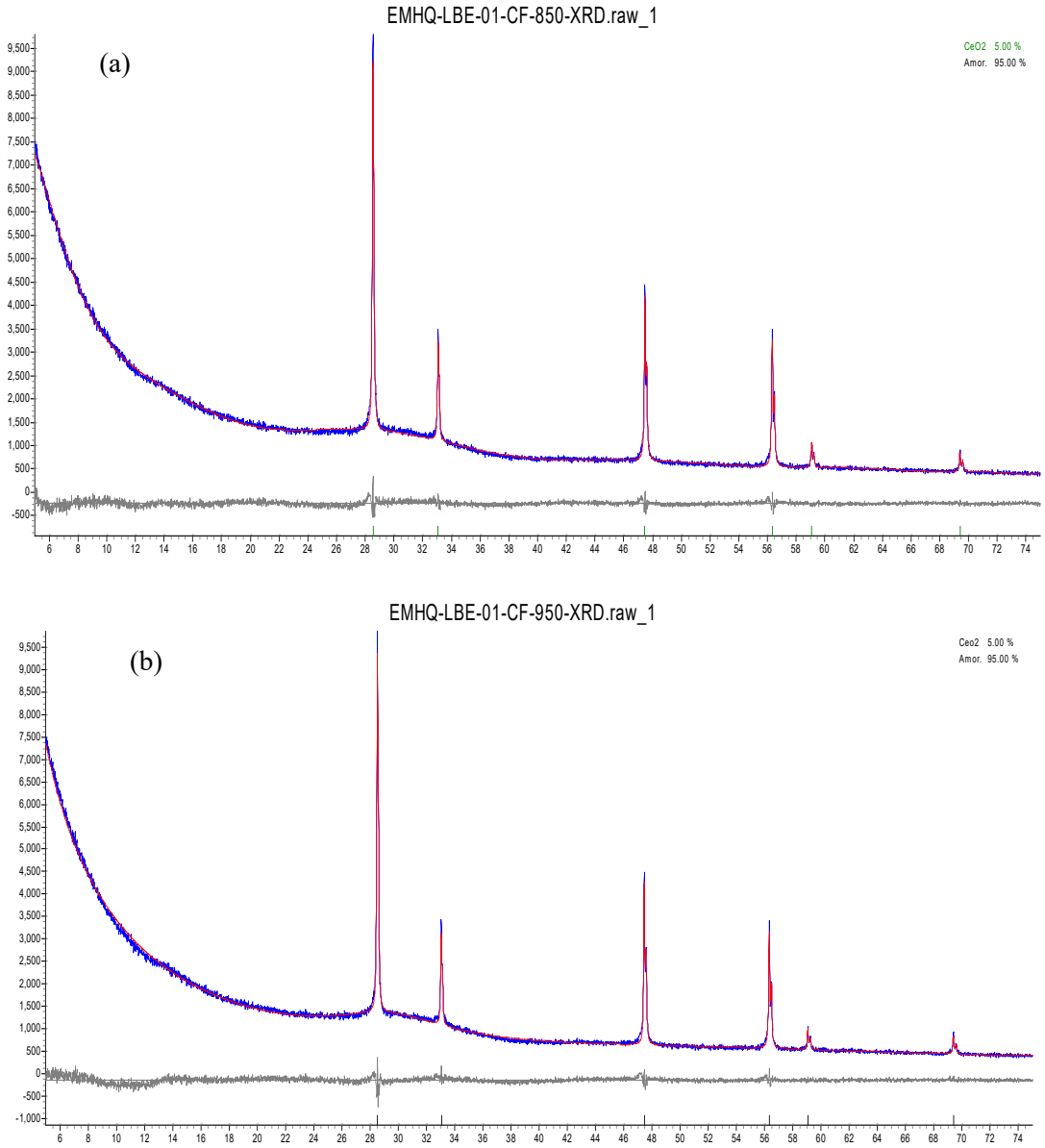

Figure G.1. XRD Spectrum of CF Heat-Treated Glass EMHQ-LBE-01 (a) 850 °C (b) 950 °C

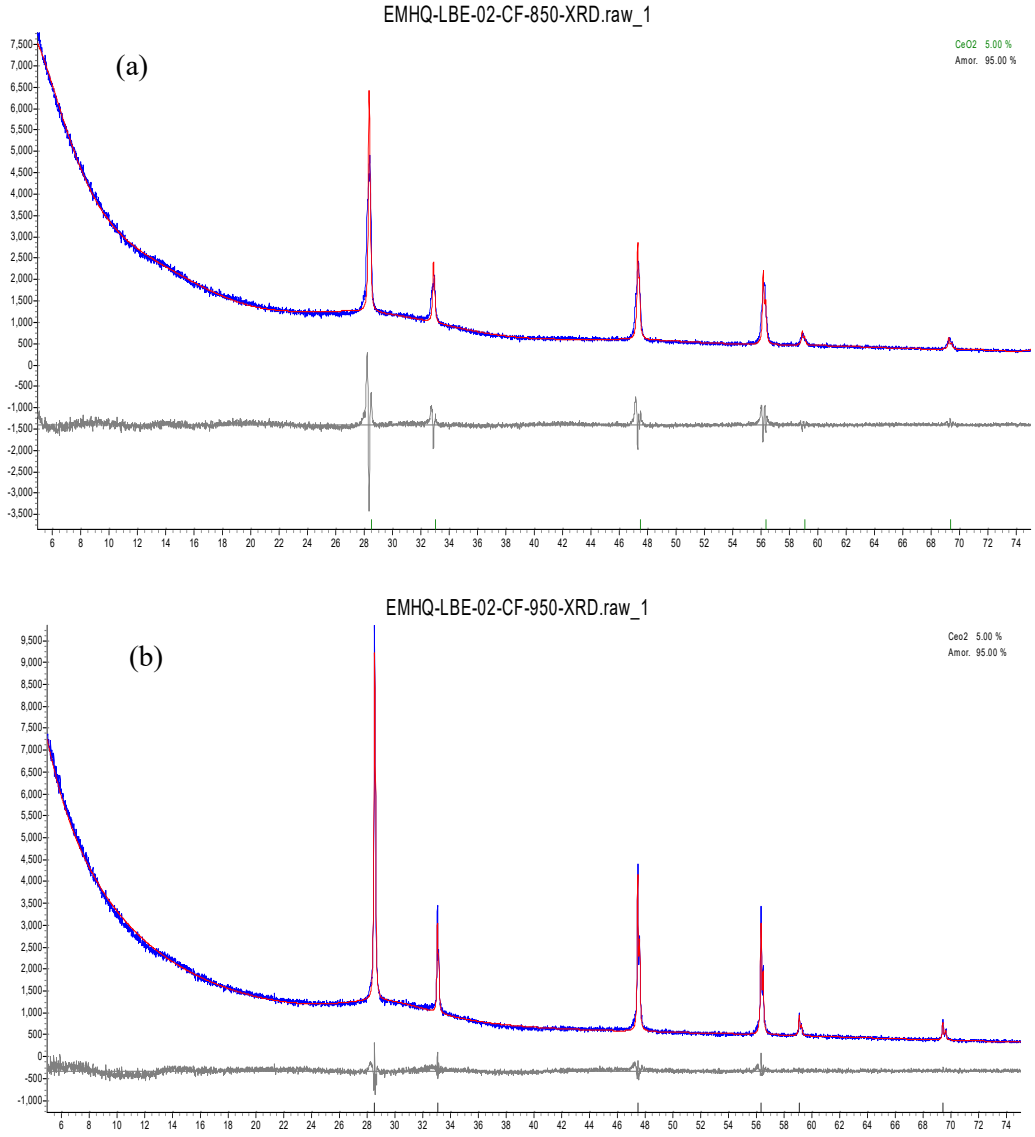

Figure G.2. XRD Spectrum of CF Heat-Treated Glass EMHQ-LBE-02 (a) 850 °C (b) 950 °C

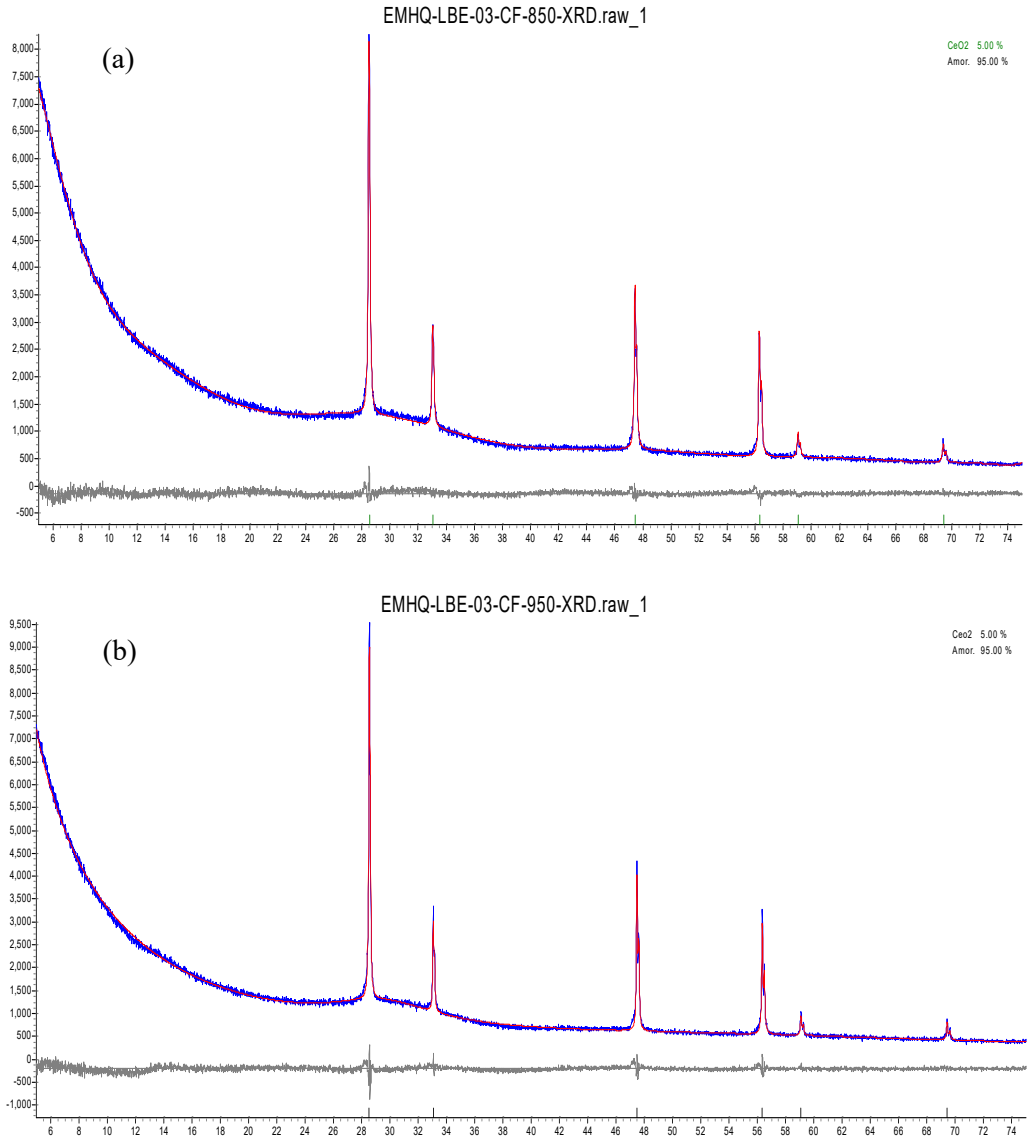

Figure G.3. XRD Spectrum of CF Heat-Treated Glass EMHQ-LBE-03 (a) 850 °C (b) 950 °C

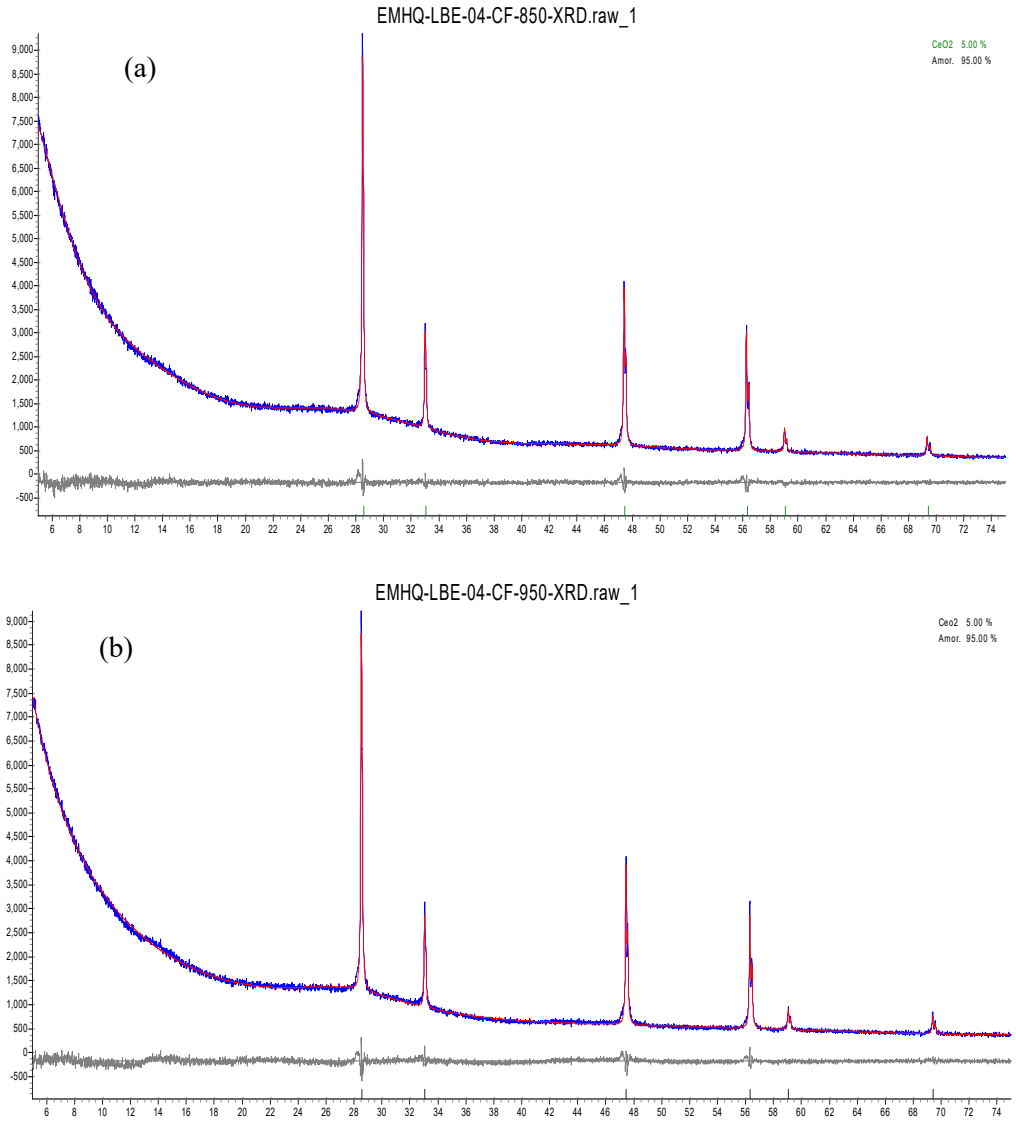

Figure G.4. XRD Spectrum of CF Heat-Treated Glass EMHQ-LBE-04 (a) 850 °C (b) 950 °C

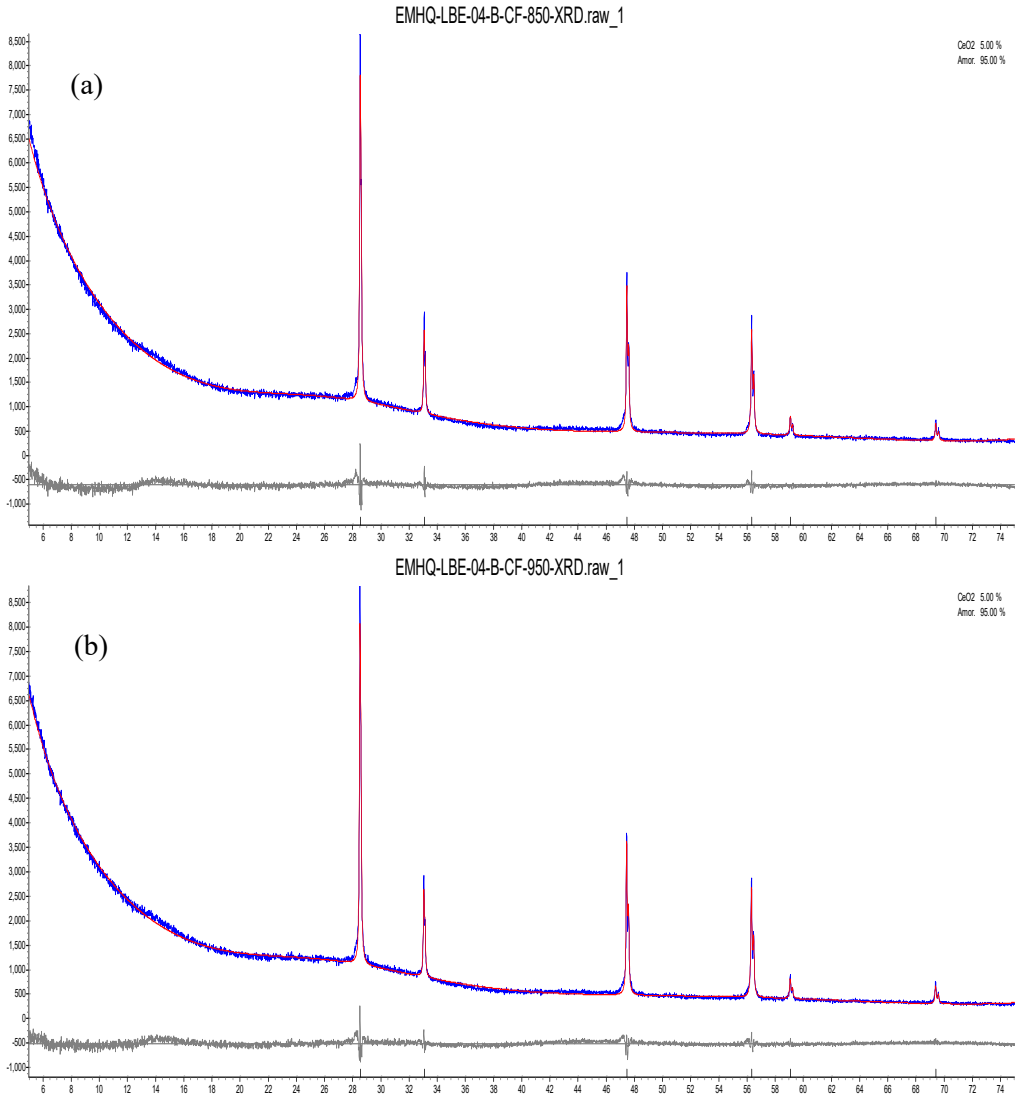

Figure G.5. XRD Spectrum of CF Heat-Treated Glass EMHQ-LBE-04B (a) 850 °C (b) 950 °C

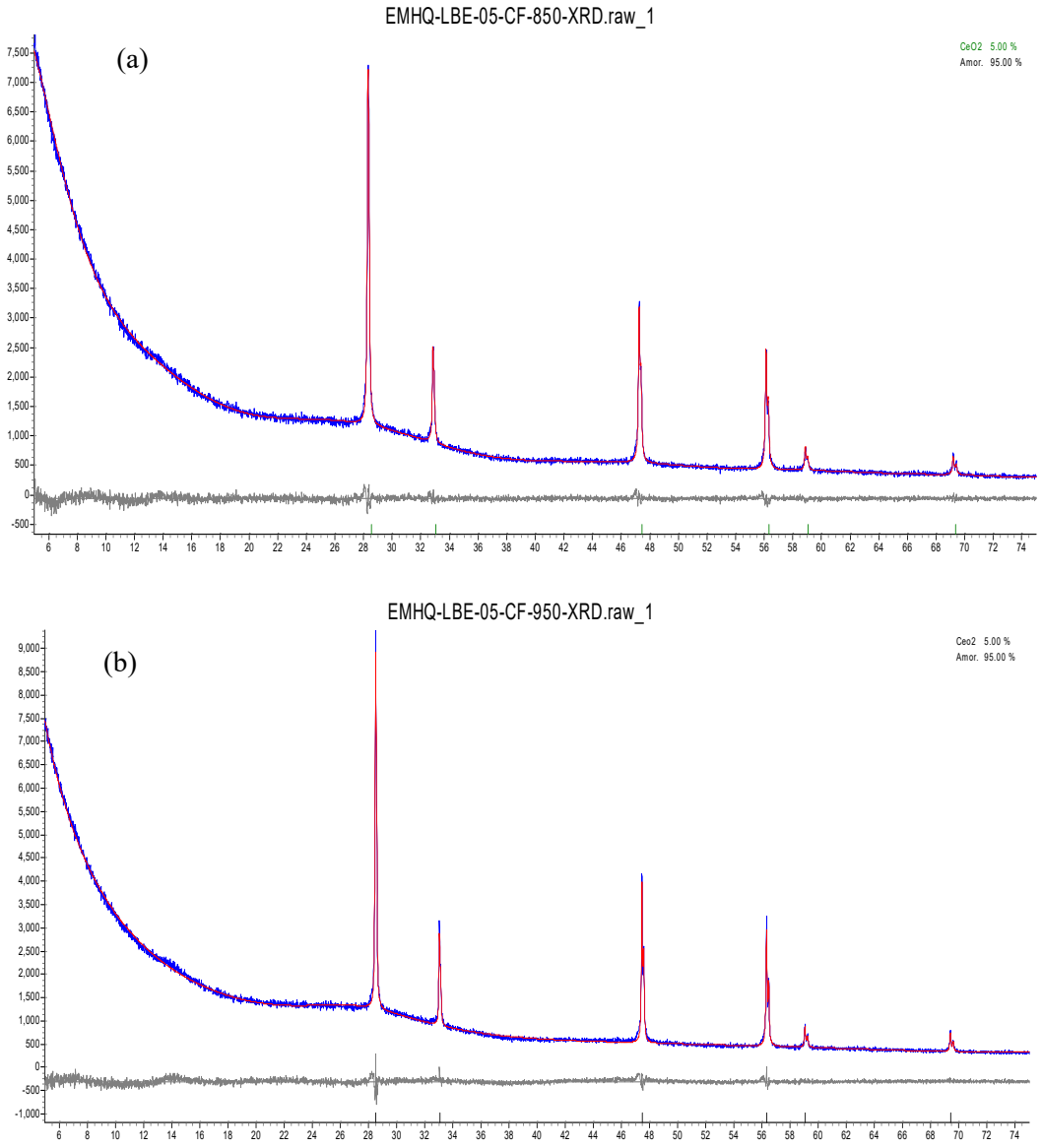

Figure G.6. XRD Spectrum of CF Heat-Treated Glass EMHQ-LBE-05 (a) 850 °C (b) 950 °C

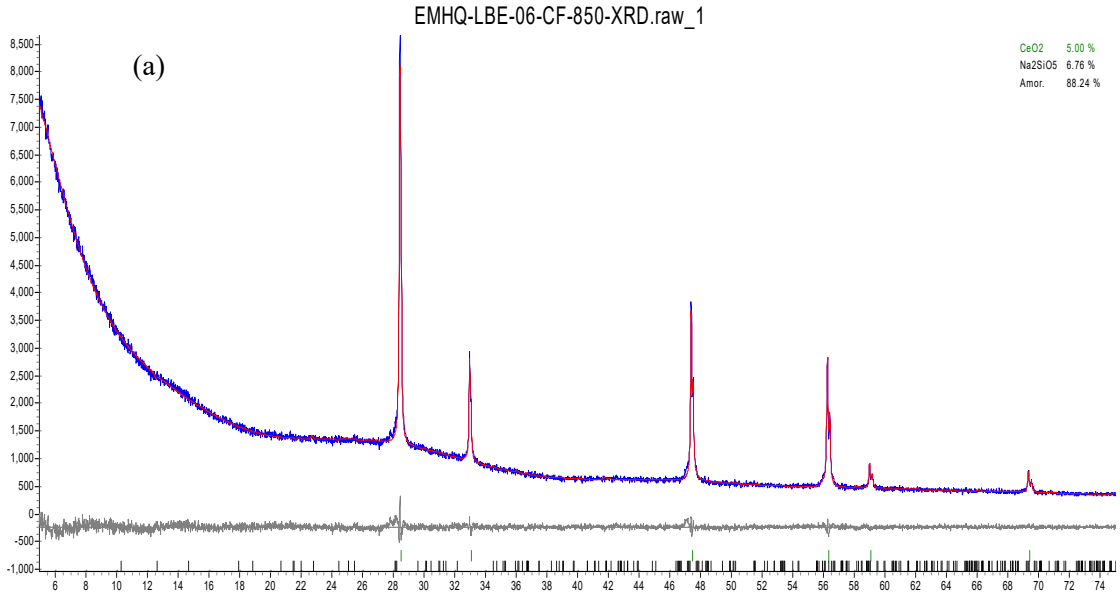

Phase Name	Wt% of Spiked	Wt% in Spiked Sample	Wt% in Original Sample
CeO_2	4.996	4.996	0.000
Na_2SiO_5	0.000	7.094	7.467

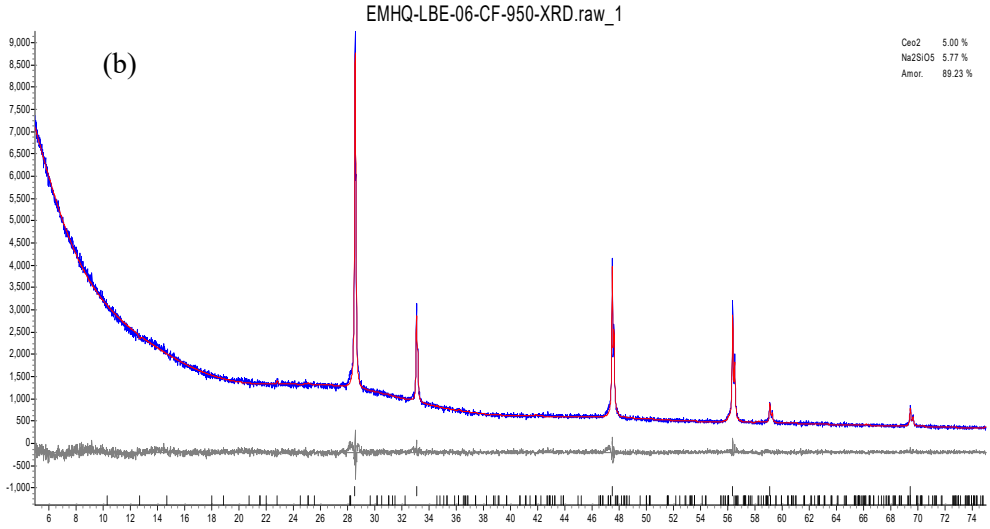

Phase Name	Wt% of Spiked	Wt% in Spiked Sample	Wt% in Original Sample
CeO_2	5.002	5.002	0.000
Na_2SiO_5	0.000	5.774	6.078

Figure G.7. XRD Spectrum of CF Heat-Treated Glass EMHQ-LBE-06 (a) 850 °C (b) 950 °C

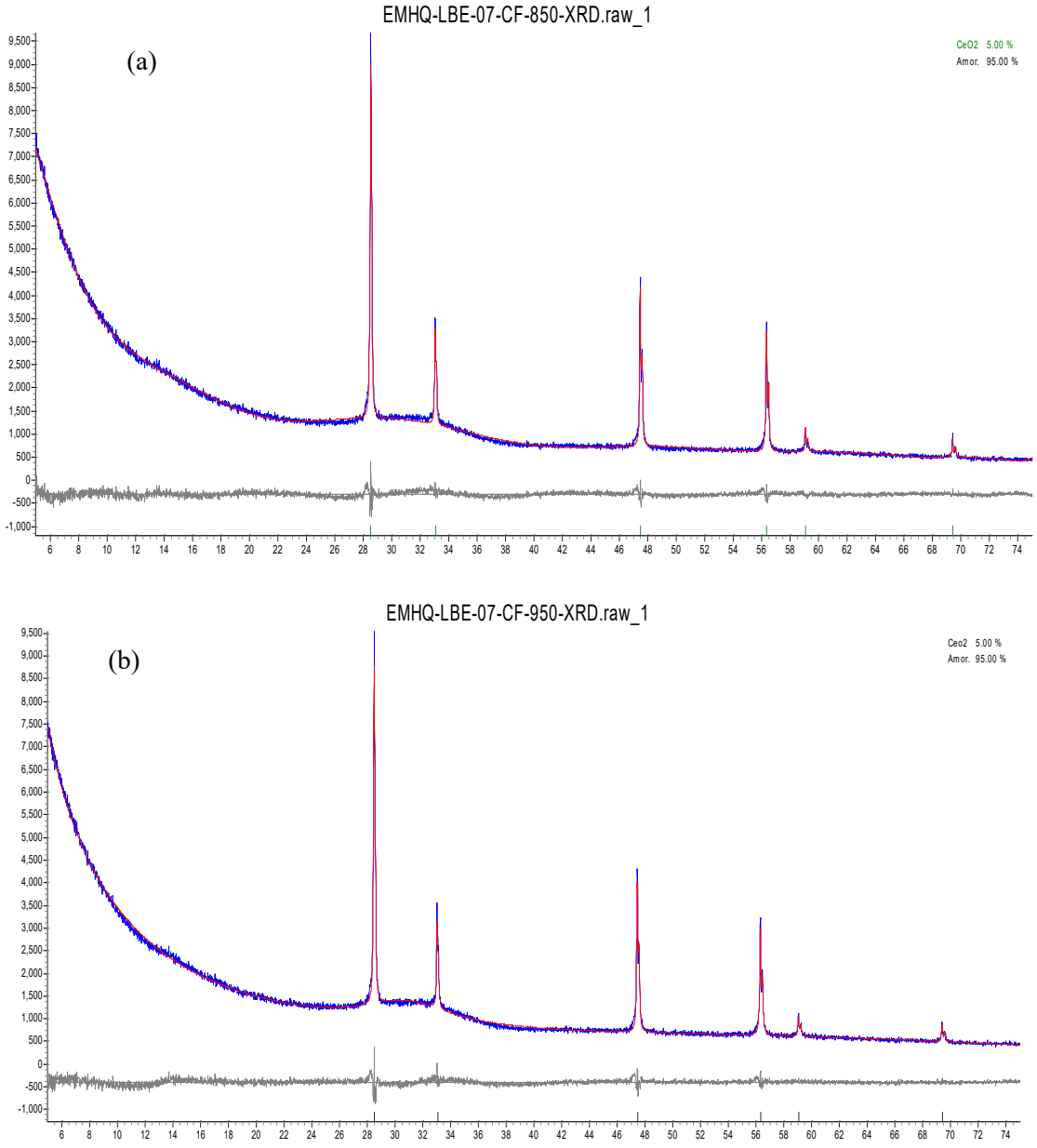

Figure G.8. XRD Spectrum of CF Heat-Treated Glass EMHQ-LBE-07 (a) 850 °C (b) 950 °C

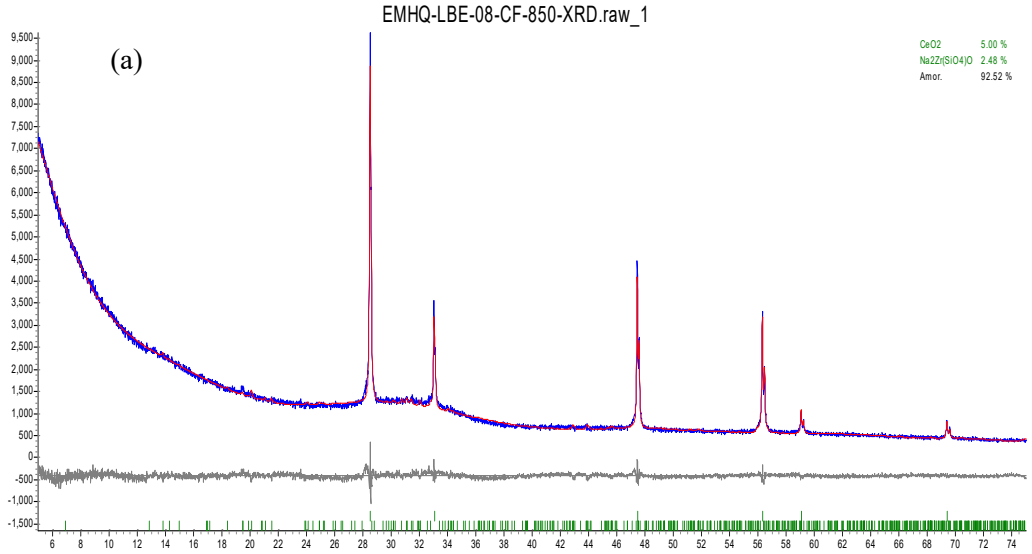

Phase Name	Wt% of Spiked	Wt% in Spiked Sample	Wt% in Original Sample
CeO_2	5.001	5.001	0.000
$Na_2Zr(SiO_4)O$	0.000	2.471	2.602

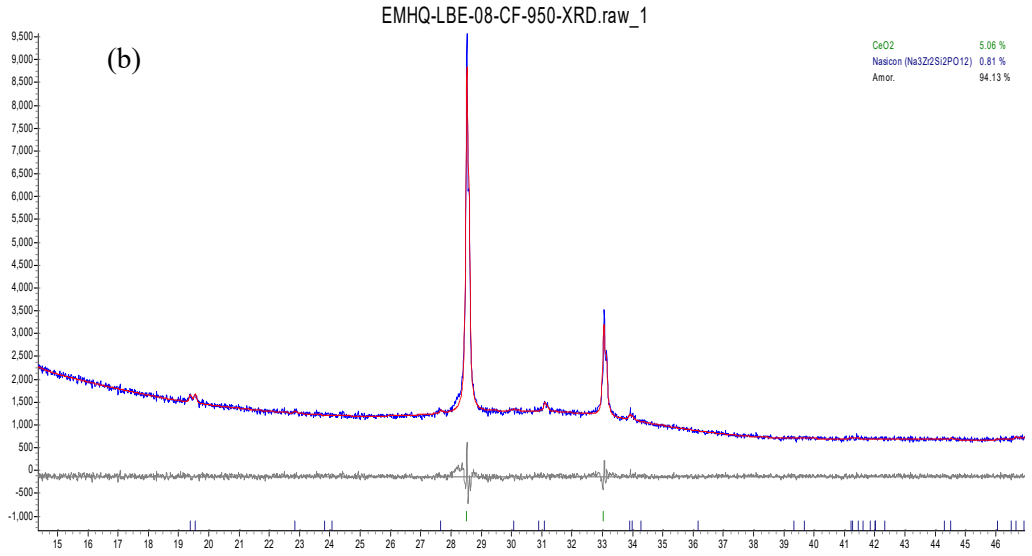

Phase Name	Wt% of Spiked	Wt% in Spiked Sample	Wt% in Original Sample
CeO_2	5.001	5.001	0.000
Nasicon ($Na_3Zr_2Si_2PO_{12}$)	0.000	1.058	1.114

Figure G.9. XRD Spectrum of CF Heat-Treated Glass EMHQ-LBE-08 (a) 850 °C (b) 950 °C

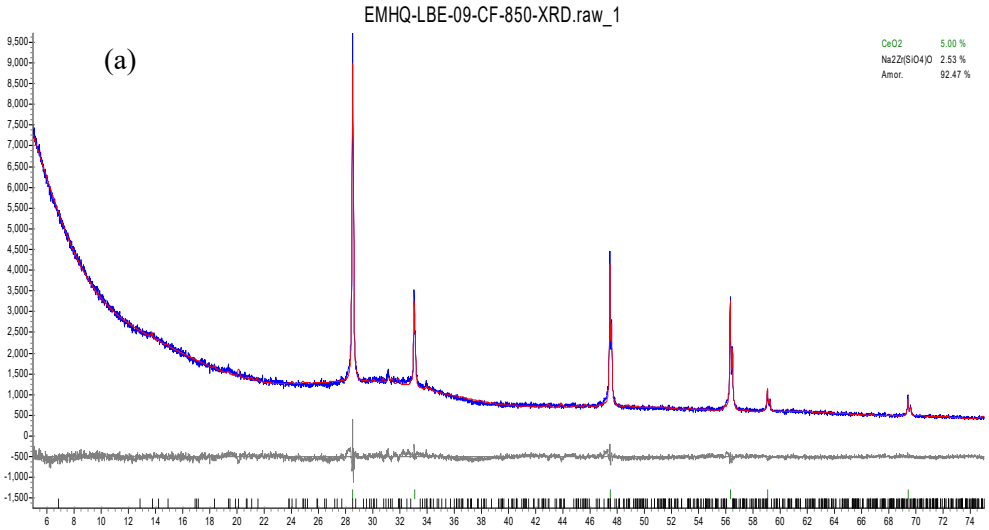

Phase Name	Wt% of Spiked	Wt% in Spiked Sample	Wt% in Original Sample
CeO_2	5.003	5.003	0.000
Nasicon ($Na_3Zr_2Si_2PO_{12}$)	0.000	2.509	2.641

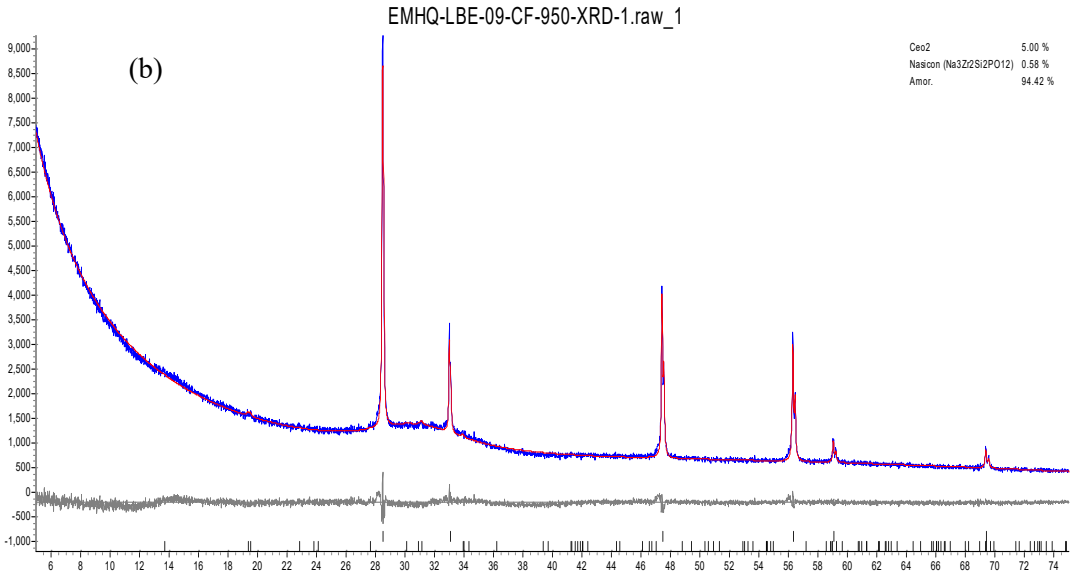

Phase Name	Wt% of Spiked	Wt% in Spiked Sample	Wt% in Original Sample
CeO_2	5.010	5.010	0.000
Nasicon ($Na_3Zr_2Si_2PO_{12}$)	0.000	0.573	0.603

Figure G.10. XRD Spectrum of CF Heat-Treated Glass EMHQ-LBE-09 (a) 850 °C (b) 950 °C

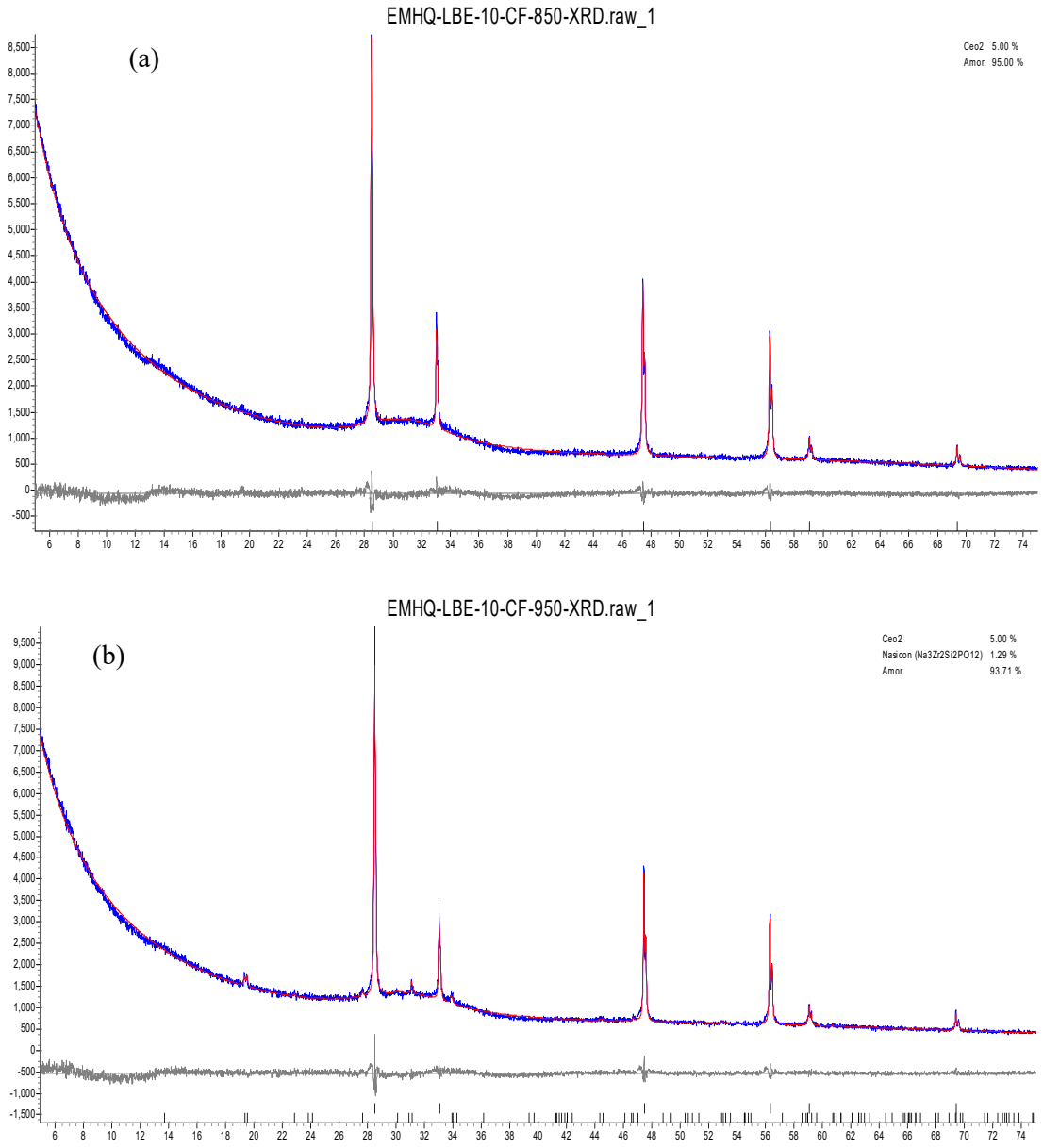

Phase Name	Wt% of Spiked	Wt% in Spiked Sample	Wt% in Original Sample
CeO_2	5.000	5.000	0.000
Nasicon ($Na_3Zr_2Si_2PO_{12}$)	0.000	1.305	1.374

Figure G.11. XRD Spectrum of CF Heat-Treated Glass EMHQ-LBE-10 (a) 850 °C (b) 950 °C

Appendix H – Pictures of Vapor Hydration Test (VHT) Glass Coupons

This appendix shows photos of the VHT samples of the EMHQ glasses both before and after testing. These photos show the variation in corrosion with the samples.

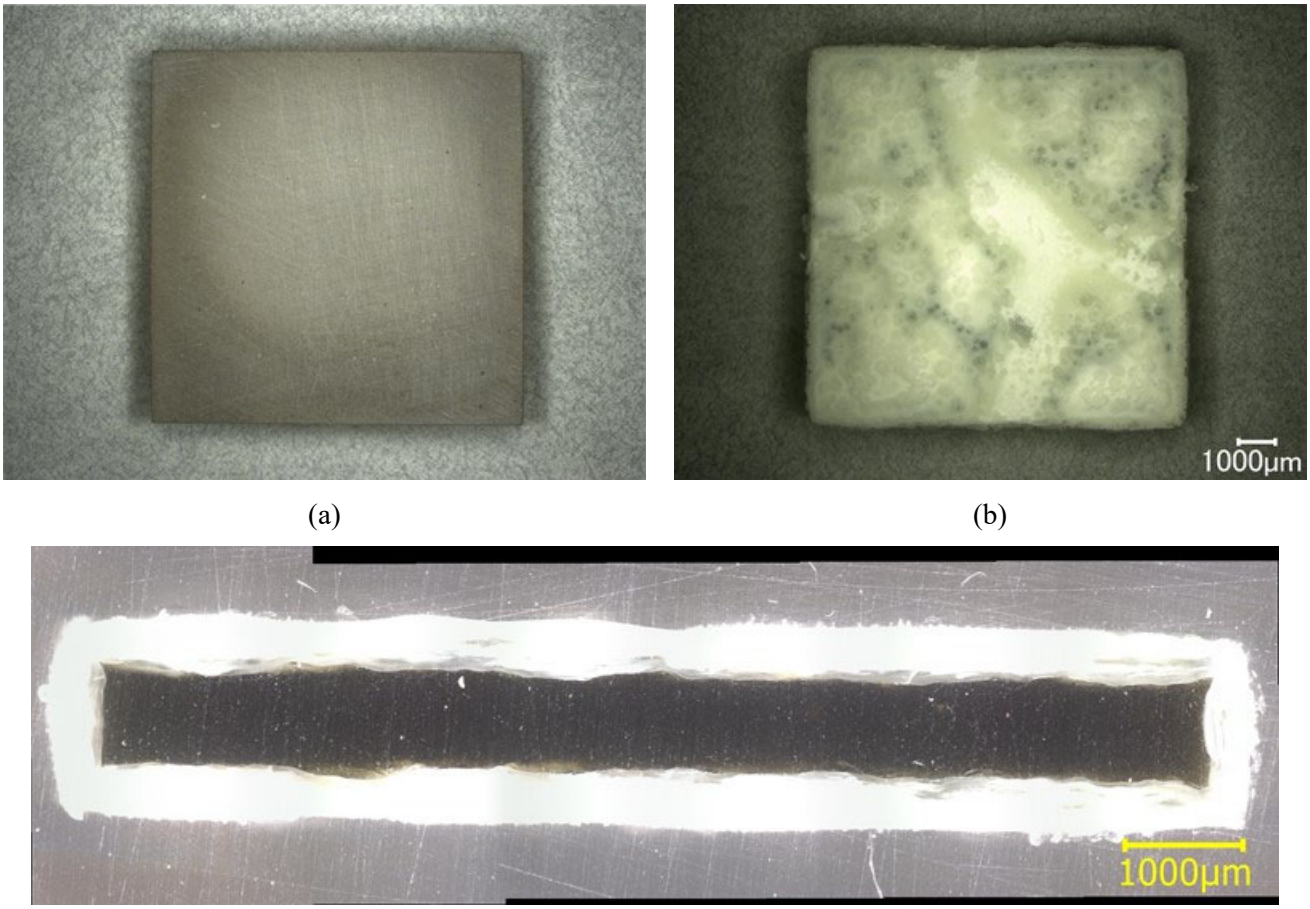

(a) (b)

(c)

Figure H.1. Quenched Glass EMHQ-LBE-01 after VHT for 24 Days: (a) glass square before VHT; (b) glass square after VHT; (c) glass cross section magnified after VHT.

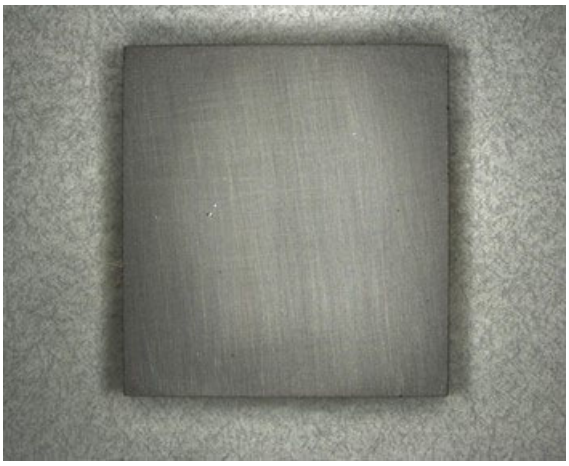

(a)

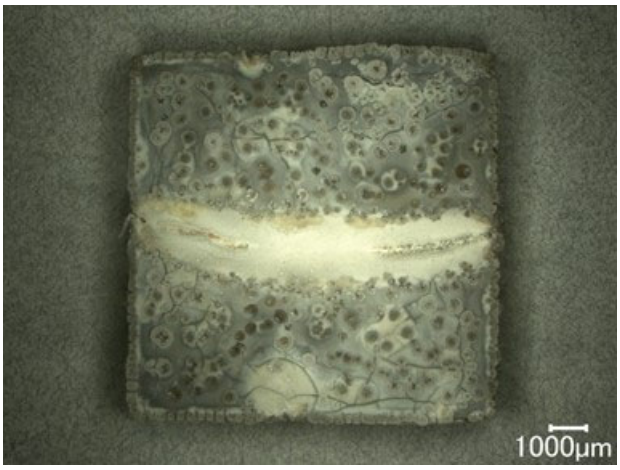

(b)

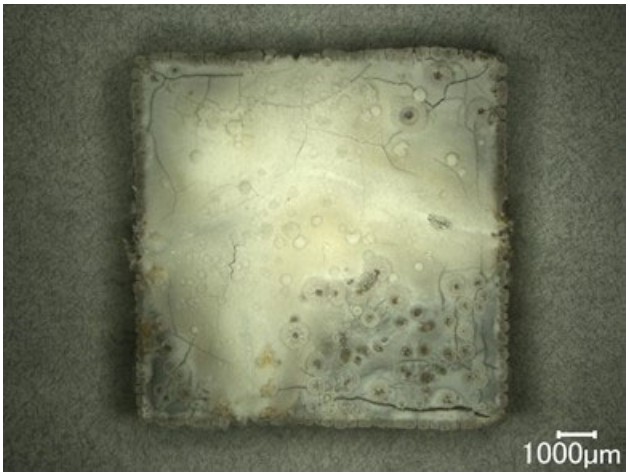

(c)

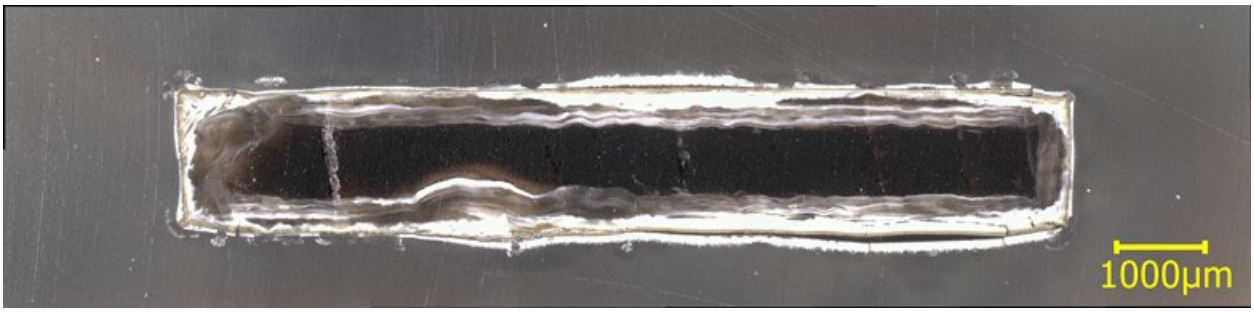

(d)

Figure H.2. Quenched Glass EMHQ-LBE-02 after VHT for 24 Days: (a) glass square before VHT; (b) glass square after VHT; (c) glass square after VHT; (d) glass cross section magnified after VHT.

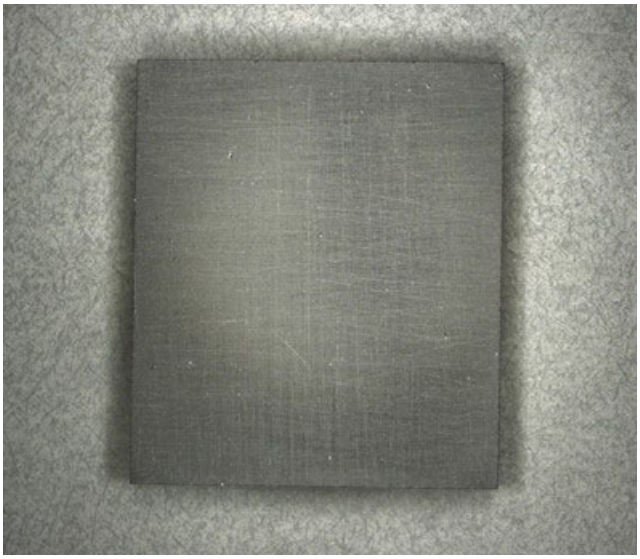

(a)

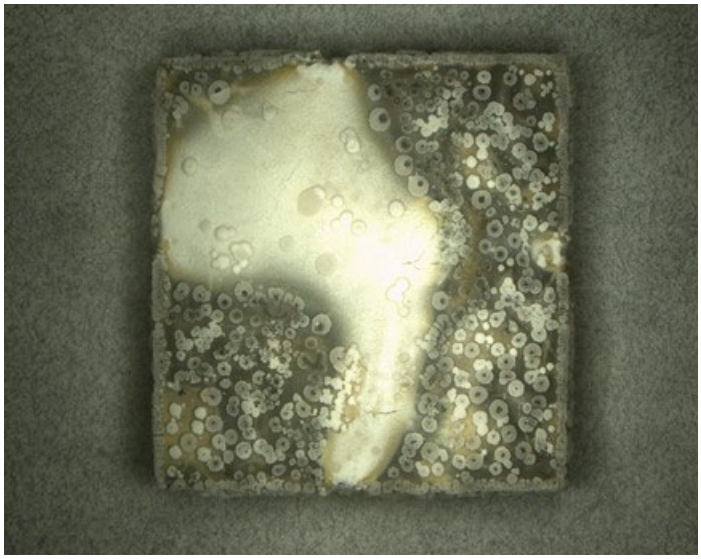

(b)

(c)

Figure H.3. Quenched Glass EMHQ-LBE-03 after VHT for 24 Days: (a) glass square before VHT; (b) glass square after VHT; (c) glass cross section magnified after VHT

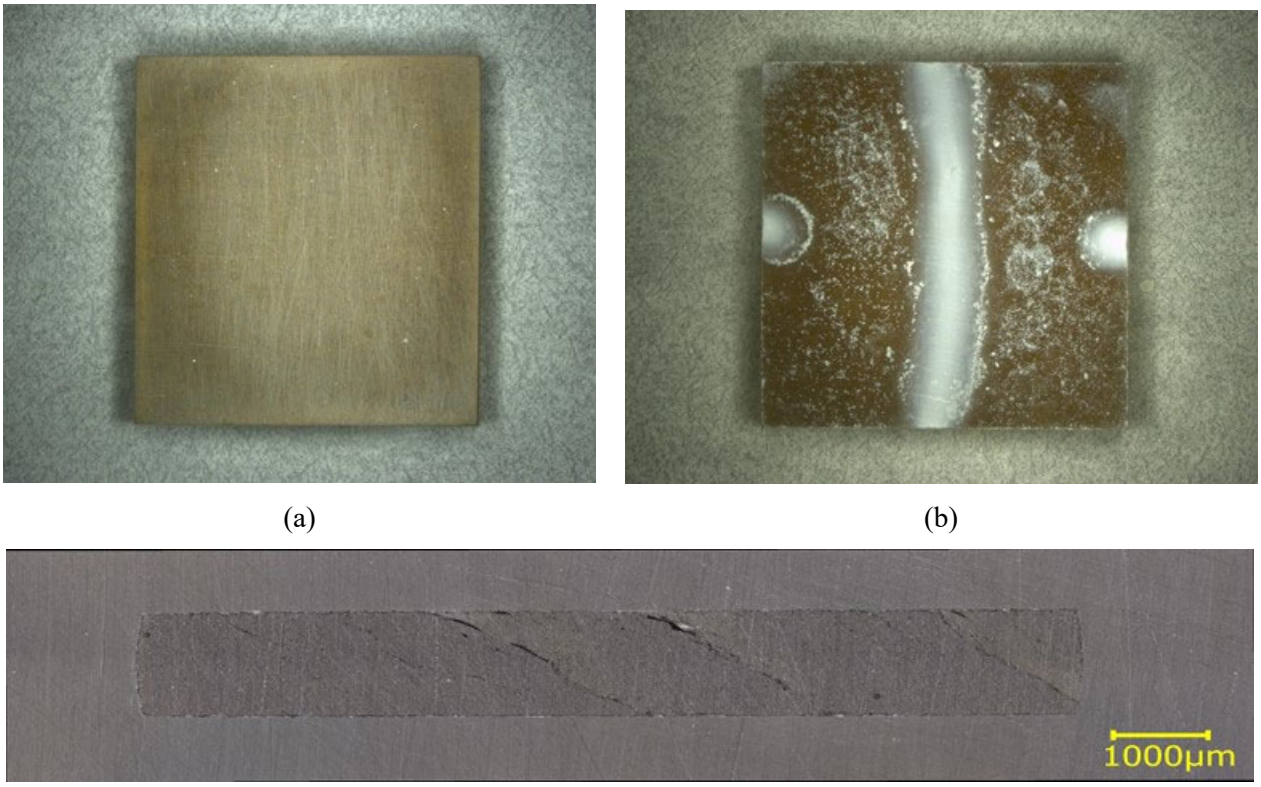

(a) (b)

(c)

Figure H.4. Quenched Glass EMHQ-LBE-04 after VHT for 24 Days: (a) glass square before VHT; (b) glass square after VHT; (c) glass cross section magnified after VHT

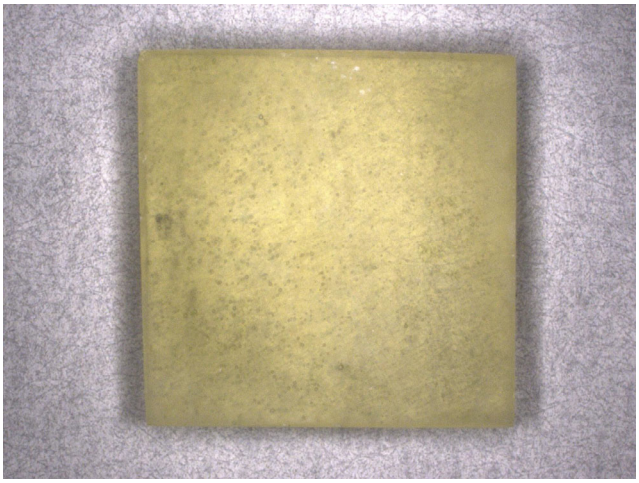

(a)

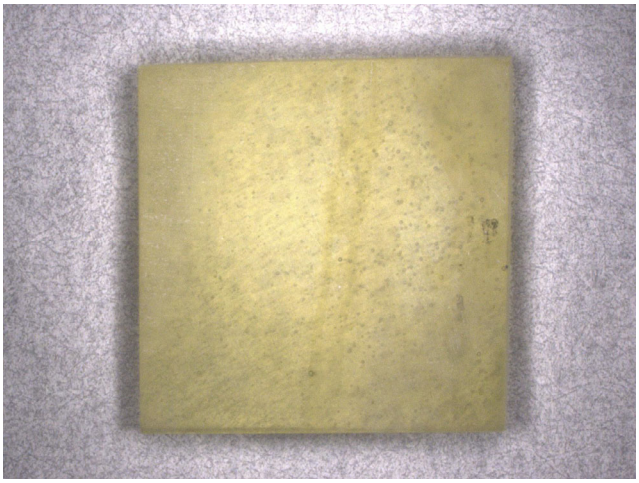

(b)

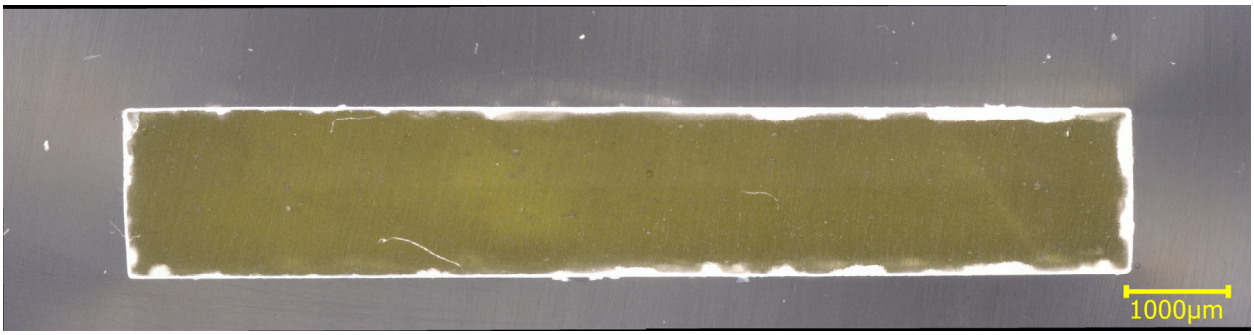

(c)

Figure H.5. Quenched Glass EMHQ-LBE-04B after VHT for 24 Days: (a) glass square before VHT; (b) glass square after VHT; (c) glass cross section magnified after VHT

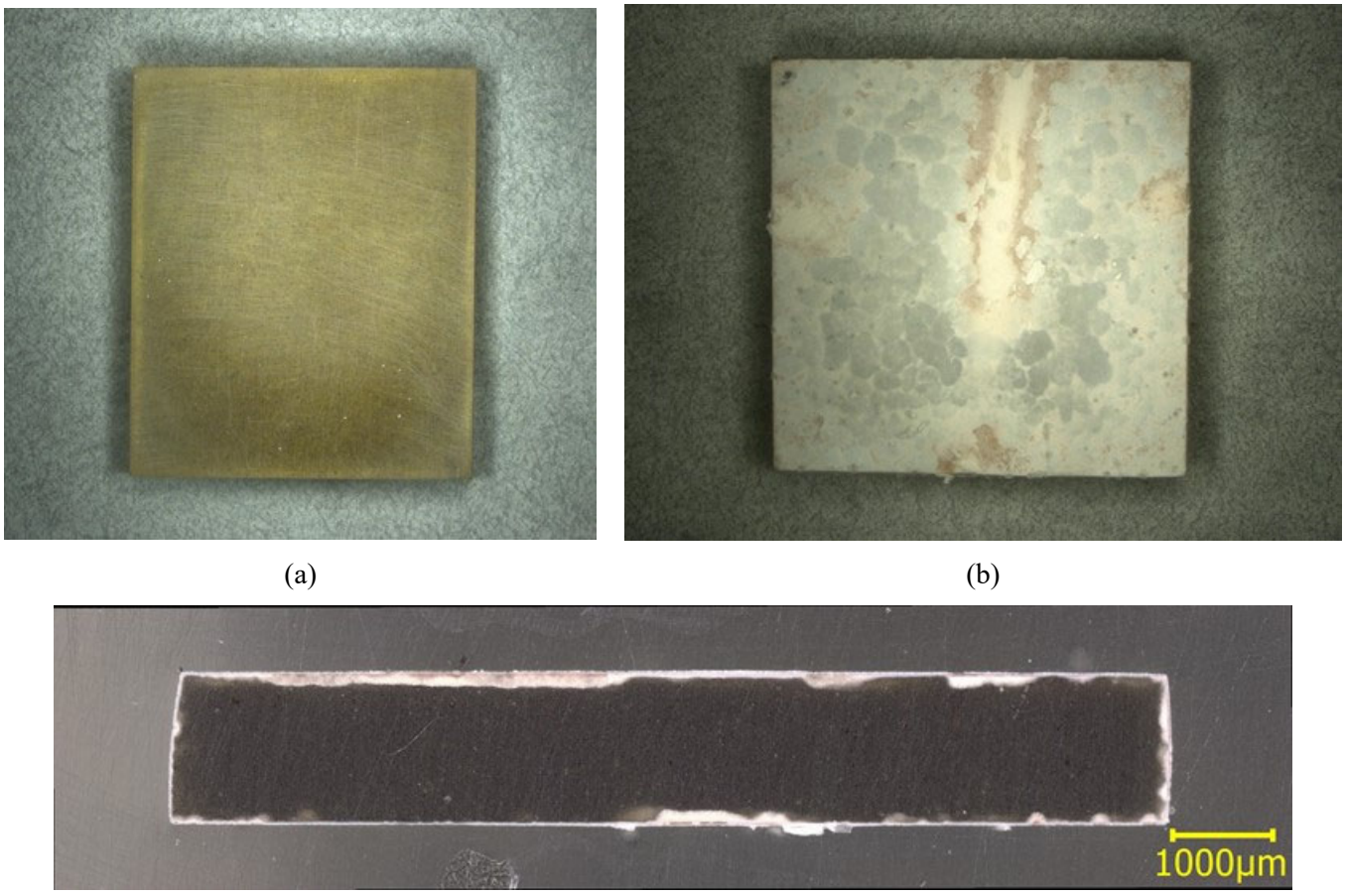

(a) (b)

(c)

Figure H.6. Quenched Glass EMHQ-LBE-05 after VHT for 24 Days: (a) glass square before VHT; (b) glass square after VHT; (c) glass cross section magnified after VHT

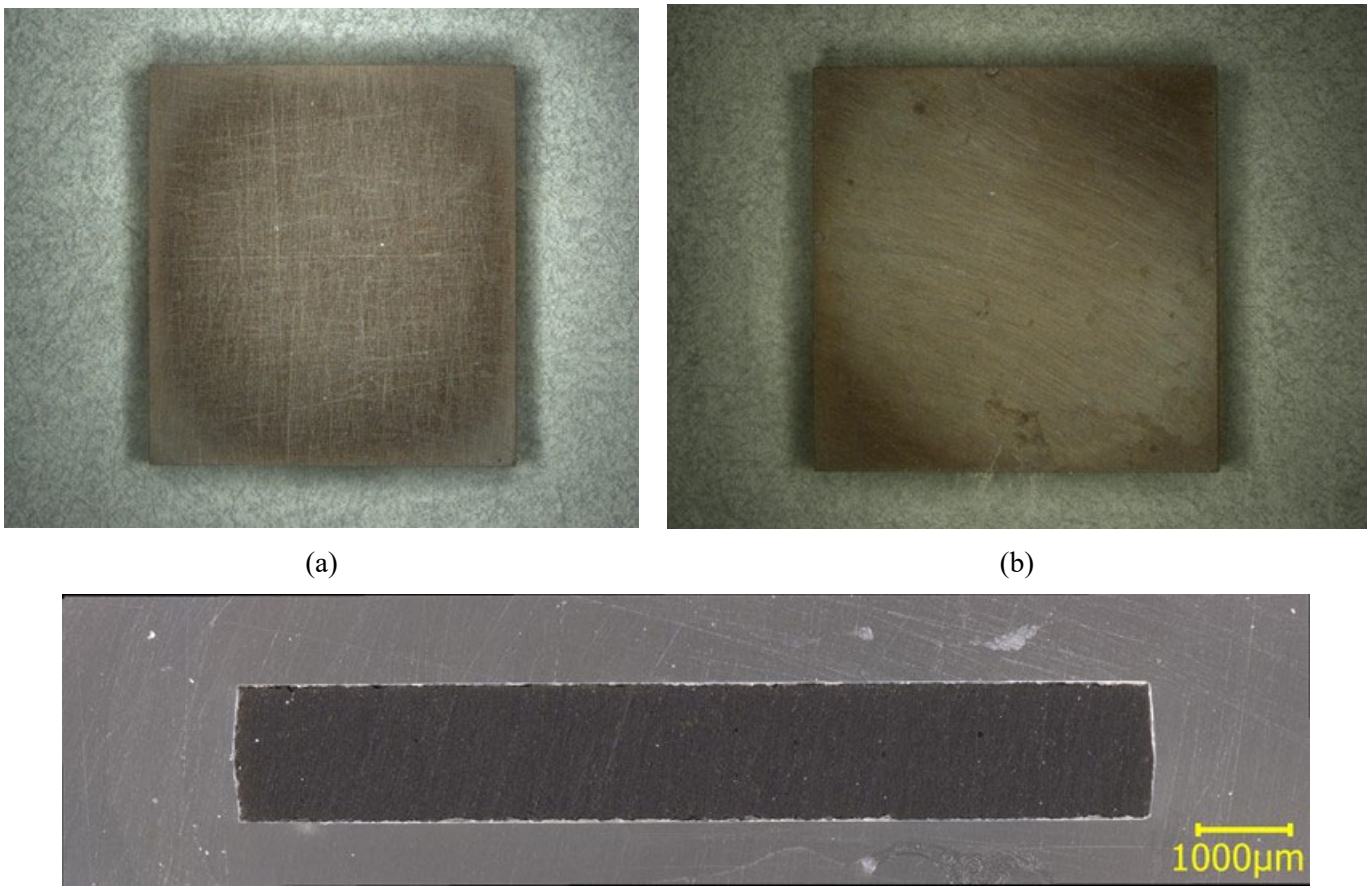

Figure H.7. Quenched Glass EMHQ-LBE-06 after VHT for 24 Days: (a) glass square before VHT; (b) glass square after VHT; (c) glass cross section magnified after VHT

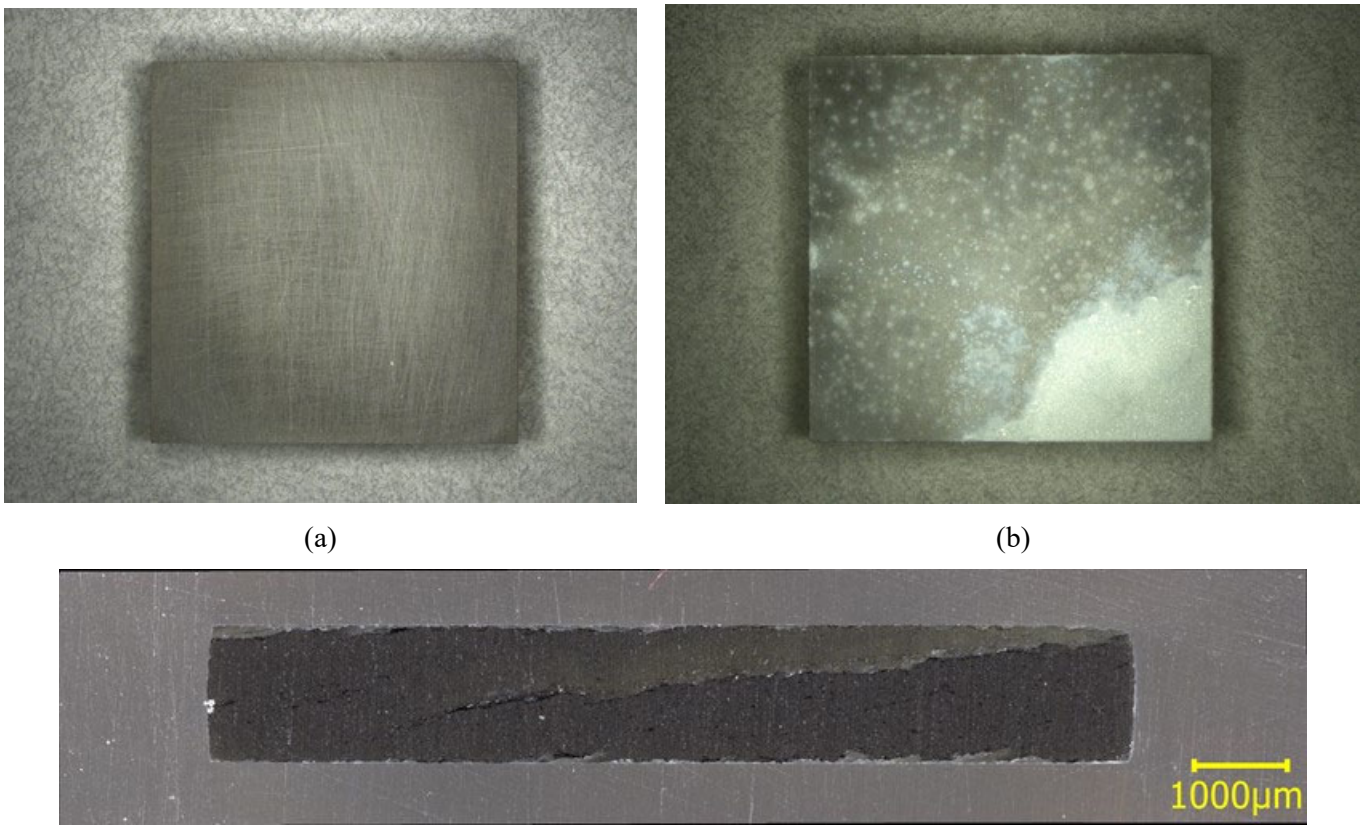

(a) (b)

(c)

Figure H.8. Quenched Glass EMHQ-LBE-07 after VHT for 24 Days: (a) glass square before VHT; (b) glass square after VHT; (c) glass cross section magnified after VHT

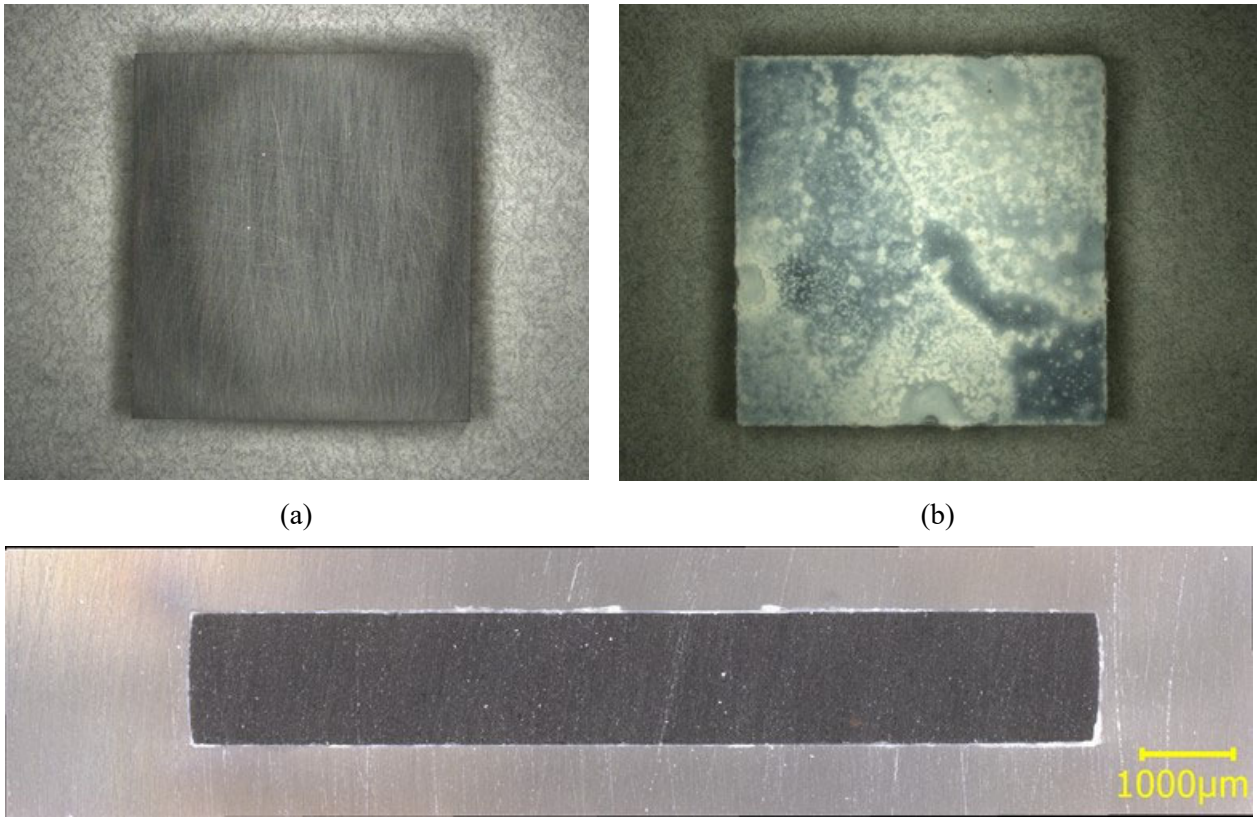

(a) (b)

(c)

Figure H.9. Quenched Glass EMHQ-LBE-08 after VHT for 24 Days: (a) glass square before VHT; (b) glass square after VHT; (c) glass cross section magnified after VHT

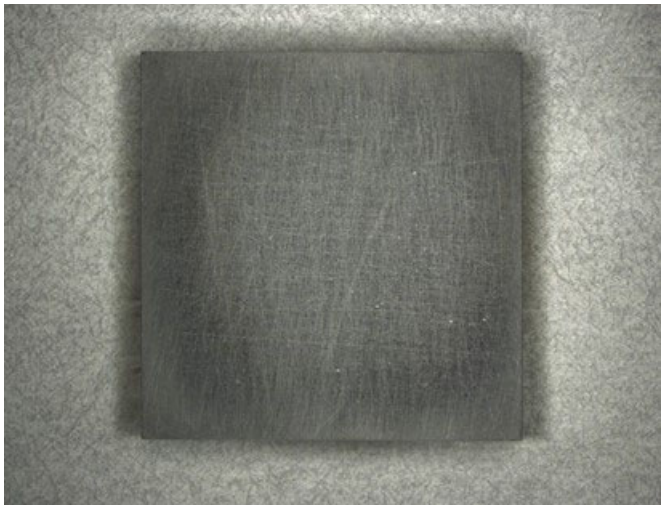

(a)

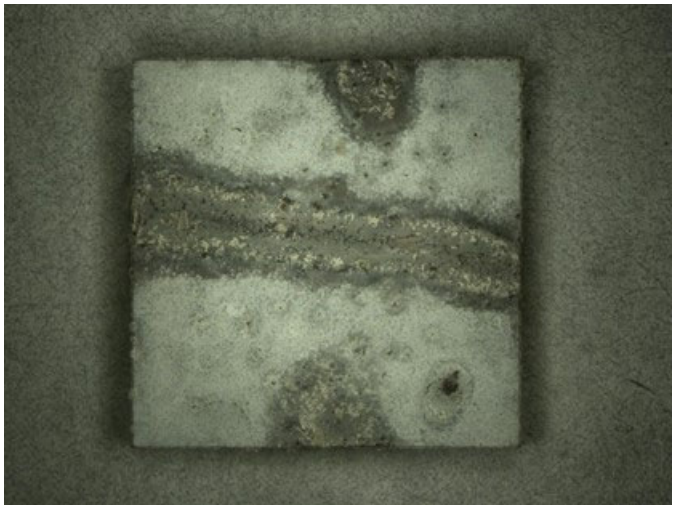

(b)

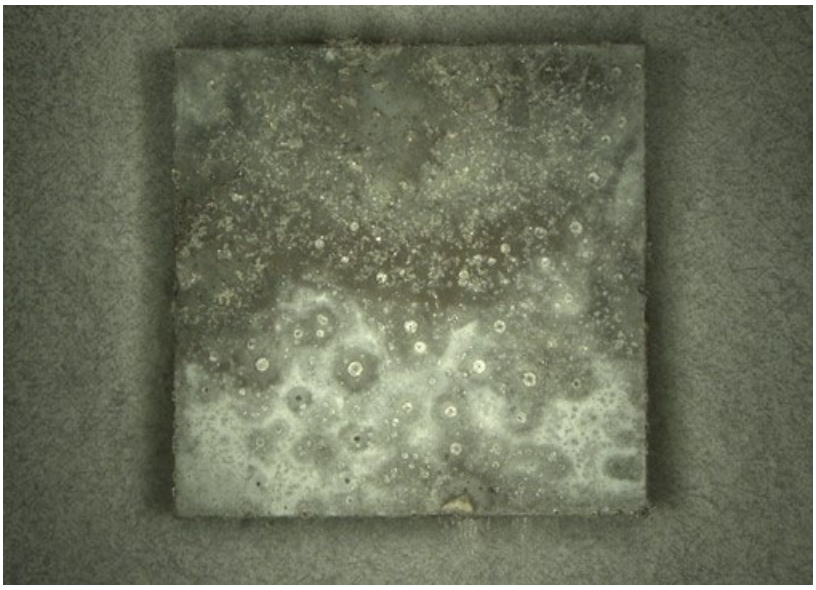

(c)

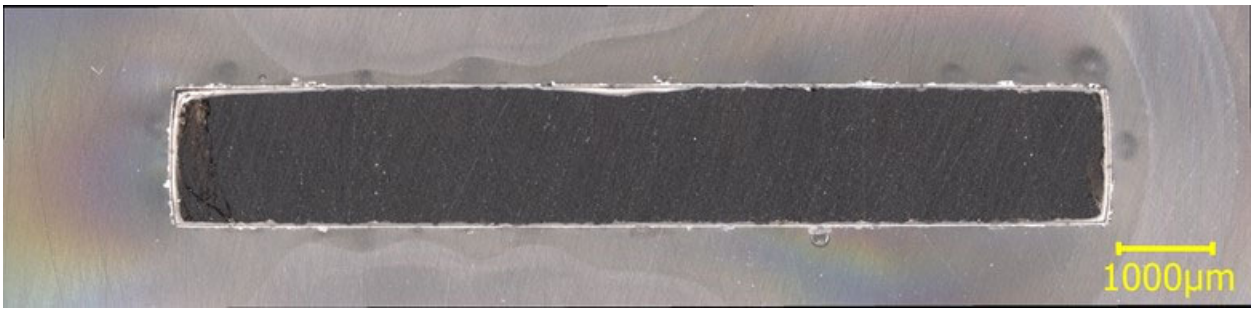

(d)

Figure H.10. Quenched Glass EMHQ-LBE-09 after VHT for 24 Days: (a) glass square before VHT; (b) glass square after VHT; (c) glass square after VHT; (d) glass cross section magnified after VHT

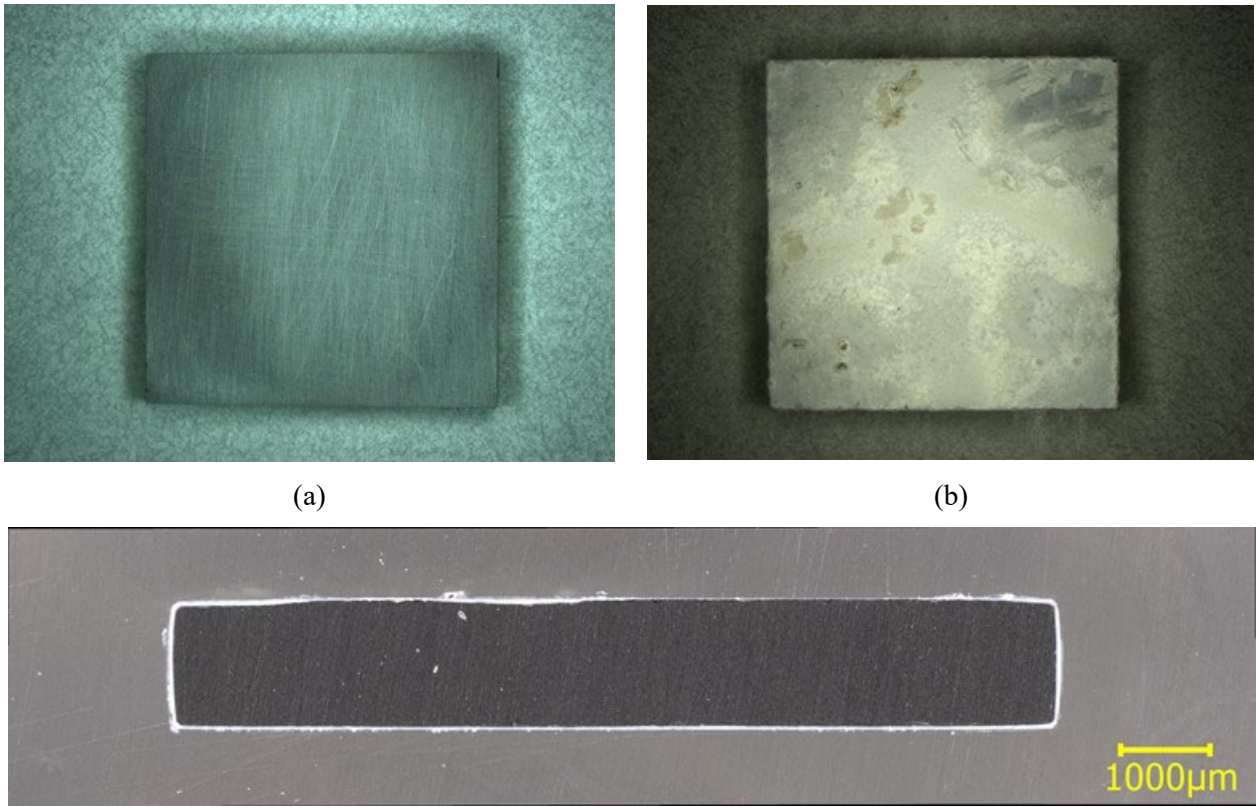

(a) (b)

(c)

Figure H.11. Quenched Glass EMHQ-LBE-10 after VHT for 24 Days: (a) glass square before VHT; (b) glass square after VHT; (c) glass cross section magnified after VHT

Appendix I – Analyses for Quenched and Sulfur Saturated Glasses and Sulfur Wash Solutions

This appendix presents and compares the normalized compositional analyses of the quenched and sulfur-saturated glasses and wash solutions using inductively coupled plasma – optical emission spectrometry and ion chromatography. This shows how much sulfur was retained in the glass as well as what was lost from the glass.

Table I.1. Normalized Measured Compositions (mass fractions) for Quenched and Sulfur-Saturated Versions of the LAW Boundary Expansion Waste Glasses EMHQ-LBE-01, EMHQ-LBE-02, EMHQ-LBE-03, EMHQ-LBE-04

	Glass ID											
	EMHQ-LBE-01			EMHQ-LBE-02			EMHQ-LBE-03			EMHQ-LBE-04		
Components	Quenched	Sulfur-saturated	% Diff	Quenched	Sulfur-saturated	% Diff	Quenched	Sulfur-saturated	% Diff	Quenched	Sulfur-saturated	% Diff
Al_2O_3	5.41	5.30	-2.08	5.32	5.28	-0.76	5.36	5.31	-0.94	3.58	3.36	-6.55
B_2O_3	11.8	11.7	-0.85	11.8	11.7	-0.85	11.7	11.7	0.00	12.4	12.1	-2.48
CaO	9.34	9.82	4.89	9.31	9.74	4.41	9.25	9.79	5.52	11.6	11.8	1.69
Cl	0.104	0.0459	-126.6	0.101	0.0454	-122.5	0.107	0.0425	-151.8	0.0679	0.0313	-116.9
Cr_2O_3	0.0476	0.0436	-9.17	0.0483	0.0383	-26.11	0.0484	0.0614	21.17	0.0223	0.0239	6.69
F	0.0936	0.0714	-31.09	0.0859	0.0711	-20.82	0.0913	0.0667	-36.88	0.0708	0.0507	-39.64
Fe_2O_3	0.118	0.121	2.48	0.125	0.124	-0.81	0.118	0.128	7.81	0.120	0.122	1.64
K_2O	0.100	0.0977	-2.35	0.0984	0.0968	-1.65	0.0943	0.0965	2.28	0.0557	0.0628	11.31
Li_2O	<0.215	<0.215	NA	<0.215	<0.215	NA	<0.215	<0.215	NA	1.85	1.73	-6.94
MgO	0.165	0.157	-5.10	0.161	0.157	-2.55	0.159	0.161	1.24	0.197	0.19	-3.68
MnO	<0.0129	<0.0129	NA	0.524	0.516	-1.55	0.520	0.534	2.62	<0.0129	<0.0129	NA
Na_2O	20.5	19.8	-3.54	20.1	19.3	-4.15	20.2	18.9	-6.88	11.5	12.9	10.85
P_2O_5	0.274	0.259	-5.79	0.275	0.268	-2.61	0.271	0.266	-1.88	0.144	0.139	-3.60
SiO_2	40.1	40.4	0.74	39.8	40.2	1.00	39.7	40.1	1.00	47.8	46.5	-2.80
SnO_2	<0.127	<0.127	NA	<0.127	<0.127	NA	<0.127	<0.127	NA	<0.127	<0.127	NA
SO_3	1.38	2.10	34.29	1.41	2.14	34.11	1.40	2.12	33.96	1.35	2.38	43.28
TiO_2	0.137	0.114	-20.18	0.111	0.114	2.63	0.109	0.116	6.03	0.0746	0.0756	1.32
V_2O_5	3.99	3.75	-6.40	3.99	3.70	-7.84	3.94	3.68	-7.07	4.02	3.80	-5.79
ZrO_2	3.69	3.73	1.07	3.63	3.71	2.16	3.64	3.69	1.36	1.96	1.90	-3.16
Total	97.6	97.9	0.31	97.3	97.5	0.21	97.0	97.1	0.10	96.9	97.2	0.31

Table I.2. Normalized Measured Compositions (mass fractions) for Quenched and Sulfur-Saturated Versions of the LAW Boundary Expansion Waste Glasses EMHQ-LBE-05, EMHQ-LBE-06, EMHQ-LBE-07, EMHQ-LBE-08

	Glass ID											
	EMHQ-LBE-05			EMHQ-LBE-06			EMHQ-LBE-07			EMHQ-LBE-08		
Components	Quenched	Sulfur-saturated	% Diff	Quenched	Sulfur-saturated	% Diff	Quenched	Sulfur-saturated	% Diff	Quenched	Sulfur-saturated	% Diff
Al_2O_3	3.51	3.42	-2.63	3.52	3.31	-6.34	8.82	8.45	-4.38	8.86	8.43	-5.10
B_2O_3	12.2	12.2	0.00	12.3	11.9	-3.36	8.02	7.88	-1.78	8.02	7.81	-2.69
CaO	11.6	12.0	3.33	11.5	11.6	0.86	7.55	7.93	4.79	7.45	7.92	5.93
Cl	0.0629	0.0284	-121.5	0.0695	0.0297	-134.0	0.0657	0.0272	-141.5	0.0635	0.0270	-135.2
Cr_2O_3	0.0257	0.0262	1.91	0.024	0.0416	42.31	0.153	0.128	-19.53	0.157	0.0728	-115.7
F	0.0682	0.0476	-43.28	0.0711	0.0487	-46.00	0.0647	0.0532	-21.62	0.0624	0.0542	-15.13
Fe_2O_3	0.139	0.131	-6.11	0.128	0.126	-1.59	0.117	0.117	0.00	0.131	0.133	1.50
K_2O	0.0536	0.0614	12.70	0.0527	0.0566	6.89	0.0521	0.0519	-0.39	0.0514	0.0522	1.53
Li_2O	1.81	1.80	-0.56	1.81	1.70	-6.47	<0.215	<0.215	NA	<0.215	<0.215	NA
MgO	0.200	0.192	-4.17	0.198	0.191	-3.66	0.130	0.130	0.00	0.133	0.130	-2.31
MnO	0.524	0.513	-2.14	0.527	0.516	-2.13	<0.0129	<0.0129	NA	0.525	0.528	0.57
Na_2O	11.5	12.5	8.00	11.3	12.5	9.60	22.9	22.8	-0.44	22.7	22.4	-1.34
P_2O_5	0.146	0.140	-4.29	0.141	0.129	-9.30	0.297	0.266	-11.65	0.294	0.258	-13.95
SiO_2	47.3	46.7	-1.28	47.6	45.9	-3.70	38.6	38.9	0.77	38.9	38.6	-0.78
SnO_2	<0.127	<0.127	NA	<0.127	<0.127	NA	4.30	4.27	-0.70	4.28	4.23	-1.18
SO_3	1.37	2.47	44.53	1.35	2.31	41.56	0.193	1.32	85.38	0.196	1.30	84.92
TiO_2	0.109	0.0763	-42.86	0.0746	0.0759	1.71	0.133	0.134	0.75	0.131	0.135	2.96
V_2O_5	4.02	3.56	-12.92	3.98	3.72	-6.99	<0.179	<0.179	NA	<0.179	<0.179	NA
ZrO_2	2.00	1.93	-3.63	1.94	1.86	-4.30	5.73	5.76	0.52	5.69	5.70	0.18
Total	96.8	98.0	1.22	96.8	96.1	-0.73	97.5	98.7	1.22	98.0	98.1	0.10

Table I.3. Normalized Measured Compositions (mass fractions) for Quenched and Sulfur-Saturated Versions of the LAW Boundary Expansion Waste Glasses EMHQ-LBE-09, EMHQ-LBE-10, and EMHQ-LBE-04B

Components	EMHQ-LBE-09			EMHQ-LBE-10			EMHQ-LBE-04B		
	Quenched	Sulfur-saturated	% Diff	Quenched	Sulfur-saturated	% Diff	Quenched	Sulfur-saturated	% Diff
Al_2O_3	8.84	8.56	-3.27	8.84	8.38	-5.49	3.62	3.34	-7.73
B_2O_3	7.94	7.86	-1.02	7.97	7.78	-2.44	12.7	12.5	-1.57
CaO	7.51	7.95	5.53	7.55	7.83	3.58	12.7	12.1	-4.72
Cl	0.0690	<0.0274	NA	0.0658	<0.0262	NA	0.0704	0.0419	-40.48
Cr_2O_3	0.153	0.0694	-120.5	0.153	0.0753	-103.2	<0.0365	0.0411	NA
F	0.0678	0.0583	-16.30	0.0662	0.0561	-18.00	0.0707	0.0405	-42.72
Fe_2O_3	0.107	0.113	5.31	0.108	0.111	2.70	0.119	0.128	7.56
K_2O	0.0524	0.0490	-6.94	0.0476	0.0526	9.51	0.0592	0.0593	0.17
Li_2O	<0.215	<0.215	NA	<0.215	<0.215	NA	1.96	1.77	-9.69
MgO	0.128	0.127	-0.79	0.129	0.128	-0.78	0.203	0.196	-3.45
MnO	0.530	0.529	-0.19	0.268	0.267	-0.37	<0.0129	<0.0129	NA
Na_2O	22.6	22.2	-1.80	22.9	22.4	-2.23	11.6	13.4	15.52
P_2O_5	0.289	0.261	-10.73	0.293	0.258	-13.57	<0.229	<0.229	NA
SiO_2	38.6	38.9	0.77	38.6	38.3	-0.78	48.8	48.5	-0.61
SnO_2	4.27	4.24	-0.71	4.30	4.20	-2.38	NA	NA	NA
SO_3	0.190	1.25	84.80	0.188	1.30	85.54	1.39	2.5	79.86
TiO_2	0.136	0.140	2.86	0.134	0.140	4.29	0.0799	0.0771	-3.50
V_2O_5	<0.179	<0.179	NA	<0.179	<0.179	NA	4.27	3.75	-12.18
ZrO_2	5.72	5.74	0.35	5.74	5.65	-1.59	1.88	1.85	-1.60
Total	97.7	98.4	0.71	97.7	97.3	-0.41	99.8	100.54	0.74

PNNL-32826, Rev. 0
EWG-RPT-039, Rev. 0

Pacific Northwest National Laboratory

902 Battelle Boulevard
P.O. Box 999
Richland, WA 99354
1-888-375-PNNL (7665)

www.pnnl.gov